*122397*

R - 673

# CHARLES STARK DRAPER LABORATORY
### A Division of Massachusetts Institute of Technology • Cambridge, Mass
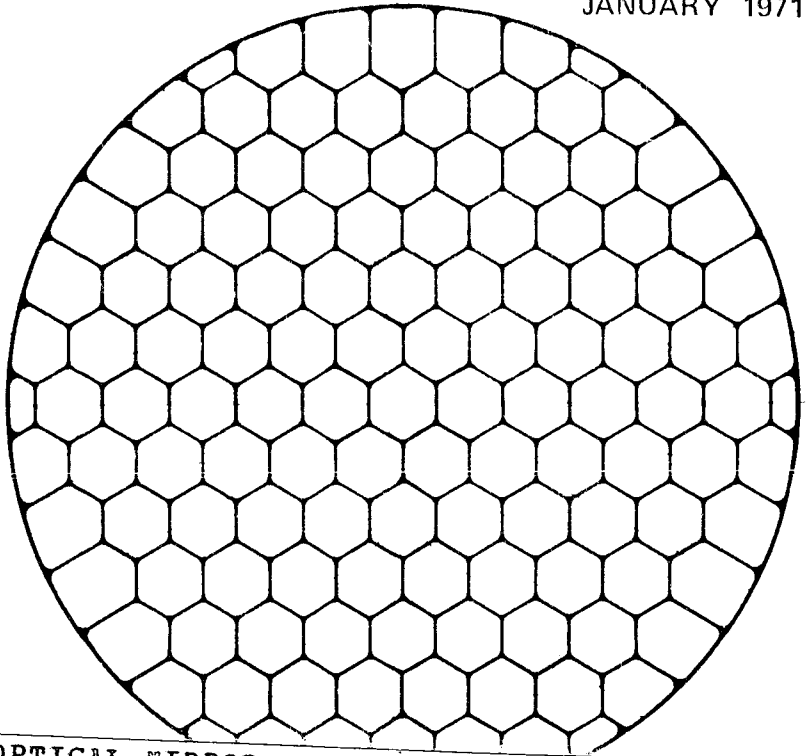
# DESIGN OF OPTICAL MIRROR STRUCTURES

KETO SOOSAAR
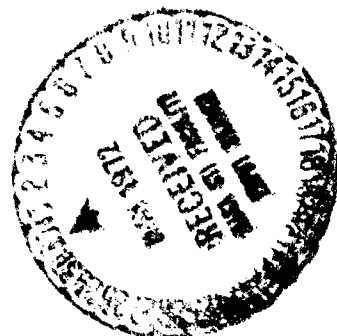
# DESIGN OF OPTICAL MIRROR STRUCTURES

by

Keto Soosaar

January 1971

## MASSACHUSETTS INSTITUTE OF TECHNOLOGY
### CHARLES STARK DRAPER LABORATORY
### CAMBRIDGE, MASSACHUSETTS 02139

This report covers research conducted
between May 1969 and November 1970.
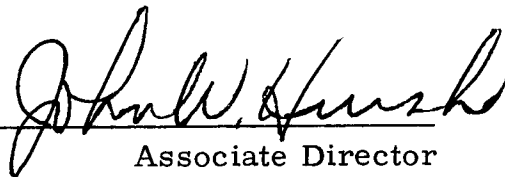
Approved: _____
Associate Director
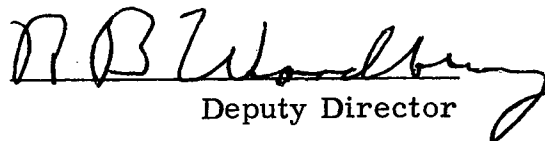
Approved: _____
Deputy Director

# ACKNOWLEDGMENT

# DESIGN OF OPTICAL MIRROR STRUCTURES

## ABSTRACT

The structural requirements for large optical telescope mirrors have been studied in this report with a particular emphasis placed on the three-meter Large Space Telescope primary mirror. Analysis approaches through finite element methods have been evaluated with the testing and verification of a number of element types suitable for particular mirror loadings and configurations. The environmental conditions that a mirror will experience have been defined and a candidate list of suitable mirror materials with their properties compiled. The relation of the mirror mechanical behaviour to the optical performance is discussed and a number of suitable design criteria are proposed and implemented. A general outline of a systematic method to obtain the best structure for the three-meter diffraction-limited system is outlined. Finite element programs, using the STRUDL II analysis system have been written for specific mirror structures encompassing all types of active and passive mirror designs. Parametric studies on support locations, effects of shear deformation, diameter to thickness ratios, lightweight and sandwich mirror configurations, and thin shell active mirror needs have been performed. Suggestions for further studies are presented.

# TABLE OF CONTENTS

# CHAPTER 1

## INTRODUCTION

The design objective of any measuring instrument is to reduce the inherent systematic and random errors in that device to at least an order of magnitude smaller than the random errors in the measured phenomenon. This goal is no less true with the astronomical telescope. Earth-based telescopes are generally bounded in their resolving power by the disturbances experienced by the light in passing through the atmosphere, but even with this generally lenient design requirement, considerable engineering skill has been required. An orbiting telescope, on the other hand, need not use this particular environmental bound and could instead be designed to the limits of diffraction.

A limiting characteristic in the behaviour of an optical telescope stems from the elasticity of the mirror material. Gravity and heat will distort the surface of any mirror, no matter how expertly prepared, and can greatly degrade the image quality. In some cases this degradation is small, but with large telescope optics some form of active compensation or adjustment, even if not continually administered, is quite vital.

While it is relatively easy to determine the mirror thermal and elastic properties and to define the gravity and temperature loadings, the prediction of their consequences through structural analysis has been evasive for some time. The optical mirror does not, in its normal configuration, belong to any group of elasticity problems that can be adequately solved by a series of simplifying assumptions. As a consequence, the structural design of mirrors has remained less a

science than an art, often subject to dark superstitions and violent disputes. While a full-scale or reduced-scale test could always be performed to settle the issue, it was, to say the least, a very costly and inadequate means.

Within the past few years a major breakthrough has occurred in the analysis of elastic continua. By means of the finite element method it is, in theory, possible to determine the stresses and displacements of any elastic body under any type of loading environment. Recent applications of this theory by means of large-scale digital computers indicate that the objective is nearly at hand.

One of the goals of this study is to develop a bridge between the information needs of the stress-deformation behaviour of optical mirrors and the existing analytical capabilities in the elasto-mechanics field. The other objective is to begin defining some of the critical structural design parameters for a 3-meter diffraction-limited orbiting optical telescope. This report represents an interim summary of efforts to date and concerns itself primarily with a collection and evaluation of appropriate criteria and methodology, and with the development of all necessary computer programs, and less with the solution of specific cases. In the final report on this study, such emphasis will be reversed.

The basic approaches in structural analysis are outlined in Chapter 2, with a discussion of the suitable elements for different mirror types and loadings. Chapter 3 outlines the environmental conditions an optical mirror must face in its journey from raw material to orbit. Chapter 4 considers a number of suitable mirror materials and presents criteria for selection of a suitable candidate. The relations of the structural performance to optical performance are discussed in Chapter 5. Chapter 6 outlines in detail the fundamental structural problems that must be solved for the primary mirror of the Large Orbiting Telescope, and presents a number of design approaches with specific examples. Chapters 7 and 8 present conclusions and further necessary extensions of the research, respectively.

# CHAPTER 2

# STRUCTURAL ANALYSIS METHODS

## 2.1 Closed-Form Solutions - Classical Methods

Occasionally in technical elasticity, an ideal situation occurs; a mathematical model for the physical world can be formulated, and a closed-form solution is found. Whenever such a solution exists it is, of course, the most accurate and should be used if available. Too often, however, the problem at hand approximates the mathematically soluble case in only some of its more superficial characteristics, further assumptions must be made, and recourse to experimental evidence may be needed. Generally this is the gray area of analysis, where personal opinions carry weight, where disputes can easily arise, and where the large errors are made. Many engineering problems nevertheless lie in this area, and the designer should check back constantly to the assumptions of the theory in order to retain confidence in his results.

Most optical mirror structures lie in this gray area. The structure is usually either a thick isotropic or sandwich slab, a shallow shell or plate with stiffeners that may or may not be orthogonal. It is supported either continuously on rings or discretely at points, and may be either symmetrically or unsymmetrically loaded. Closed-form solutions for thick dished slabs are available for only one or two very special cases, and these do not generally correspond to the real-world physical mirrors. Thin plate theory, where a lot of closed-form solutions exist, is generally not applicable for precision studies, although it is moderately useful in order-of-magnitude and trade-off studies. Orthotropic plate analysis can be used in some cases for

rib-stiffened mirrors, but this too is not generally enough applicable to form a fully reliable design tool.

At times it is possible to formulate the governing equations and boundary conditions for an elasticity problem, although a closed-form solution cannot be found. In some of these instances, finite-difference methods can be validly applied, but with many cases error propagation in computational algorithms has been fatal. Therefore, the structural theoreticians have now abandoned the search for closed-form or finite-difference approximation solutions, and virtually all progress in elasticity has been concentrated on development of the finite element technique. This method shows, at last, much promise in reducing the gray area in mirror structural analysis.

## 2.2 Finite Element Methods

The most important development in structural mechanics since Hooke's Law, one which has really revolutionized civil and aeronautical engineering problem analysis, is the finite element approach. [1][2][3]* This purely computer-oriented method permits the analyst to treat problems of continuum mechanics as well as trusses and frames in a completely general way.

The method operates by dividing a two- or three-dimensional continuum into small segments, triangles, rectangles, or cubes, over each of which the analyst assumes that the strain is either uniform or distributed according to some known variation. These segments are usually assumed connected by nodes at the vertices or at mid-points along the sides. The individual force-deformation response, that is the element stiffness matrix, is known from simple elasticity using the assumed strain function. To assure that all common joints between elements deform equally, a number of equations of joint compatibility must be formulated and solved. This leads to matrix operations and to the absolute need for high-speed large-capacity computers.

---

*References in Bibliography

The absolute generality of the method and the ease of use makes the finite element method an ideal tool for treating such complex elasto-mechanics problems as will arise in the design, manufacture, and operation of telescope mirror structures.[4] [5]

### 2.2.1   Matrix Structural Analysis

The following steps outline very broadly the procedure followed in finite element (as well as general frame element) formulation.[2]

Assume a relationship between the internal displacements f and the node displacements $\delta$ of an element

$$(f)^e = [N] \cdot (\delta)^e \tag{2.1}$$

Strains are obtained from displacements

$$(\varepsilon)^e = [B] \cdot (\delta)^e \tag{2.2}$$

introducing stress strain relationships

$$(\sigma)^e = [D]^e \cdot ( (\varepsilon) - (\varepsilon_o) )^e \tag{2.3}$$

imposing virtual nodal displacements and using the principle of stationary potential energy, the force-displacement relationships become

$$(F)^e = \left[ \int [B]^T [D] [B] \, d(vol) \right] (\delta)^e - \int [B] [D] (\varepsilon_o) \, d(vol)$$
$$- \int [N]^T (p) \, d(vol) \tag{2.4}$$

The element stiffness matrix is defined by

$$[k]^e = \int [B]^T [D] [B] \, d(vol) \tag{2.5}$$

Nodal forces due to distributed loads are

$$(F)^e_p = - \int [N]^T (p) \, d(vol) \tag{2.6}$$

Initial strain effects

$$(F)^e_{\varepsilon_o} = - \int [B]^T [D] (\varepsilon_o) \, d \, (vol) \tag{2.7}$$

or

$$(F)^e = [k]^e (\delta)^e + (F)^e_p + (F)^e_{\varepsilon_o} \tag{2.8}$$

Node equilibrium at node i, p is external forces

$$p_i = \sum_{m=1}^{n} F_i \tag{2.9}$$

Replacing $F_i$

$$p_i = \sum_{m=1}^{n} [k_{im}]^e (\delta)^e + (F_i)^e_p + (F_i)^e_{\varepsilon_o} \tag{2.10}$$

Then the overall equations are summed over nodes i

$$P = [K] \cdot (\delta) + (F)_p + (F)_{\varepsilon_o} \tag{2.11}$$

As a specific example, consider a two-dimensional region divided into triangular elements (Figure 2.1).
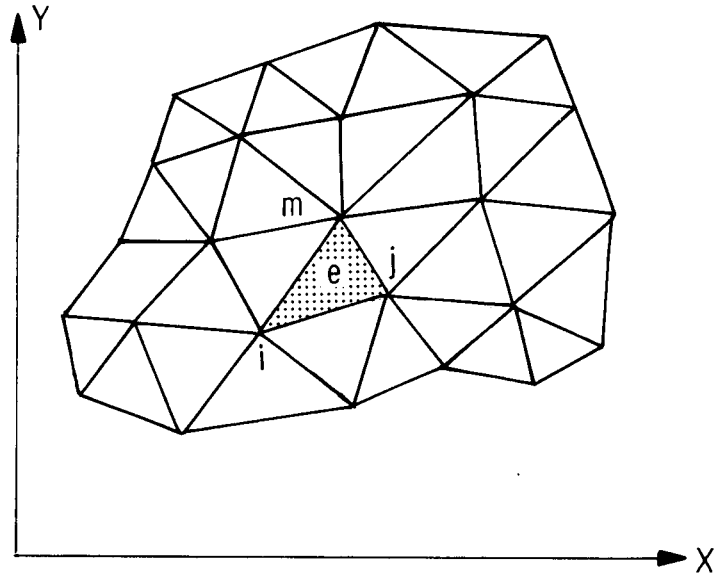


Figure 2.1   Planar region divided in triangular elements.

Then, taking an individual element of this assembly and formulating its elastic behaviour (Figure 2.2),
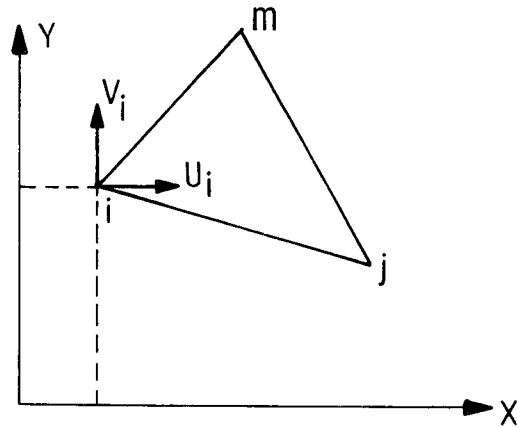


Figure 2.2   Element formulation.

assuming a constant strain element, then the displacement function is,

$$u = \alpha_1 + \alpha_2 x + \alpha_3 y$$

$$(2.12)$$

$$v = \alpha_4 + \alpha_5 x + \alpha_6 y$$

In terms of joints i, j, m

$$\begin{Bmatrix} U_i \\ U_j \\ U_m \end{Bmatrix} = \begin{bmatrix} 1 & x_i & y_i \\ 1 & x_y & y_j \\ 1 & x_m & y_m \end{bmatrix} \begin{Bmatrix} \alpha_1 \\ \alpha_2 \\ \alpha_3 \end{Bmatrix}$$

$$(2.13)$$

Inverting this to get $\alpha_1$, $\alpha_2$, $\alpha_3$ in terms of $U_i$, $U_j$, $U_m$, the joint displacements, a general expression of u is obtained. An expression for v is obtained in the same manner.

Hence,

$$(f)^e = \begin{Bmatrix} u \\ v \end{Bmatrix} = [N] \cdot (\delta)^e$$

$$(2.14)$$

This relationship is that expressed in Equation ( 2. 1 ). Thus, the formulation and solution can proceed.

## 2.3    Finite Element Systems

A large number of finite element programs have been developed by industry, but most of them are oriented towards special-purpose applications  and  are not necessarily more efficient than general-purpose systems.

A small number of general-purpose analyzers have also been developed, primarily to collect the elements and to standardize the solution

methodology. Even these vary enormously in their scope, capacity, and limitations. Some typical systems are ASKA,[6] SAMIS,[7] ELAS,[8] NASTRAN[9] and STRUDL II.[10] The last of these, which was developed by the Civil Engineering Department at MIT is one of the most comprehensive and powerful of these systems.

STRUDL II was developed to standardize and collect a large number of existing element types and to organize them in a modular way such that very complex problems involving intermixes of bar and continuous elements can be handled with equal ease. All of this was done within a problem-execution environment which has the following general characteristics.

## 2.3.1 Problem-Oriented Language

The input-output language of STRUDL II is the language an engineer uses in his everyday work. The structure is specified as to geometry, topology, loadings, and types of behaviour element. All of these commands are then translated into FORTRAN-like statements and the execution proceeds from there.

## 2.3.2 Dynamic Memory Allocator (DMA)

It is difficult to specify the primary/secondary computer storage needed for a complex problem unless one is intimately familiar with the basic operations performed. Then, too, for optimum storage use the arrays should be shifted from primary to secondary when no longer needed. This tends to make the analyst a computer systems programmer. The STRUDL II (DMA) obviates both needs by allocating the requisite amounts of storage completely automatically at execution time and moves the arrays between secondary and primary storage only when the need arises. A small problem may be solved entirely in core.

## 2.3.3 Modularity

While the library of available elements is very extensive, the user may find that the one he needs is still not available. He can add this by specifying the general stiffness matrix for an element, the

9

array needs for one such element and add it to the general library or include this as part of the input at problem execution time. Completely free intermix of bar, plate and solid elements is permitted, even if elements have unequal degrees of freedom at connecting joints. Substructure analysis exists, as well, as a user-specified option.

## 2.3.4 General Capability

At the present time the capability of the system extends to trussed, framed, folded plate, shell, and solid elements under the following conditions (Figure 2.3):

      (i)      linear static analysis

      (ii)     non-linear and buckling analysis

      (iii)    dynamic analysis

      (iv)    optimization

A systems flowchart for the essential STRUDL II capabilities is shown in Figure 2.3. Optimization occurs as a larger loop which includes Figure 2.3 as a component.

## 2.4 Finite Element Types

At the present time the STRUDL II finite element system has a library of approximately forty elements which can be broadly divided into the line, surface and solid types. Line elements include primarily the truss and frame members which are, however, seldom encountered in mirror problems.

The surface elements include pure bending, plane stress/plane strain, bending and stretching, and shell types. For many applications, these elements represent the types needed for optical mirror analysis. For a sufficiently thin mirror supported with its optical axis in line with the load direction, bending elements of various types may be used. As the plate tends towards a slab, i.e., when its span to thickness ratio drops to 8 or 10, the effects of shear deformation must be included and a more sophisticated element used. For general parametric or order of magnitude studies, however, the Kirchoff bending element is generally sufficient besides being enormously cheaper to run.
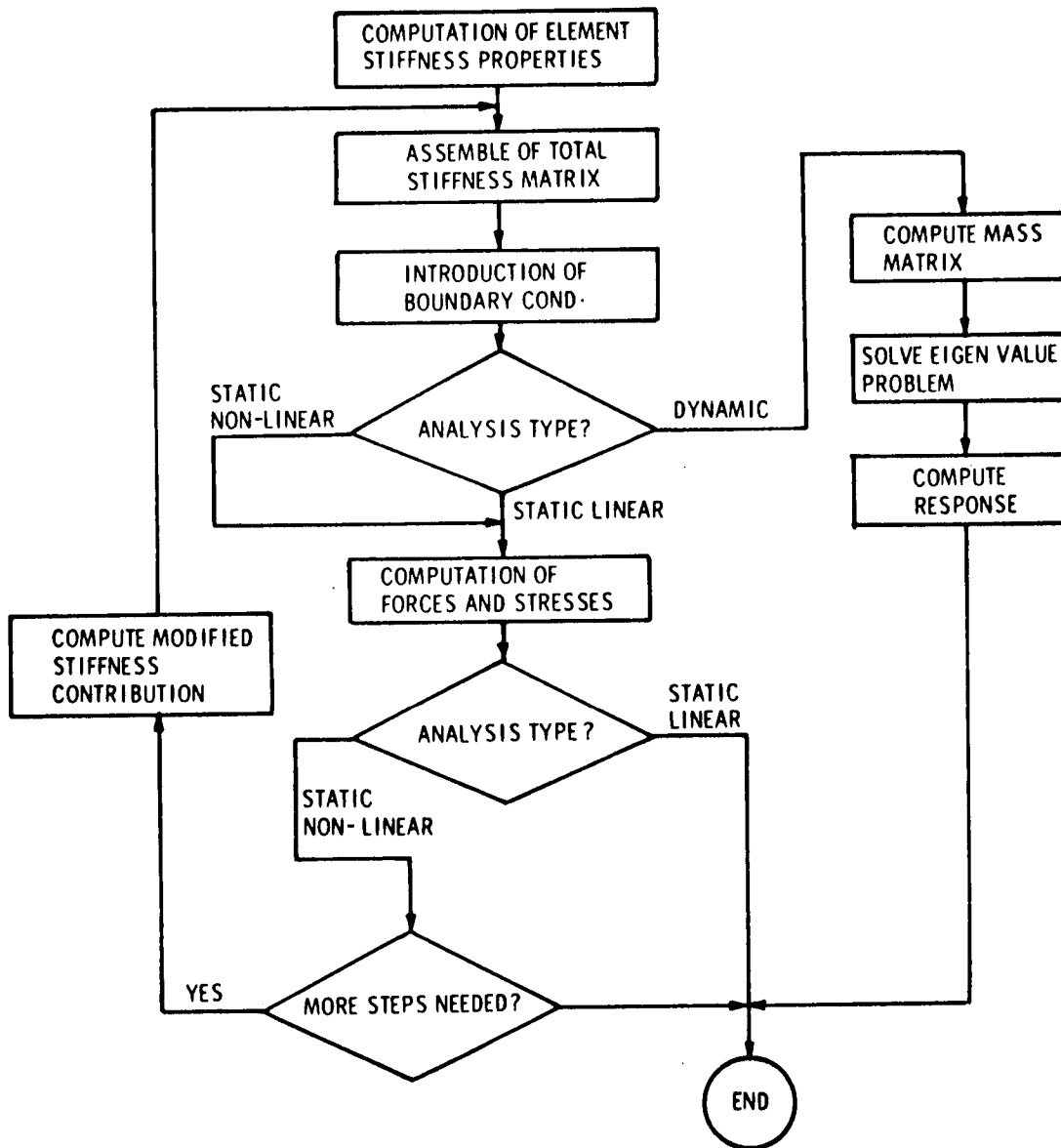
Figure 2.3 STRUDL II analysis procedure.

11

Occasionally it is of interest to determine the behavior of a mirror with its optical axis perpendicular to the load direction. In this case, plane stress elements can lead to a first-order approximation if the mirror deflections are sufficiently small.

In recent years, ribbed or "light-weight" mirrors have become quite popular and it is necessary to analyze these quite precisely as well. It is a grievous mistake here to rely on a purely equivalent bending stiffness approach as the shear deflections **often** dominate. These structures can be readily and accurately analyzed by subdividing the face and rib plates into bending/stretching elements. The approach used here is essentially identical to folded plate structural analysis. Bending/stretching elements can also be used for analysis of shell-type mirrors.

If available, shell and shallow shell elements are the most suitable for general-purpose analysis of thin mirrors, such as are encountered in thin active systems. The obvious advantage here is, of course, having the element properly curved to avoid angular intersections between adjacent elements which may often lead to unconservative results.

With the use of any of the above elements, the elasticity problem has to be defined as belonging to a particular class of problems, where known behavior assumptions would reduce the complexity. Sometimes, in elastic mechanics, and quite often in optical mirror structures, the problem cannot be reduced from the general 3-dimensional elasticity problem to a simpler, more tangible form. In such an instance, the only recourse is a solid element. With such an element, a true picture of the stresses and deformations can be obtained, though at the price of high computer running times.

A recent addition to the STRUDL II library is the isoparametric group of solids. Originally formulated by Irons[11] at the University of Swansea, they permit the user to specify "solids" with straight, parabolic, cubic or even higher order boundary curves. Intermediate nodes are required as well to satisy the high-order internal displacement functions.

These elements now permit the analyst to solve the completely general three-dimensional elasticity problem.

Figure 2.4 shows some of the typical elements that would be encountered in an optical mirror study.

1) BENDING

LOADS ALONG OPTICAL AXIS

2) STRETCHING

LOADS NORMAL TO OPTICAL AXIS

3) BENDING AND STRETCHING (1 AND 2)

GENERAL LOADS, "LIGHTWEIGHT" MIRRORS
THIN SHALLOW SHELL MIRRORS

4) SHALLOW SHELL

LIGHTLY CURVED THIN MIRRORS

5) SHELL

STRONGLY CURVED THIN MIRRORS

6) SOLID ELEMENTS

SOLID THICK MIRRORS WITH MAJOR SHEAR
AND TRACTION EFFECTS
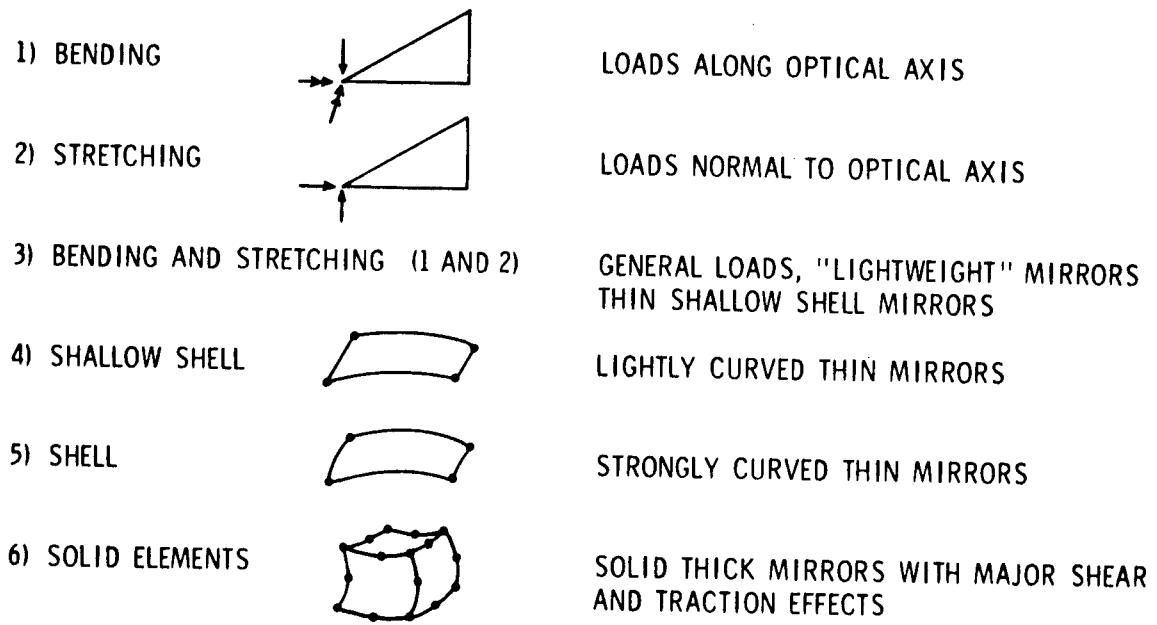
Figure 2.4   Finite element types for optical mirror problems.

14

# CHAPTER 3

# MIRROR STRUCTURE ENVIRONMENTAL CONDITIONS

## 3.1  Introduction

While the space telescope mirror structure is primarily designed to operate in orbital conditions, it is subject to several other loading environments under which it must meet either the performance or survival specifications. In a chronological order these include manufacture, earth testing, launch and orbital operation.

Previous mirrors have been fabricated, tested, launched, and now are operating in orbit with considerable success. In many of these cases, an exhaustive analytical study was not necessary as the performance specifications were less stringent. The diffraction-limited requirements on the 120" Large Space Telescope mirror, however, do not permit any a priori assumptions in this regard, and the effects of all possible loading environments should be evaluated.

This chapter will outline a minimum number of loading conditions which could serve to degrade or destroy the figure or structural integrity of the mirror. It should be observed, however, that while some of the conditions may be evaluated immediately with candidate structures, a large majority are highly system-dependent and the environment specification will evolve with the progressing design. For this reason, the emphasis here is more on the qualitative than the quantitative.

## 3.2  Manufacture

It is very difficult to cast a solid from a liquid melt without the inclusion of some degree of residual internal stress. This occurs

with all materials, but is of considerable importance with optical glass. Low-expansion materials, minimal heats of fusion, carefully-controlled cooling procedures followed by proper annealing will reduce, but never eliminate, material and stress inhomogeneities.

A cooled mirror blank has basically achieved internal stress equilibrium, with the faces in compression, the core in tension. The process of grinding and polishing will, however, remove a finite surface layer at the location of the greatest compressive stresses and disturb this equilibrium. As a result, the mirror blank will distort. Kumanin[12] gives a relationship between the deformation, the residual stress, and thickness of layer removed

$$f = K \cdot \frac{D^2}{L^2} \cdot \delta \cdot H \qquad (3.1)$$

where

$f$ = magnitude of deformation

$H$ = thickness layer removed

$\delta$ = internal stress parameter

$D$ = diameter of disc

$L$ = thickness of disc

$K$ = proportionality factor

This relationship is approximate, as it assumes uniform internal stresses and the removal of a uniform thickness of material. The general case can be solved with finite elements if the internal stress level and distribution prior to grinding can be defined.

Heat generation in grinding and the slight viscoelasticity of glass will tend to give further distortions which will not be immediately apparent after surface figuring. These effects will be added then to the distortions resulting from the release of gravity body forces in the orbital environment.

With ribbed or honeycombed lightweight mirror structures, new internal stresses or stress redistributions are produced by the "welding" and coring procedures. These will be further changed by the grinding and polishing action.

Local mirror surface deviations at the ribs can be expected due to nonuniform elastic deformations caused by the grinding tools. With a solid mirror blank, the action of the tool contact is more of a point effect on a uniform semi-infinite solid. With ribbed mirrors, the elastic resistance of the mirror is considerably higher immediately on the rib than in the plate action areas between. As a result, a rigid tool removes more of the stiffer zone than of the flexible. Critical here, also, are the supports of the mirror during the figuring process. If these are similar to the operating mounts, and if the mirror is not permitted to deform elastically during figuring, then the surface deviations will be small. If not, then the ribs will be "seen" in the resulting deformation pattern. Again, with the gravity loads removed in orbital operation, these effects will be amplified.

It is possible to evaluate these manufacturing effects analytically using finite element techniques, but some fundamental data is still needed on the initially-stressed condition after cooling, and on the nature of the loading intensities expected in the grinding and polishing process. The knowledge of this data will determine the permissible load levels for handling, testing, launch and, if necessary, active control actuators. A thorough analysis prior to manufacture may very well be cheaper than a catastrophic mirror breakage.

3.3    Earth Testing

Even though the mirror will eventually operate in a gravity-free environment, the basic optical testing of the system must be performed under gravity conditions. An important consideration here is whether or not an attempt should be made to design the mirror to perform at or close to the final specifications within the earth environment.

If the mirror deformations due to gravity effects are several orders of magnitude greater than the desired orbital performance, then special precautions must be taken to establish, on earth, that the desired performance level in orbit will be met.

The orbital behaviour may be obtained by factoring out the

17

gravity effects using the data from an adequately precise theoretical model or by testing the mirror in a reversed gravity-field. Such an evaluation will require the taking of differences of almost equal large numbers. If the gravity effects are several orders of magnitude larger than the orbital effects, then the noise to signal ratio of the net results could be very poor. Contributors to such "noise" would be minor shifts and alterations in the support locations or in support friction, and even slight inhomogeneities in the mirror material properties. It is highly desirable, therefore, for a reliable passive system to obtain a design which comes close to satisfying the desired performance even within the gravity environment.

For the active figure control system, it will be assumed that the gravity effects will be completely removed by the actuators. The critical structural parameters for earth testing of an active system must then ensure that the actuators have sufficient movement and strength to neutralize the gravity effect, and that the resultant mirror stresses do not exceed the strength levels of the mirror material. It should be kept in mind, however, that the stresses from the actuators will be additive with the internal stresses remaining from the manu-facturing.

## 3.4   Launch Effects

The launch dynamics problem is especially severe for the tele-scope structure. The mirror itself must survive the complex shock, vibrational and acoustic environment without exceeding permissible material stress levels. It is as important, however, to evaluate the dynamic effects of the mirror on the rest of the telescope system.

In the passive configurations, the mirror system will be suf-ficiently heavy and stiff to represent a considerable lumped mass which must be restrained by the relatively flexible launch vehicle structure. This mass will be of sufficient magnitude to be a major contributor to the overall vehicle dynamics. With the active config-uration, the stiffness and weight of the mirror is much less, although because of actuators, backing-plates and control hardware the total

system weight will probably remain high.

There is, moreover, a functional incompatibility between the precision supports needed for the mirror in orbital operation and the substantial restraints required for the launch phase. It is anticipated that two independent support systems would be necessary with the final telescope alignment occurring in orbit. It is difficult to estimate, at this time, the nature of the launch support system required, as it will be strongly influenced by the nature of the launch vehicle, and on the location of the mirror in that vehicle.

## 3.5 Orbital Operation

The mirror in orbit will experience disturbances from a number of sources. Some of these may be minor, such as the inertial effects during attitude change, the dynamics resulting from docking with the space station (with the mirror on operational 'optical' supports), or from the slight but measurable accelerations resulting from instrumentation actuators. The controlling disturbances presumably will be thermal.

Unless active thermal means are employed, the mean operating temperature of the mirror structure in orbit will be considerably below that experienced for earth assembly and testing. Low-expansion mirror materials may be employed, but these are effective only within a limited temperature range. Thus, deformations will occur and the mirror figure will change. The magnitude of this change will be primarily dependent on the entire telescope structural and thermal configuration.

In addition to the change in the mean temperature, short-term temperature fluctuations will be experienced. The primary source of this is the radiative transfer from the sun, moon, earth, and the space station impinging on the telescope. Some contributions will be expected as well from the on-board instrumentation. Part of the energy will reach the mirror directly, some of it will conduct through the supports. Under these conditions, however, the mirror must deliver the desired performance. Unless the disturbances are found

to be very slight, the passive optics approach will require the solution of a highly coupled heat transfer-thermoelasticity problem. For the active optics concept, the material thermal and elastic properties are much less critical, but it is necessary to provide sufficient actuator strength and stroke, yet assure that mirror over-stressing does not occur during a corrective phase.

# CHAPTER 4

## MIRROR MATERIALS

## 4.1 Introduction

The success of any engineering design depends highly on the
proper choice from available materials. When diffraction-limited
optical performance is desired for the space telescope, such a choice
becomes even more difficult since a number of equally important en-
vironmental criteria pull in opposite directions. Any one of the re-
quirements, taken individually, is relatively easy to fulfill; jointly, a
compromise must be attained.

The minimum material requirements are:

1. High-quality durable optical surface.
2. Minimum stresses and deformations under laboratory-
   testing conditions.
3. Launch survival.
4. Minimum thermal distortions in operation.
5. Adequate long-term dimensional stability.

## 4.2 Criteria and Candidates

The initial choice, obviously, must be narrowed to the can-
didates that can be manufactured to the desired optical figure. Major
considerations for acceptance will include material homogeneity,
isotropy, porosity, the ability to achieve a proper polish, or to
accept a necessary optical coating. Schroeder[13] reports on per-
centages of scatter from a number of optical materials at two
different wavelengths (Table 4-1). While a certain trend is
evident, tending towards rejection of beryllium, considerably more
work is needed here with the other materials as well, especially if
the system is to be optimized for a more restricted band-width.

# Table 4-1

## Scatter Measurements (Schroeder)

| Material | Percent Scatter | |
| --- | --- | --- |
| | $\lambda = 6328$ Å | $\lambda = 1.9$ Å |
| CER-VIT | 0.11 | 20 |
| FUSED SILICA/ULE | 0.05 | 9 |
| SILICON | | 15 |
| BERYLLIUM | 0.5 | 30 |

Experience with the manufacture of large-diameter mirrors (80" to 120") has been limited to fused silica and CER-VIT. Some doubts have, however, been expressed by manufacturers that a homogenous isotropic beryllium mirror of that size can be produced by present fabrication techniques.

Under laboratory testing conditions the thermal environment may be controlled, but gravity deformation effects cannot be eliminated. A high elastic modulus to material density ratio $(E/\rho)$ is necessary here. Also of importance is the microyield level of the material to avoid excessive permanent straining caused by testing procedures. This level is generally defined as that stress producing a permanent strain of 1 micro in/in.

Launch survival, too, is a function of the stiffness to density ratios although it is anticipated that the launch supports will be provided to minimize the response of the mirror both in stress and deformation. Of some importance here is the damping capacity of the various materials, although very little published data on this exists.

For an active flexible system, the value of the elastic modulus is of considerable importance, as the force in the actuators is limited and a stiff mirror will require a large number of these devices.

In orbital operation it is desirable to minimize the thermal distortions of the mirror. A measure of this, known as the Thermal Distortion Index, indicates the capacity of the material to resist distortions

caused by thermal gradients. This index is the ratio of the coefficient of thermal expansion to the thermal diffusivity and is independent of the mirror geometry. A desirable material will have a low numerical value of this index.

$$\text{Thermal Distortion Index} = \theta = \frac{\alpha}{\frac{K}{\rho C p}} \tag{4.1}$$

where

$\alpha$ = coefficient of linear expansion

K = thermal conductivity

Cp = specific heat

$\rho$ = material density

Additional material considerations for orbital operations can be included under "creep" and ionizing radiation. The former includes a number of effects which can be related to activation-type effects and are thus influenced by time, temperature and internal stress considerations. Some data has been gathered by various investigations,[14] but conclusive information on sufficiently large samples is yet unavailable. In an active system the creep, as well as the thermal distortion errors, can be almost entirely corrected.

Ionizing radiation has a measurable effect on the mechanical and thermal properties of the mirror material and coatings. Elastic and thermal constants will change and, in an active system, alter the coefficients of the control matrix. The coatings are subject to degradation and contamination with accompanying reflectance charges.[15]

Mechanical and thermal data for a number of materials has been summarized in Table 4-2. The listing is made in the order of decreasing stiffness to density ratio. Microyield data is presented for the materials where this is available and finally the values for the Thermal Distortion Index ($\theta$) are presented and a desirability ranking of materials on the latter basis is also shown.

Stainless steel and titanium have both mediocre performance thermally and from the point of view of relative stiffness, and can then be eliminated from further consideration. Super Invar is the top choice

23

Table 4-2

Mechanical and Thermal Properties of Mirror Candidate Materials

| Material | $E$ $10^6$ #/IN$^2$ | $\rho$ #/IN$^3$ | $E/\rho$ $10^6$ IN | $\sigma_{my}$ #/IN$^2$ | $\alpha$ $10^{-6}$/°F | $C_p$ BTU/LB-°F | $K$ BTU/HR-FT-°F | $\theta$ | $\theta$ RANK |
|---|---|---|---|---|---|---|---|---|---|
| Beryllium | 42 | 0.066 | 635 | 8000 | 6.4 | 0.45 | 104 | 18 | 4 |
| CER-VIT C-101 | 13.4 | 0.090 | 149 | | 0.08 | 0.22 | 0.97 | 16 | 3 |
| Fused Silica (7940) | 10.6 | 0.079 | 134 | | 0.28 | 0.17 | 0.77 | 49 | 6 |
| ULE Fused Silica (7971) | 9.8 | 0.079 | 124 | | 0.03 | 0.18 | 0.5 | 5.7 | 2 |
| Aluminum | 10.2 | 0.097 | 105 | 25000 | 13.2 | 0.23 | 80 | 37 | 5 |
| Titanium | 16.5 | 0.16 | 103 | 80000 | 5.0 | 0.13 | 9.8 | 106 | 7 |
| Stainless Steel | 28 | 0.29 | 97 | | 9.2 | 0.12 | 9.4 | 340 | 8 |
| Super Invar | 21 | 0.29 | 72 | | 0.1 | 0.12 | 8.0 | 4.4 | 1 |

24

thermally, though the worst mechanically, and has never been reportedly used as an optical mirror. It is therefore, at this time, difficult to recommend it as a candidate. Aluminum falls short of middle in both the thermal and stiffness performance groups and it appears difficult to manufacture a figure to the tolerances needed.

Of the remaining group, beryllium has the best stiffness properties, but is only moderately good thermally. At the present time (1970) it is not possible to fabricate a 120" mirror of this material with the requisite figure. This technology may change by the time the mirror is prepared for launching and it will be retained as a final candidate. Fused silica is poor thermally, but a large field of experience exists with large-diameter mirrors and it will be used in the analysis for comparative purposes. CER-VIT and ULE are the remaining candidates and the most likely to be actually launched. The mirror preliminary design should then keep comparing the virtues and disadvantages of these four.

An important consideration to remember with low-expansion materials such as CER-VIT and ULE is that the thermal properties are, nevertheless, a function of the absolute temperature. Low expansions can be maintained only if the range of temperature variation is limited. Problems can be anticipated if it is desired that the mirror perform as adequately under laboratory room conditions as in the actual cryogenic space operating environment.

There are materials which have not been considered here at all, some of which have good thermal and/or mechanical properties. Scarcity, lack of optical experience with these, or fabrication difficulties have forced their omission at this time. The large group of material composites which have become available in recent years for air and spacecraft skins should be investigated at some time as potential sources for mirror materials. It is at present too early to speculate on their usefulness.

# CHAPTER 5

# DESIGN EVALUATION CRITERIA

## 5. 1  General Performance Criteria

A design objective of the Large Space Telescope is to achieve diffraction-limited optical performance with the three-meter system. In the structural evaluations of the candidate mirrors, the mechanical deformations of the mirror optical surface must be related to this desired criterion for optical performance.

A diffraction-limited optical system produces a nearly perfectly spherical wave-front to form the image of a point source in a limited region of object space. The inclusion of "nearly" is due to the fact that diffraction theory sets a predictable unsharpness of the image of a point source. If an optical device produces so nearly spherical a wave-front that the realized image is indistinguishable from that predicted by diffraction theory, it is said to be diffraction limited. These departures from true spherical wave form may not exceed the upper bound of one quarter the wave-length of light.

Analytical relation of diffraction theory to generalized mechanical deformations of a telescope mirror is at present tremendously complicated, if not impossible. A multi-staged series of approximating but substantiable discrete criteria is therefore proposed.

The wave-front may be distorted by two types of surface error: large-scale systematic surface deformations, and the locally-occurring random effects. In the first category, the gravity, thermal and large-scale manufacturing defects may be included. For a passive mirror system, these form the major sources of error and they will

be directly measured against the fundamental design goals. The use of active optics will readily reduce the large-scale systematic distortions, but the residual effects of local actuator loads or localized random thermal, material or manufacturing inhomogenieties will remain. In active optics it is these residuals that must then be evaluated against the desired optical criteria.

For the purposes of this discussion, it will be assumed that all of the distortions of the wave-front originate from elastic deformations of the primary mirror. It follows then that errors due to decentering, tilt and separation, which are really rigid-body movements, should be adjustable by some active means during the operation of the telescope. Alterations in the focal length, caused by elastic deformations can then also be corrected by simple realignments of the secondary mirror.

The simplest structural performance criterion compares the maximum mirror surface distortions to some previously defined fraction of the operating wavelength. This is of some value in cases where the separation of the primary and secondary must remain fixed or in situations where a speedy comparison between different mirror thicknesses, materials, and support parameters is desired. For precision evaluations it is, however, inadequate.

## 5.2 Optical Path Difference

A more realistic evaluation of the gross deformation effects is based on the resulting optical path difference. This criterion measures the difference between the wave reflected by the mechanically distorted mirror and a wave reflected by a perfect mirror represented by a best-fit paraboloid to the distorted mirror (Fig. 5-1). As the incident light ray has to reflect from the imperfect segment and return, a double pass is needed and thus the optical path difference is twice the total surface deviation. This total may be based on the sum of the absolute values of maximum positive and maximum negative

27

$$1/2 \text{ OPTICAL PATH DIFFERENCE} = |a_1| + |a_2|$$

$$b = \text{FOCUS CHANGE}$$
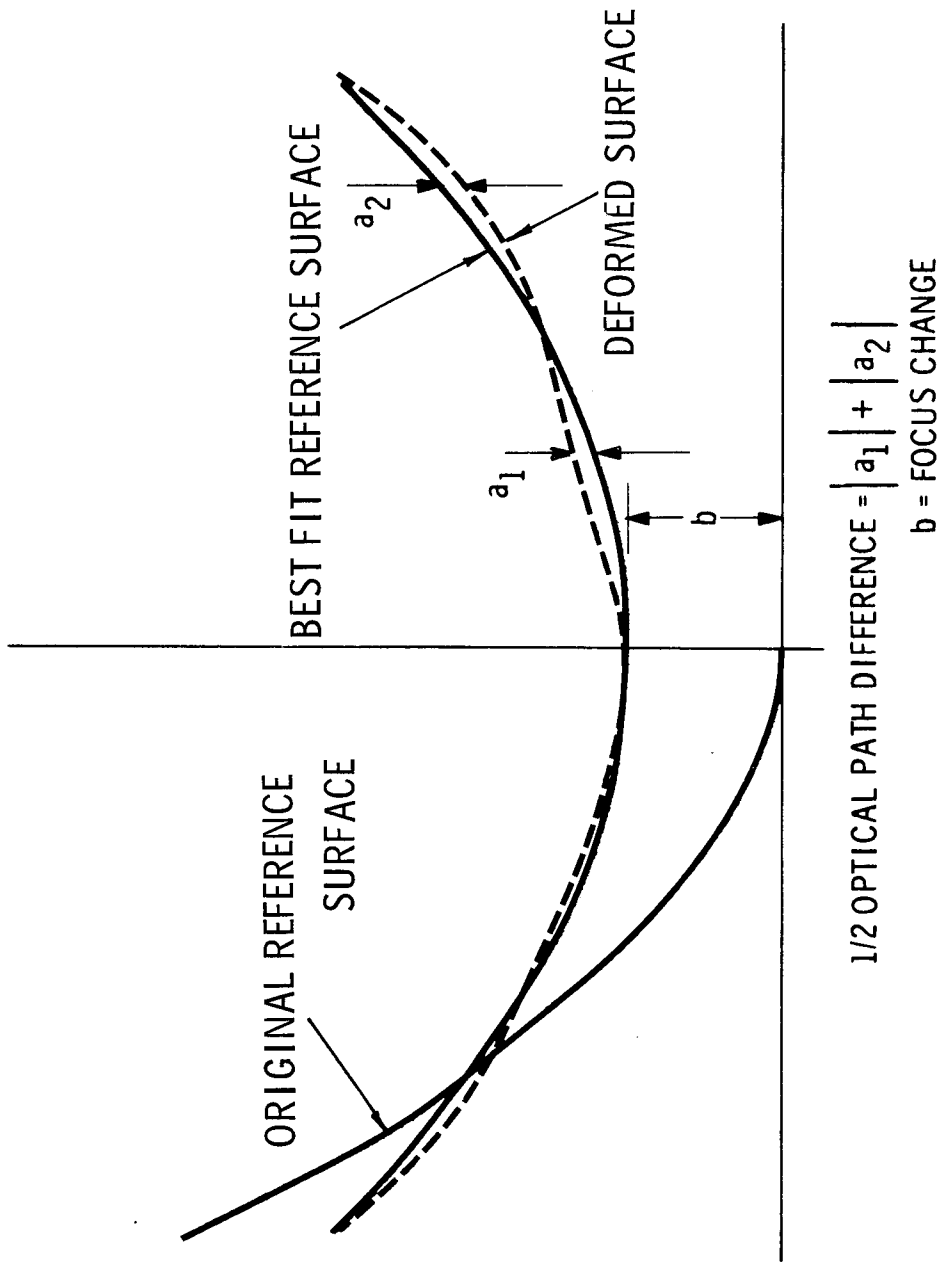
Fig. 5-1  Optical Path Difference

deviations from the best-fit surface, or it may also be based on a surface-wide rms definition. The design criterion then specifies that half the optical path difference must not exceed a given fraction of the operating wavelength.

The actual tolerance permitted for the surface distortions of the primary mirror will be some fraction of the total error budget permitted to the system. Classically the Rayleigh criterion of $\lambda/4$ has been the "diffraction limited" condition, but in this case that will not be adequate if the passive optics concept is used. The primary deformations, it will be recalled, are large-scale and systematic, and it is very unlikely that the distorted surface forms a new paraboloid. The residuals, or the optical path differences, i.e., the difference between the distorted surface and the best-fit reference surface, will still be systematic and will result in considerable reduction of the intensity at the diffraction focus.

The specific degradation level in the central Airy disc caused by the optical path difference must be defined by the designers of the entire optical system. It is clear that approaching too close to the Rayleigh limit of $\lambda/4$ will lead to a very poor design. Once a permissible optical path difference limit is imposed, a clear analytic constraint can be obtained for the mirror structural design.

5.3  Strehl Ratio

An active optical system should be able to remove the systematic surface distortions to well below the Rayleigh limit. If an adequate number of actuators are used, the residual deformations will then be distributed randomly in magnitude and location. The non-systematic errors in a passive optics system should also be constrained to at least below this limit. A possible means to evaluate the diffraction quality of the mirror figures in these instances is the Strehl intensity ratio.

The Strehl ratio is defined as "the ratio of the light intensity at the peak of the diffraction pattern of an aberrated image to that at the peak of an aberration-free image."[17] (Fig. 5-2). If previous corrections have reduced the peak to valley distortions below $\lambda/4$, the diameter of the central Airy disc and the intensity will change. Thus, the Strehl ratio permits a measure of the amount of energy going into the central disc of the diffraction pattern, but now resulting from random mirror surface errors.

Analytically, Marechal[18] has shown that starting from the fundamental definition of the Strehl ratio, and in view of the studies of Rayleigh (1879),

$$SR = \left| \frac{1}{A} \iint_A \exp(ikW)dA \right|^2 \tag{5.1}$$

where for a perfect lens SR = 1. If the value of kW is small, i.e., errors less than $\lambda/4$,
where

$$k = 2\pi/\lambda$$

and

$W = W(x, y)$, the wave-aberration referred to the sphere
centered at the focal point

the expression in (5.1) may be simplified to

$$SR = \left\{ 1 - \left(\frac{2\pi}{\lambda}\right)^2 \cdot E \right\}^2 \tag{5.2}$$

where E is the variance of the wave-aberration

$$E = \overline{W^2} - \left(\overline{W}\right)^2 \tag{5.3}$$
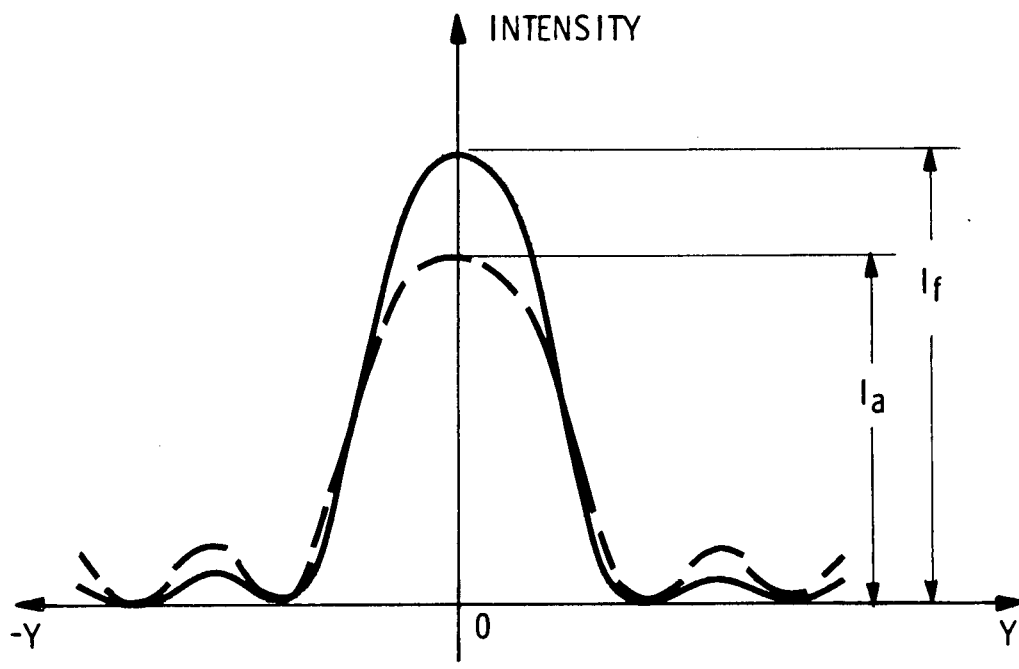
Fig. 5-2 Strehl Ratio

31

where from an integral definition

$$\overline{W^2} = \frac{1}{A} \iint_A W^2 dA \qquad (5.4a)$$

and

$$\overline{W} = \frac{1}{A} \iint_A W dA \qquad (5.4b)$$

or for large discrete sums of equal weight

$$\overline{W^2} = \frac{1}{N} \sum_N W_N^2 \qquad (5.5a)$$

$$\overline{W} = \frac{1}{N} \sum_N W_N \qquad (5.5b)$$

that is, the variance (E) of the surface distortions may be obtained in (5.3) and a measure of the image quality can be obtained from (5.1).

For random statistical errors in the mirror surface, a limiting value for E has been imposed by Marechal and Francon[18] to

$$E \leq \lambda^2/180 \qquad (5.6)$$

this value, substituted in (5.2) then gives a lower bound to the Strehl ratio

$$SR \geq 0.79 \qquad (5.7)$$

which is approximately equivalent to a systematic surface error of $\lambda/8$ (Table 5.1). Recalling the definition of the variance

$$E = \sigma^2 \qquad (5.8)$$

the standard deviation of the wave-front error must be

$$\sigma \leq \left(\frac{\lambda^2}{180}\right)^{1/2} \tag{5.9}$$

or

$$\sigma \leq \frac{\lambda}{13.4}$$

since this is the tolerance in the wave-front standard deviation, the actual value of the mirror surface deviations from the "best-fit" surface must not exceed half of this or $\lambda/26.8$ to achieve diffraction-limited performance. In general, this error represents the total error budget of the optical systems. Until the remainder of the optical system is adequately defined, however, this will be used as the design criterion for the random errors in the primary mirror. Ultimately, the primary mirror surface deviations may be limited to the range of $\lambda/50$ rms.

# CHAPTER 6

# MIRROR ANALYSIS AND DESIGN

## 6. 1   Outline of General Problem

The ultimate objective of this structural study is to contribute towards defining the specifications for the manufacture, testing and operation of the 3-meter diffraction-limited Large Space Telescope. In previous chapters the methodology of structural analysis, the types of environmental conditions expected, the available mirror materials, and optical performance criteria were discussed and summarized. This chapter will attempt to bring these altogether to formulate a strategy for the design.

It is safe to say at this time that given a mirror configuration with the material properties defined and the static, dynamic or thermal conditions specified, the computation of the structural re-sponse, for any type of mirror, can be performed by finite elements with reasonable ease and sufficient accuracy. The objective of en-gineering is, however, not analysis, but design. It is necessary not only to test, by computer simulation, a candidate structure for adequacy, but also to find the best solution amongst a large number of alternatives.

There is at this time no unique mirror configuration that is immediately and obviously much superior to any of the other can-didates. The number of major families of mirrors, their genera and species are so immense that a design approach by a strictly exhaustive search is truly an enormous open-ended task. The large minority of these solution candidates will, in time, be rejected for optical reasons, for material or fabrication limitations or because of telescope system constraints. The remaining possibilities must be evaluated but without

resort to a brute force approach.

The approach at this time has, therefore, deliberately avoided choosing one type of mirror configuration and then analyzing it in great depth. The philosophy has been, rather, to consider all family types, to produce the necessary finite element programs, check their validity, and only then to present some beginning examples of the design process. This appears as the only rational means for optimizing the limited resources.

6.2   Candidate Structural Form Considerations

Three fundamental approaches have been suggested for the primary mirror for the three-meter telescope:

1. passive
2. active segmented
3. active flexible

Each of these may be subdivided into further categories based on the structural configuration and analysis methodology:

1. thin isotropic plate or shell
2. ribbed ("lightweight")
3. thick monolithic plate

In the first case the span to thickness ratio is sufficiently great so as to have pure bending or shallow shell behaviour. The ribbed mirror may be analyzed as an assembly of folded plates. The thick plate is such where the span length to thickness ratio is small, and shear deflections are equal in magnitude to the bending displacements.

Table 6-1 illustrates the possibilities available at this level and their relative desirability. A very thin passive mirror would deflect excessively in the earth's gravity field under laboratory testing. The use of ribbed or thick plates for the active flexible approach will demand actuator strength out of concert with the desired resolution accuracies. As bending-action span lengths in the active segmented approach are rather small, and thickness to span ratios may be quite substantial without excessive weight increases, the use of thin isotropic or

35

ribbed mirror structures is somewhat less likely than the conventional, easier-to-fabricate thick mirror configuration.

TABLE 6-1    TYPE VS. STRUCTURE

|  | TYPE | | |
|  | PASSIVE | ACTIVE SEGMENTED | ACTIVE FLEXIBLE |
|---|---|---|---|
| THIN PLATE | POOR | LIMITED | GOOD |
| RIBBED | LIMITED | LIMITED | POOR |
| THICK | GOOD | LIMITED | POOR |

For the final design the basic optical system has not yet been fully established. In this view it is necessary to consider both a solid mirror and one with a central opening (e.g., cassagrain).

The objectives of the Large Space Telescope program have included the testing of an 80" laboratory model as well as the 120" (3-meter) flight model. Both mirror sizes are therefore considered as basic design goals. Presumably the type and structure will be identical, but the design for one cannot necessarily be scaled for the other unless complete dimensional homology is maintained. Scaling in non-homologous cases is successful only if a single structural action, such as pure bending, predominates in both the model and prototype.

Without going into the mirror details, there exist now 6 basic structure-type candidates, with 2 optical approaches and at 2 sizes. These 24 cases are subject to the 4 separate loading environments and should be evaluated for at least 4 available materials. A number of further design variables must be determined for each case. The optimum mirror thickness must be obtained,and whether or not this thickness will be constant or varies across the mirror face. Optimum number and location of supports must be determined. If a ribbed mirror structure is used, then the grid type, rib spacing, rib thickness and the thicknesses of the face and back plate must be established. With the active flexible mirror, the location and the number of segments, and the relative proportions of each must be found. (Table 6-2)

If an exhaustive systematic study is truly required, the amount of separate finite element studies can run into the tens of thousands. This does not include studies of element layout. Clearly all this is far out of the question, so major efforts must be made to reduce the structural study to a tangible format.

TABLE 6-2     MIRROR DESIGN VARIABLES

| TYPES OF MIRRORS | PARAMETERS |
|---|---|
| 1) PASSIVE ISOTROPIC | a) MATERIALS<br>b) THICKNESS<br>c) SUPPORT LOCATIONS AND TYPE |
| 2) PASSIVE RIBBED | a) MATERIALS<br>b) GRID TYPE<br>c) GRID SPACING<br>d) PLATE THICKNESS<br>e) SUPPORT LOCATIONS AND TYPE |
| 3) ACTIVE FLEXIBLE | a) MATERIALS<br>b) THICKNESS<br>c) ACTUATORS, SUPPORTS, LOCATION, NUMBER, AND TYPE |
| 4) ACTIVE SEGMENTED | a) MATERIALS<br>b) THICKNESS<br>c) SEGMENT PROPORTIONS<br>d) SUPPORT LOCATIONS |

It is obvious, however, that while certain mirror-structure combinations are more suitable than others, similar criteria can as well be postulated in the structure-material-environment conditions. The relationships here, however, are much more complex in that the elasto-mechanics and thermal problems are highly coupled. For example, if the transverse stiffness for the mirror were the only design objective, then a deep and probably "lightweight" structure would be the optimum solution. The ribs in such a structure would, however, be relatively thin, permitting little conduction of heat between the top and bottom faces, with resulting large thermal distortions. This design then, is clearly non-optimal thermally. Alternately, if in the active flexible case the design were to aim towards optimum thermo-elastic behaviour, a relatively solid, thick and hence stiff mirror would result which then would require high-strength actuators.

A simplified material-loading-mirror type tradeoff matrix is shown in Table 6-3. It is evident here how certain material charac- teristics are desirable for one type of mirror configuration under a particular loading, but are of little consequence in another, and may be undesirable in a third. Many of the necessary matrix elements are, however, highly system-dependent, so that until further data is gathered, it makes little sense to assign merit values to the elements. For the final design decision, a multi-dimensional matrix including material, loading, mirror type and structure type must be generated.

TABLE 6-3  MIRROR MATERIAL-LOADING-TYPE TRADEOFF

| LOADING ENVIRONMENT AND MIRROR TYPE | MIRROR MATERIAL CHARACTERISTIC | | | | |
|---|---|---|---|---|---|
| | HIGH E | HIGH E/$\rho$ | LOW $\theta$ | HIGH $\sigma$ | HIGH STABILITY |
| MANUFACTURE | + | + | + | + | 0 |
| TEST | | | | | |
|    PASSIVE | + | + | + | 0 | + |
|    ACTIVE SEGMENTED | + | + | + | 0 | + |
|    ACTIVE FLEXIBLE | - | + | + | + (s) | 0 |
| LAUNCH | 0 | + (s) | 0 | + (s) | 0 |
| OPERATION | | | | | |
|    PASSIVE | 0 | 0 | + (s) | 0 | + |
|    ACTIVE SEGMENTED | 0 | 0 | + | 0 | + |
|    ACTIVE FLEXIBLE | - | 0 | 0 (s) | + (s) | 0 |

| | |
|---|---|
| + | FAVOURABLE EFFECT |
| - | ADVERSE EFFECT |
| 0 | RELATIVELY INSENSITIVE |
| (s) | STRONGLY SYSTEM DEPENDENT |

40

In order to converge to such a decision matrix, a strategy for the design evaluations must be formulated.

When analysis studies are made, the computational tools used for this purpose should be the most exact that are available. For preliminary design, that is the choosing of one amongst many differing but feasible alternates, it is generally unnecessary as well as uneconomical to start with the most rigorous method. Where, however, are the limits of either approach? Several levels of solution hierarchy can be recognized in the design process.

1.  Topology:          the basic connectedness of the elastic system. Parameters such as a continuous active or a segmented active mirror; 3, 6 or "n" supports for the mirror; a ribbed or a solid mirror; how many ribs; how many actuators, etc.

2.  Geometry:          length quantities related to the topological variables. Parameters such as support or actuator locations; proportions of the various active mirror segments; rib spacings, etc.

3.  Elastic variables: cross-sectional properties on a local scale. Parameters such as mirror-thickness, and the function with which it varies; top-plate and rib thicknesses in "lightweight" mirrors, etc.

For a large majority of structures, the hierarchies are relatively independent. If a design is optimal at the topology level, the optimum solution of the joint topology-geometry problem will still preserve the original topology. This postulate generally extends to the elastic variables level as well.

It is a generally observed fact also that the topology level solution, and to some degree also the geometry level, is not too sensitive to the accuracy of the behaviour analysis model used. Often,

41

a fully adequate preliminary design may be obtained from very approximate models. The elastic variables level, which requires a very precise analyzer, will refine the design to some degree but basically retain the same topology and geometry. The advantages of using an approximate method of analysis are, however, very great in that considerably quicker convergence to the best solution is achieved at a much lower expenditure of manpower and computer rental.

Sometimes an approximate approach cannot be found for a given structure. In these cases there is little choice but to use the exact method, but it is very important then to make those studies that can be used to obtain bounds for the possible solution. It should be noted here that in the present context the finite element method is considered exact, although forces and displacements are defined only at the nodal points.

The mirror loadings, for example, will be primarily parallel to the optical axis, and hence flexural behaviour will predominante in the design of the mirror configuration. If the thickness/diameter ratio is less than one in ten with edge supports, then a pure bending model may be adequate. Most of the cases here, because of various support types, will require an exact finite element model, but as only one form of behaviour predominates, these results can be scaled, both homologously and otherwise. If a deeper mirror seems inevitable, then shear deflections begin to predominate and the new model must include this. If the distance between the mirror supports is reduced, even though the depth to diameter ratio for the mirror as a whole is high, localized shear deflection behaviour should be expected near the supports. Again, exact methods are needed here as well, but the use of a generalized enough model will allow the designer to obtain approximate data on design of "sandwich" and "lightweight" configurations.

The strategy that is proposed for the mirror design includes the following phases:

1. Establish that exact analysis methods exist for all necessary types of structural action that are expected. While all of these capabilities will not be needed immediately, they are "long lead time" items, which can be used later for exact analysis studies. These will be formulated to include gravity, thermal and dynamic capabilities.

2. Begin to develop the mirror design at the topology and geometry levels with existing approximate methods. New approximations would be developed wherever need and cost would justify. Exact analysis tests would be performed to establish benchmarks.

3. When sufficient preliminary design information exists at the topology and geometry levels, then very exact methods would be used to converge to a design. If justified by weight savings or required by tight specifications, formal optimization procedures may be further adopted.

This report marks the completion of the first phase. Examples will be presented in the following sections that include all of the necessary techniques to analyze the various mirror types. Work has progressed to an intermediate stage with the second phase, although much remains to be done.

## 6.3    Mirror Behavior - Bending Deformations

To test out some of the finite element routines, and to begin gathering design data for the monolithic mirror type, a series of support configuration studies were performed. The objective was to find, for the solid mirror, as well as the one with the central opening, the optimum number and location of the supports under a gravity load parallel to the optical axis.

For these initial studies, the pure bending element was used, as the mirror structure could then be analyzed in a generalized non-dimensional form, and the results could be scaled non-homologously throughout the limits of the behaviour assumptions. If the loading type and boundary conditions are retained, then the geometry, density and elastic properties can be varied freely to obtain much data from a limited amount of computer studies. Fundamentally, data was desired at the 80" and 120" diameters with the 4 material choices listed earlier in Chapter 4.

It is noted that as the thickness/diameter ratio of the mirror increases, the importance of the shear deflections does as well. It is intended to modify the results presented here, at a later date, with shear deflection corrections wherever necessary.

The element layout for the solid mirror is shown on Fig. 6-1. An equilateral triangle was used wherever possible to obtain best element accuracy and to make optimal use of the 3 point (statically determined) supports. The grid size was chosen as a compromise between computer running times and accuracy of results. Tripling the number of elements was found to improve the deformation accuracy only by 3% at the cost of 5 times the normal running times. While
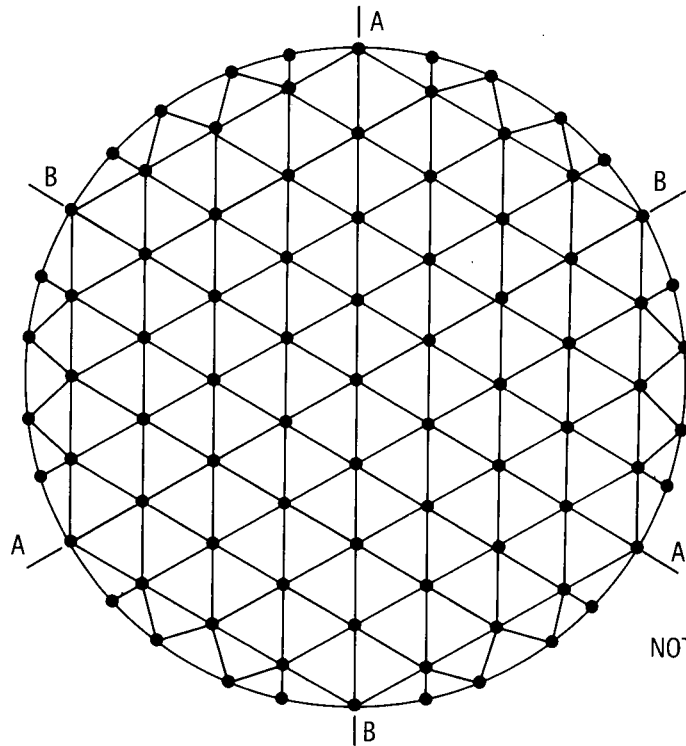
NOTE: POINTS 'A' USED FOR
3-SUPPORT STUDIES
POINTS 'A' AND 'B' USED
FOR 6-SUPPORT STUDIES

Fig. 6-1 Finite element subdivision used for solid plate and
thin shell mirror studies - both $80''\phi$ and $120''\phi$ -
transverse loading.

45

these methods do not consume excessive computer time, a considerable cost is still involved, and considering the fundamental accuracies demanded for this type of preliminary study, it was felt that the least number of elements giving a reasonably good answer should be used.

All studies were performed with a general "model" structure 80" in diameter, elastic modulus of 10,000 psi, an equivalent surface loading of 1 psi, and a mirror thickness of 1". These parameters were chosen to give best numerical significance. The scaling law for bending behaviour under surface forces is:

$$\left(\frac{\Delta p}{\Delta m}\right) = \left(\frac{E_m}{E_p}\right) \cdot \left(\frac{D_p}{D_m}\right)^4 \cdot \left(\frac{W_p}{W_m}\right) \cdot \left(\frac{t_m}{t_p}\right)^3 \qquad (6.1)$$

where

|   |   |
|---|---|
| $\Delta$ | = deflections |
| p | = prototype |
| m | = "model" |
| E | = elastic modulus |
| D | = diameter of mirror |
| W | = surface load intensities |
| t | = mirror thickness |

With the constants used for the model case, this law gives the relationship between the deflections in the prototype and model:

$$\Delta p = \Delta m \cdot 2.44 \cdot 10^{-4} \cdot \left(\frac{D_p^4 W_p}{E_p t_p^3}\right) \qquad (6.2)$$

46

Thus, deformations for all mirrors with similar loadings and boundary conditions can be obtained from this. The location where $\Delta m$ is obtained must obviously be analogous to the location where $\Delta p$ is desired.

This expression is generally valid for surface forces. The self-weight forces per unit area can be obtained from D'Alembert's law which allows the interchange of statically equivalent loads located in close proximity.

$$W_p = t_p \cdot \rho_p \qquad (6.3)$$

where

$\rho_p$ = density of prototype

Therefore, the expression (6.2) becomes

$$\Delta p = \Delta m \cdot 2.44 \cdot 10^{-4} \cdot \left( \frac{D_p^4 \rho_p}{E_p t_p^2} \right) \qquad (6.4)$$

Once the data is scaled to the prototype desired, the deformation results are interpreted to evaluate the mirror behaviour optically. At this early stage of design, a best-fit plane was passed through the deformed surface, and the RMS deviation from that surface of the element deflection points was determined. As the RMS deflection is a linear deflection quantity, it scales in the same manner as the other deflection quantities and it may be obtained once for the "model" case, and then employed afterward in expressions (6.2) or (6.4).

For the final design process, a curved mirror surface will be used, and a best-fit sphere or parabola is necessary. As the computer programs for doing this were not yet ready at the time these studies were completed, the best-fit plane, which can be calculated by hand quite readily was used for the interpretation.

The design objective of "diffraction limited" shall, at this stage, be considered (see Section 5.3):

$$(\Delta p)_{RMS} \leq \lambda/27 \qquad (6.5)$$

Assuming that the working wavelength is 5000 Å, this results in a $(\Delta p)_{RMS}$ of $0.73 \times 10^{-6}$ in. Using this as a criterion stemming from the Strehl ratio makes more sense at this time than comparing on the basis of the optical path difference, which in this (flat) case would be merely the sum of the absolute value of the largest positive and negative deflections. The RMS, on the other hand, gives the "area-weighted" deflections which are much more significant in determining optical quality. It should be noted that to do this properly, a uniform finite element size is desirable.

The following sections outline some of the data gathered for the solid mirror as well as the mirror with the center opening (Cassagrain type).

### 6.3.1 Solid Plate Mirrors

Based on the finite element layout in Fig. 6-1, a number of studies were performed. The only variables at this stage were the locations and number of the supports. The 3-support configuration is located at $120^\circ$ from each other, the 6-support at $60^\circ$. These then are moved inwards along radial lines.

The raw results for some of these studies can be seen in Figs. 6-2 to 6-7. The contours have been plotted automatically from the finite element output. The contours represent quantities of $\Delta m$ from Equation (6.2). Actual values of the contour intervals could be then determined for any dimensionally consistent set of D, $\rho$, E and t variables. Their straight-line segments obviously reflect the element size and, in spite of the cubic displacement functions in the element, a necessity to simplify the plotting routines with the use of non-uniform grid sizes. The contour interval was chosen to have no more than 6 separate contour levels per plot.

This data is interpreted, along with similar information from a closed-form solution to the continuous support in Fig. 6-8, and replaces the coefficient ($\Delta m \bullet 2.44 \bullet 10^{-4}$) in Equation (6.4). Fig. 6-9 shows a plot of this data, summarizing other data as well which is not included in Figs. 6-2 to 6-8, in terms of the $(\Delta m)_{RMS}$ for each of the cases. The best support from this interpretation is evidently the six-point support. It is recalled here that the deflected points are being corrected to a best-fit plane. With a spherical or parabolic best-fit surface, presumably another of these supports would perform best.
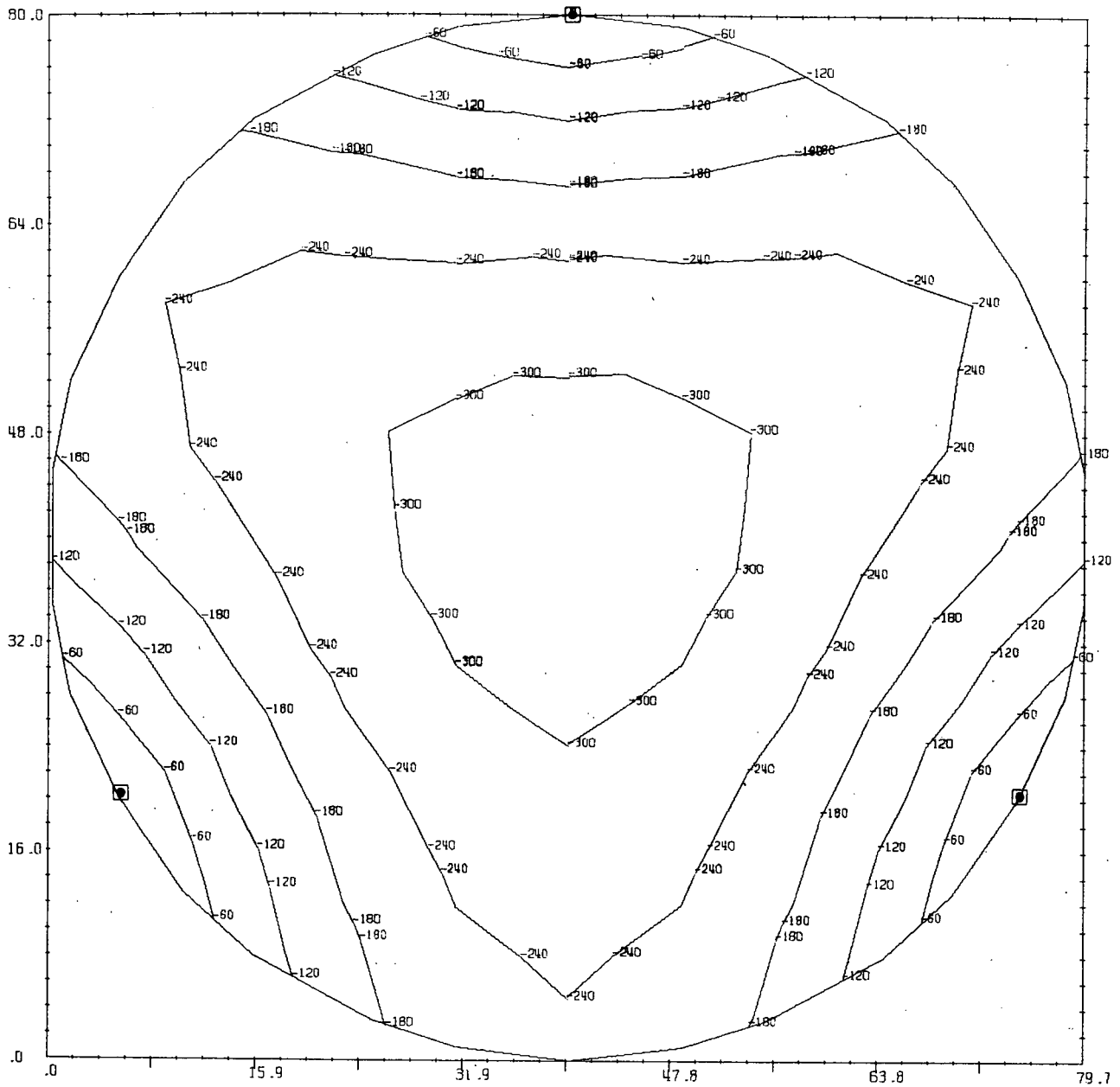
Fig. 6-2 Solid Mirror 3 Supports at Edge

◙ – SUPPORT LOCATIONS

Note: The contour intervals are presented here in a
generalized form for $(\Delta_m)$. Any specific values
desired can be obtained from Eq (6-4) by sub-
stitution of the appropriate parameters.

59
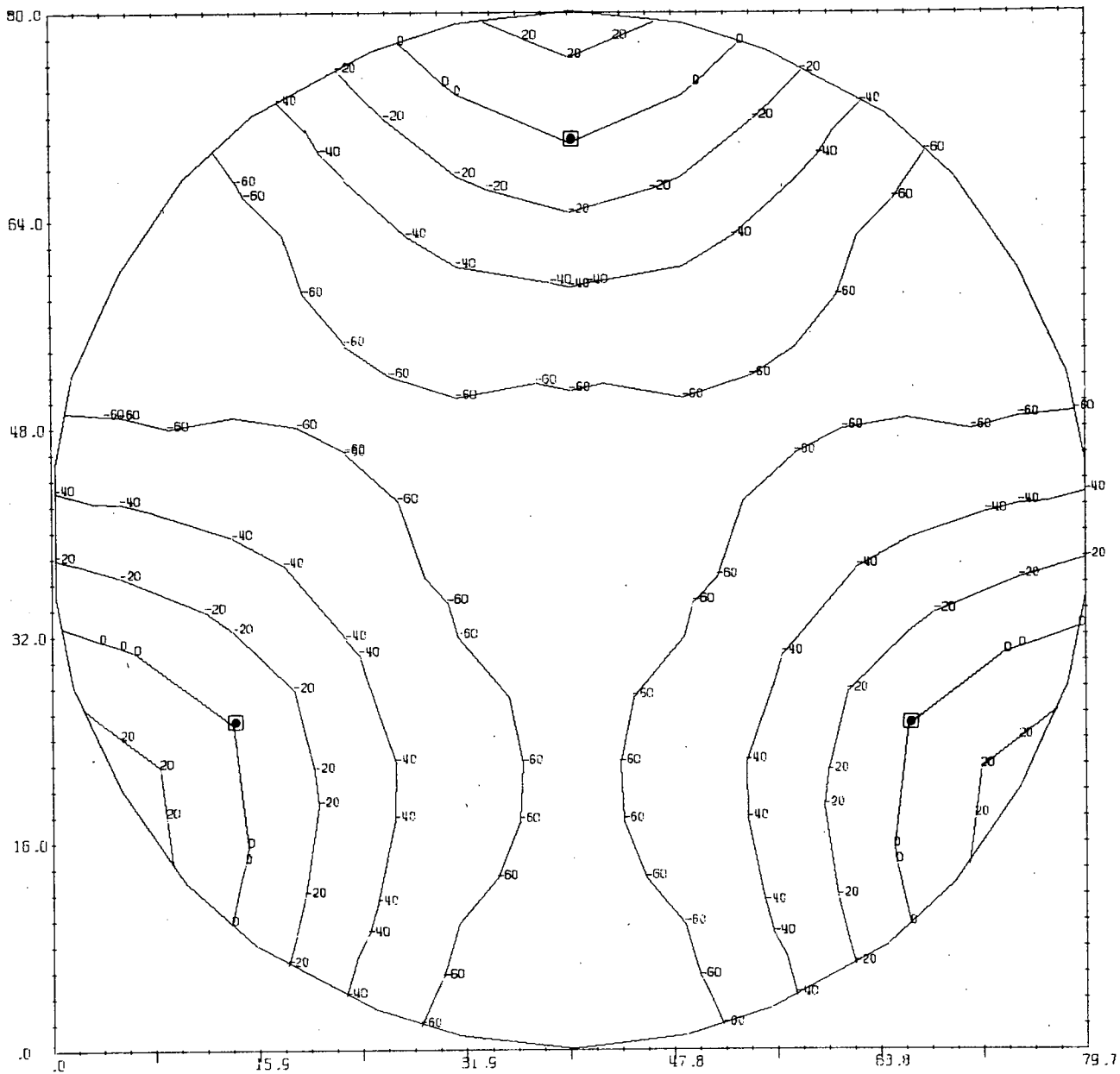
Fig. 6-3 Solid Mirror 3 Supports 25% in from Edge
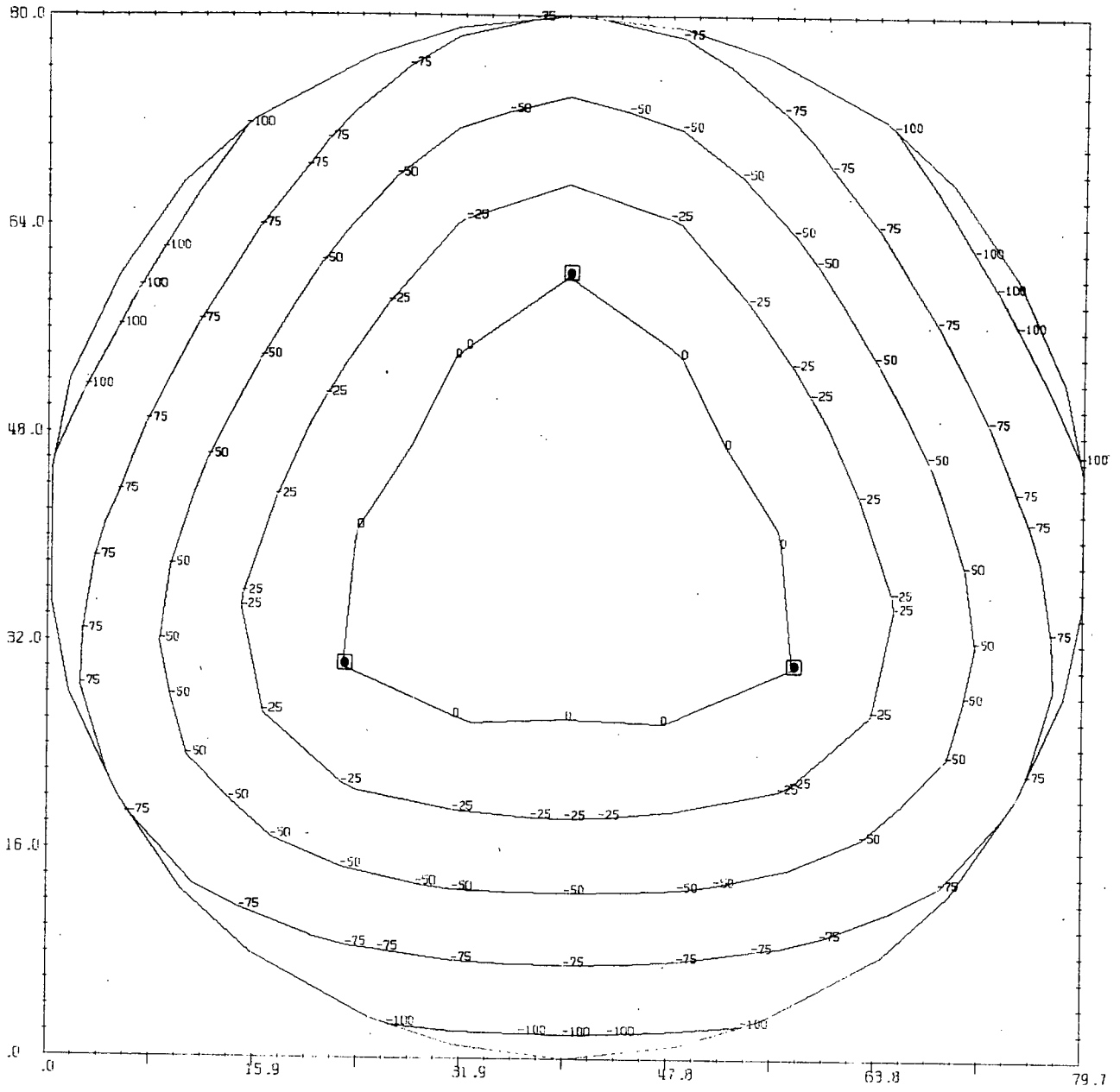
◉ - SUPPORT LOCATIONS

Fig. 6-4  Solid Mirror 3 Supports 50% in from Edge

⊡ - SUPPORT LOCATIONS

52
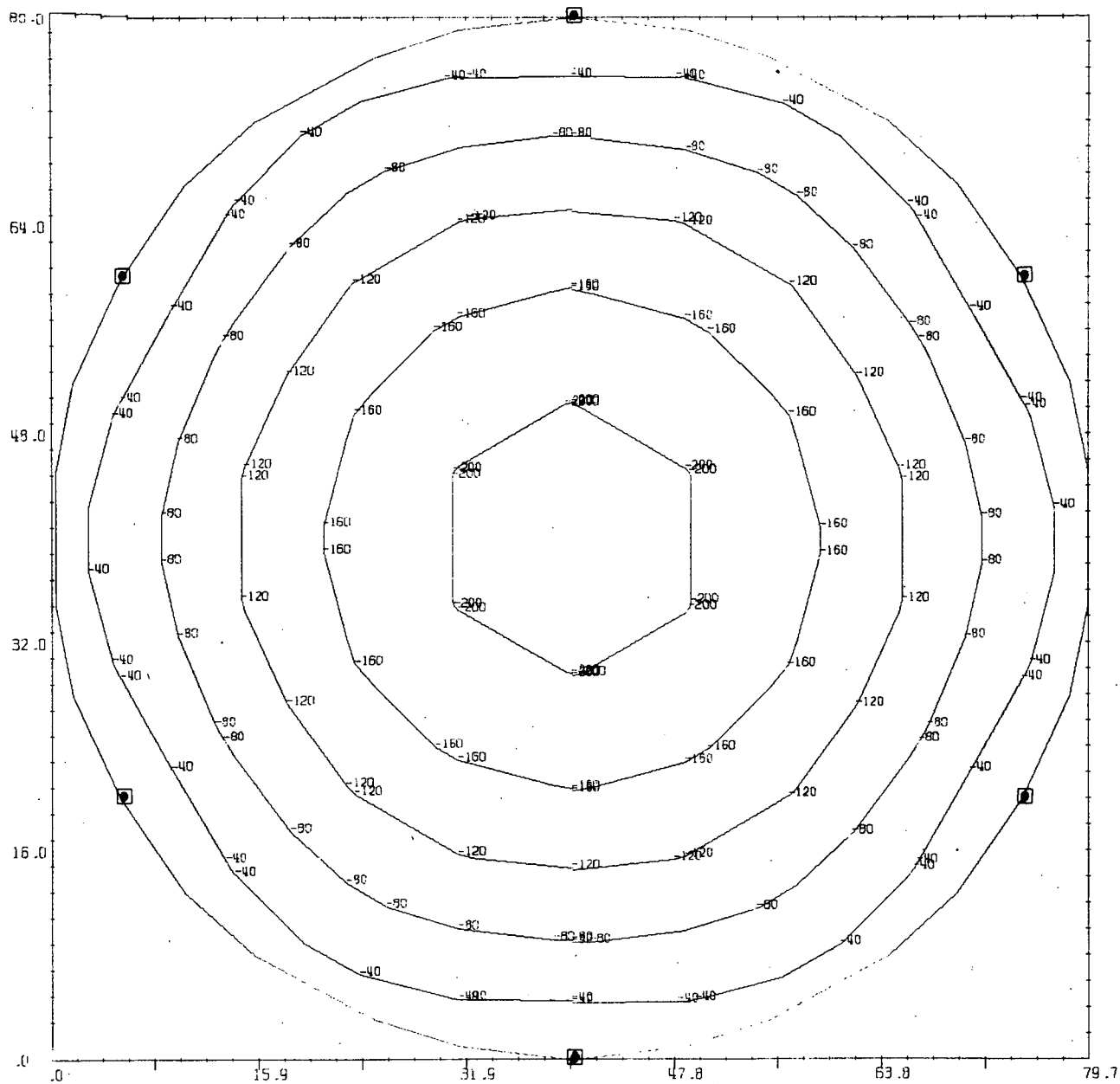
Fig. 6-5 Solid Mirror 6 Supports at Edge

◉ - SUPPORT LOCATIONS

53
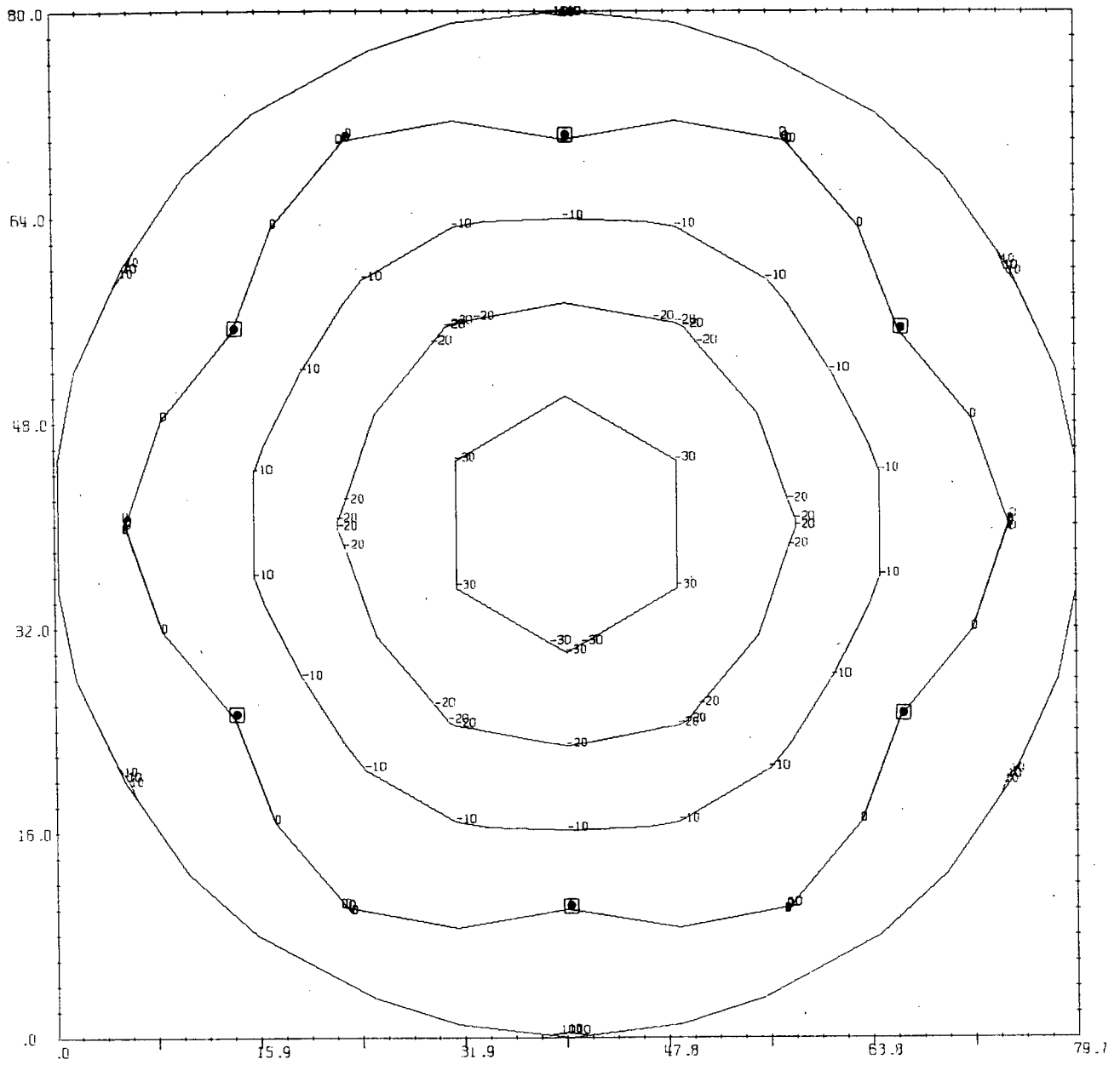
Fig. 6-6  Solid Mirror 6 Supports 25% in from Edge

⊡ - SUPPORT LOCATIONS

54

C.2
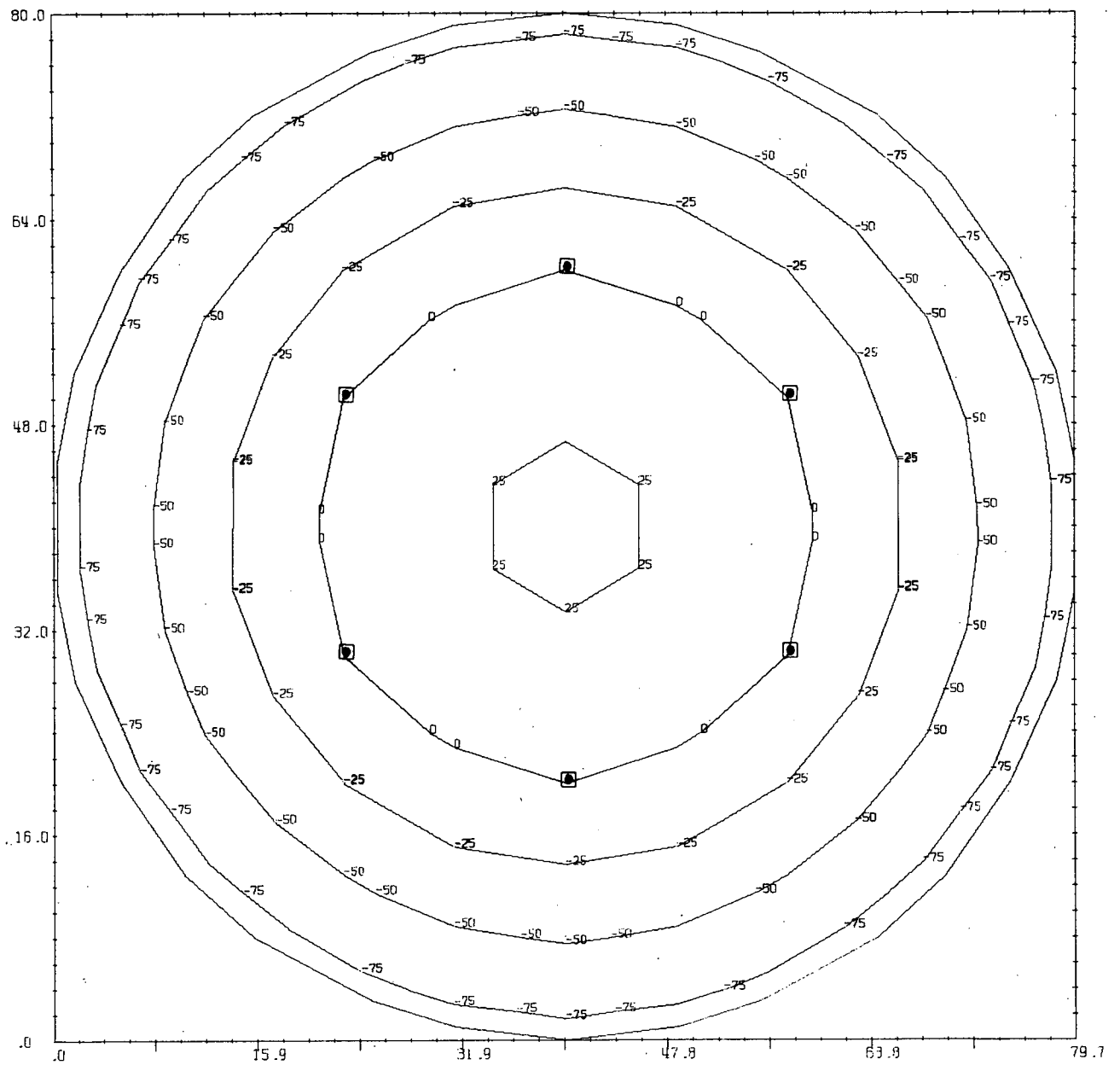
Fig. 6-7 Solid Mirror 6 Supports 50% in from Edge

◙ - SUPPORT LOCATIONS
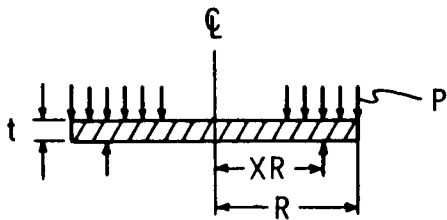
$$W = K_S \times \left(\frac{D^4 P}{E t^3}\right)$$

W = ROOT MEAN SQUARE DISPLACEMENT
D = MIRROR DIAMETER
P = UNIFORM LOAD
E = ELASTIC MODULUS
t = THICKNESS

| X | $K_S$ |
|---|---|
| 1.0 | $219 \times 10^{-4}$ |
| 0.75 | $75 \times 10^{-4}$ |
| 0.50 | $31 \times 10^{-4}$ |
| 1.0 | $140 \times 10^{-4}$ |
| 0.75 | $26.4 \times 10^{-4}$ |
| 0.50 | $90.3 \times 10^{-4}$ |
| 1.0 | $161 \times 10^{-4}$ |
| 0.75 | $58.7 \times 10^{-4}$ |
| 0.50 | $86 \times 10^{-4}$ |

Fig. 6-8 Solid circular mirror: transverse uniform loading, varying supports.
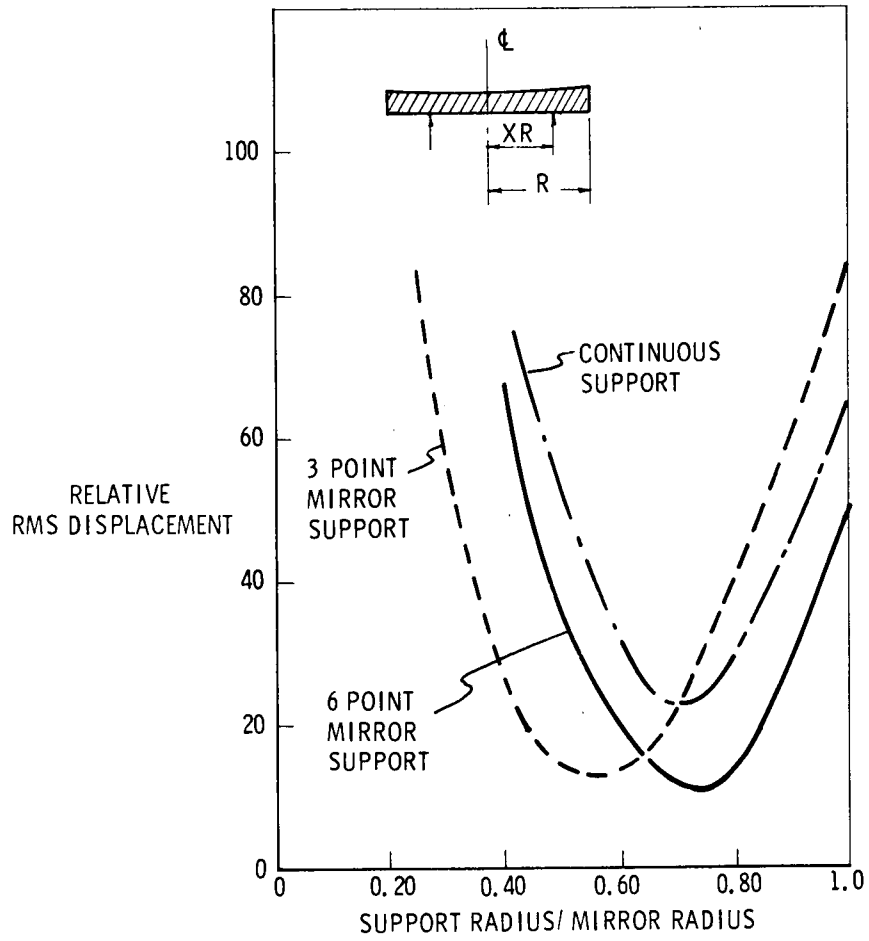
Fig. 6-9 Solid mirror - face up.

Using as a basis the 3-point support at 0.5 of the radius, the implication of these results on the mirror design are shown in Fig. 6-10. An 80" beryllium mirror is diffraction-limited under gravity effects when it has a 16" thickness. The other materials are grouped quite closely together but do not approach this level within the limits of the bending theory. At this range shear deflections are beginning to contribute an additional 10-20% to the total and for accurate later studies, an exact model should be used.

For the 120" mirror (Fig. 6-11) beryllium gives diffraction-limited performance at about 36" depth, whereas the others again fail to reach this limit.

Some measure of the weight versus deflection tradeoffs can be seen from Fig. 6-12 and Fig. 6-13 for beryllium. It is evident that the curves are very strongly asymptotic in the region of the diffraction limit, and small changes in the design variables have a large influence on the weight of the mirror. This also implies the need for a very accurate analyzer if a good design is desired.
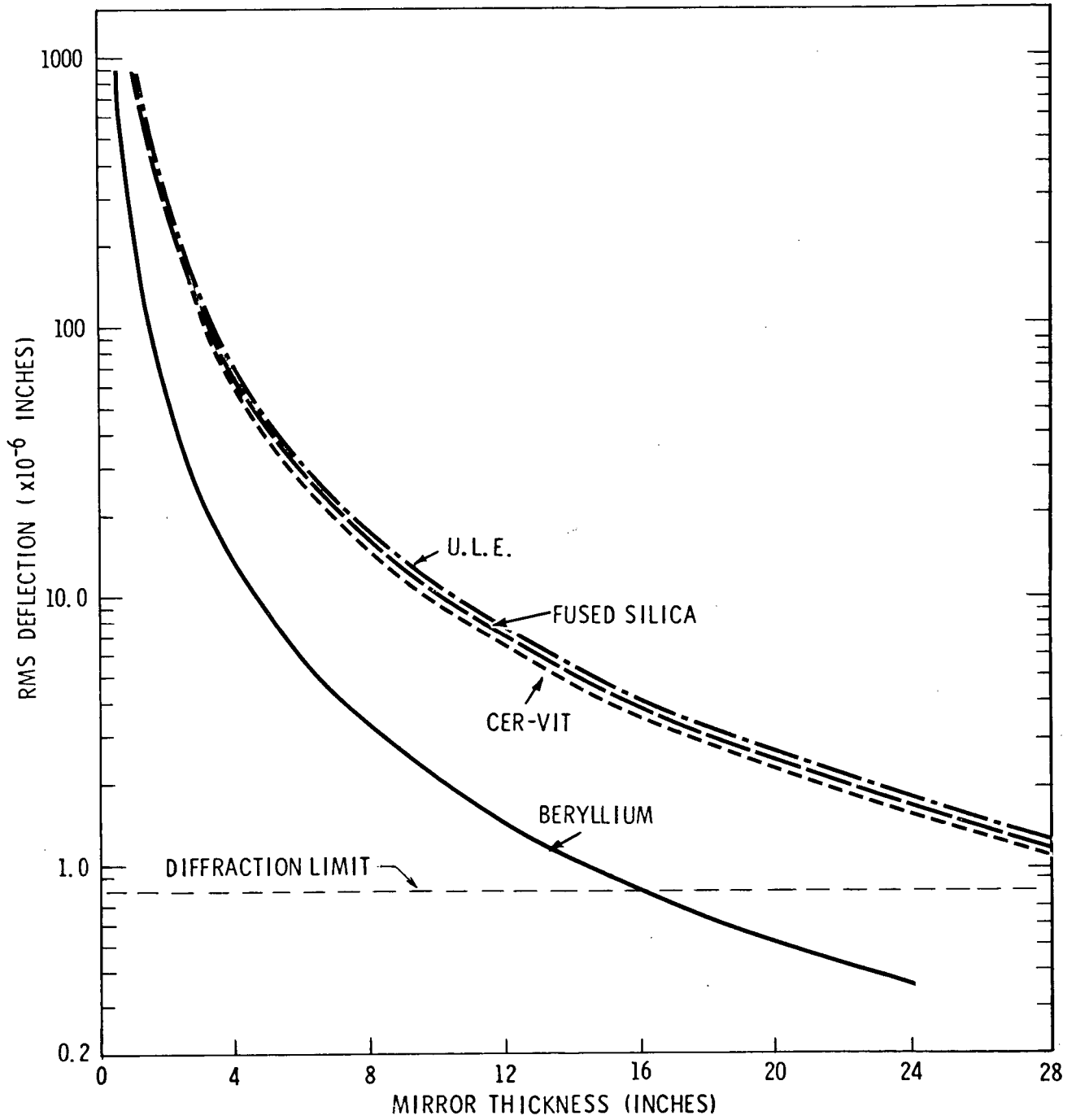
FIG. 6-10   80" SOLID MIRROR - FACE UP - 3 POINT SUPPORT AT 50% RADIUS
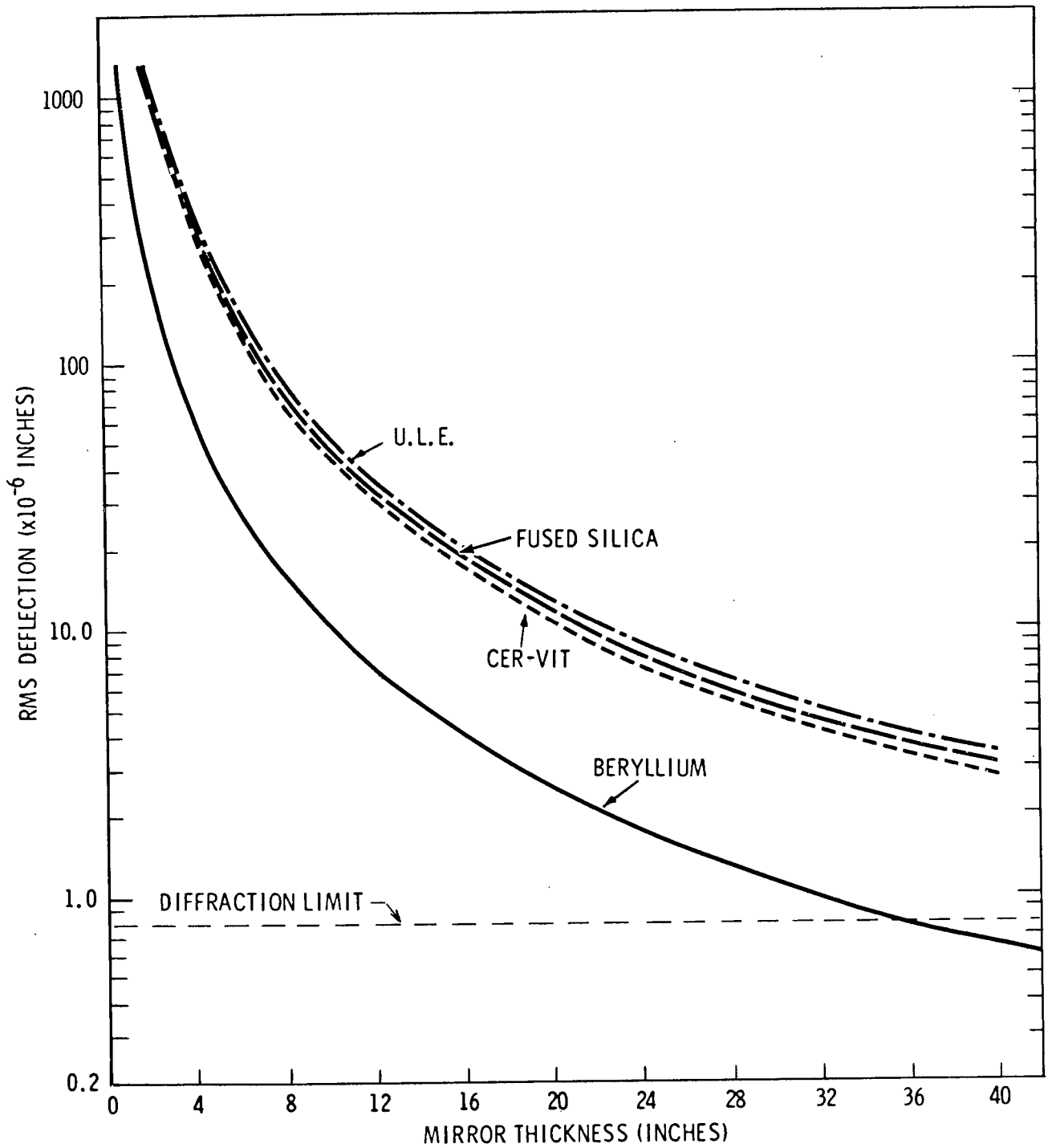
FIG. 6-11   120" SOLID MIRROR - FACE UP - 3 POINT   SUPPORT AT 50% RADIUS
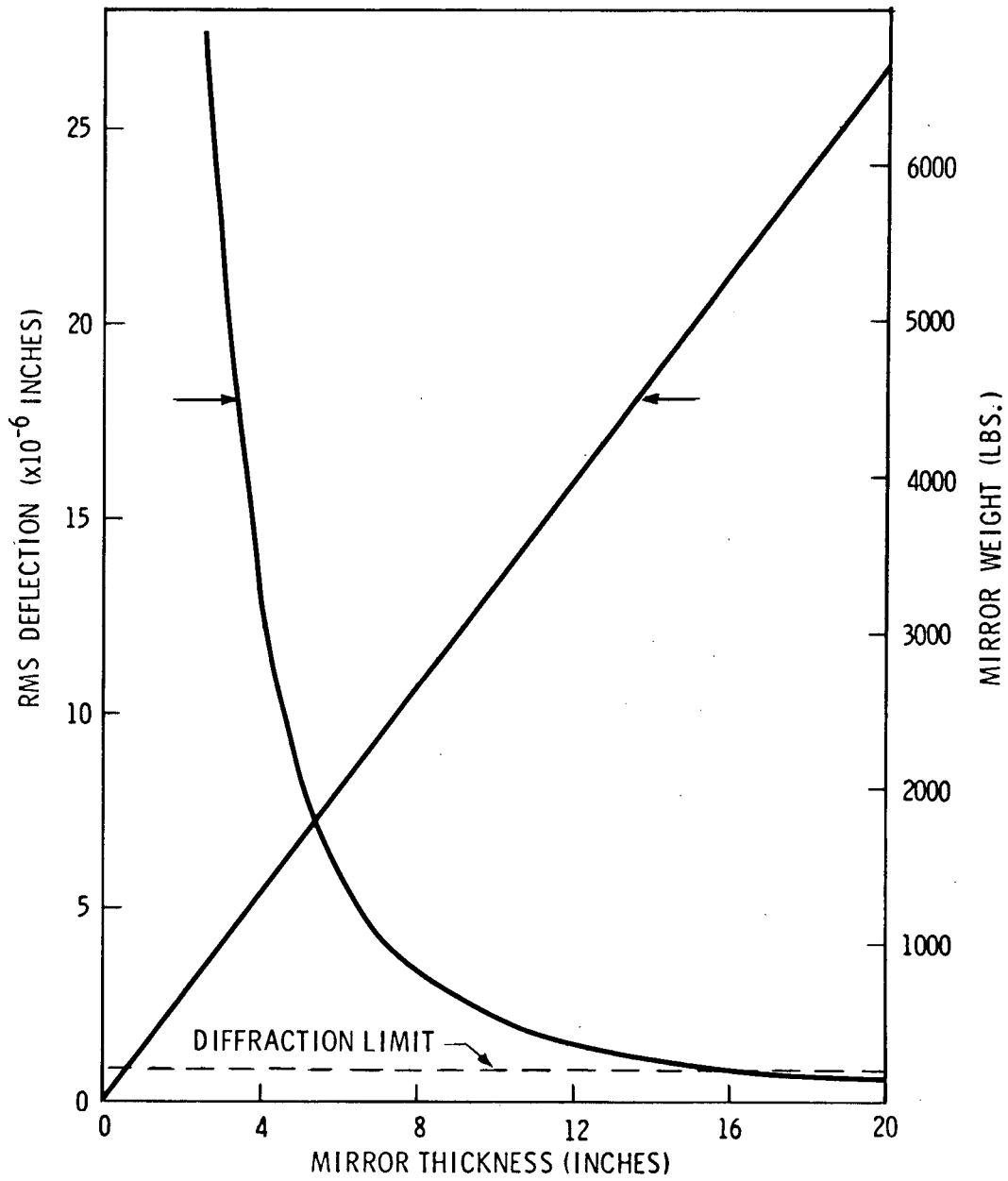
FIG. 6-12   80"φ SOLID BERYLLIUM MIRROR
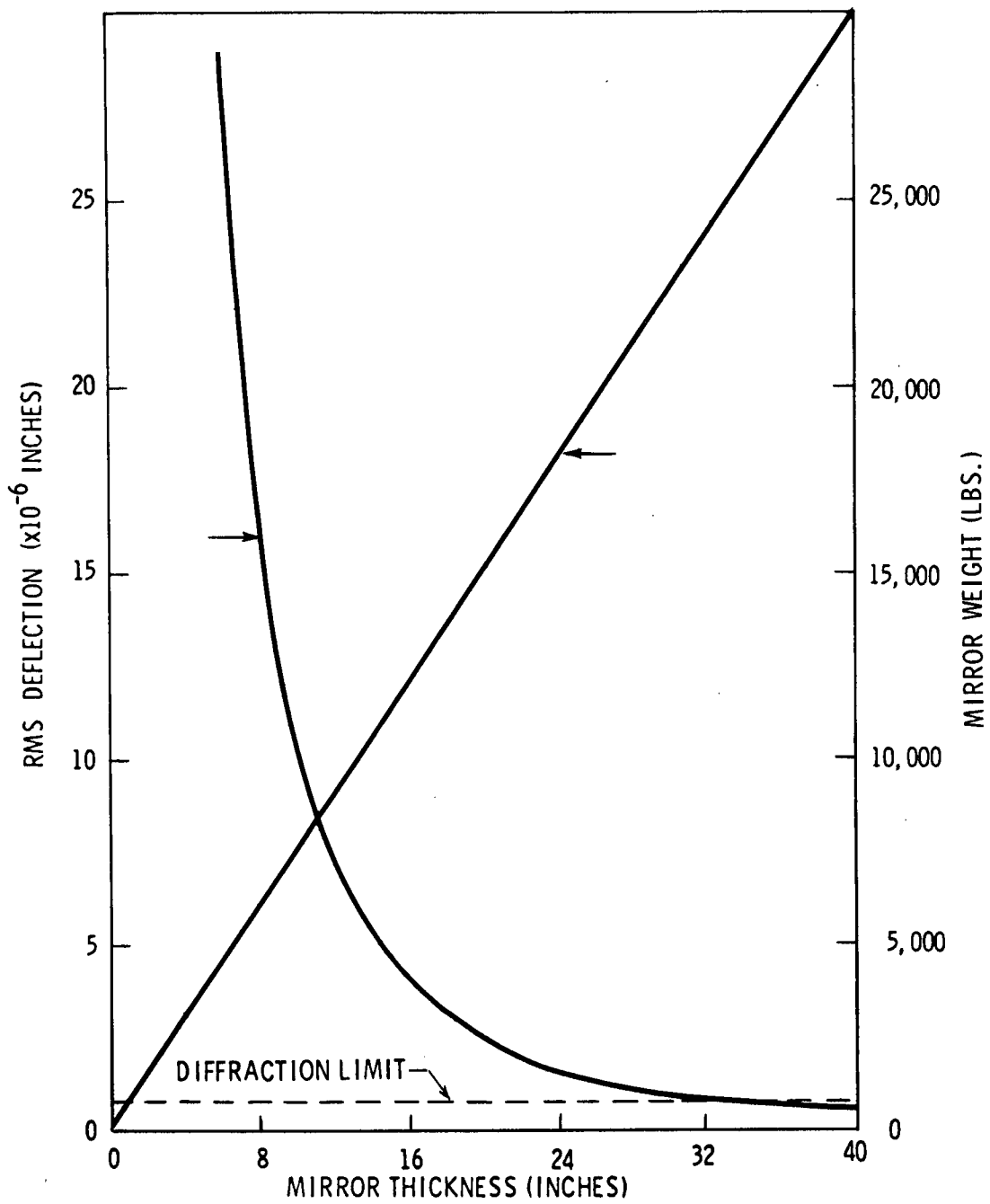
FIG. 6-13 120"ϕ SOLID BERYLLIUM MIRROR

### 6.3.2    Mirrors with Central Opening

The basic element layout is altered slightly for the mirror as shown in Fig. 6-14. The actual size of the central opening will not be known until further optical data is obtained, but a statistical average of some Cassagrain mirror openings was taken and found to be 5/16 of the main diameter. The opening was left hexagonal and not rounded, as the differences would be small and to avoid many small and odd-shaped elements in the interior. The same loading type is used and the supports are altered in a similar manner.

Fig. 6-15 to 6-20 are plots of the deformations (i. e. , $\Delta m$) taken directly from the STRUDL output. Comparison with Fig. 6-2 to 6-7 shows the effects of the opening on the deformations.

The results are again summarized in Fig. 6-21 for a number of cases. Again the surface deviations are connected to the best-fit plane and RMS deflections are computed. Again under these criteria the 6-point support appears the best at 0.7 radius. Further inter-pretation of these results is continuing.
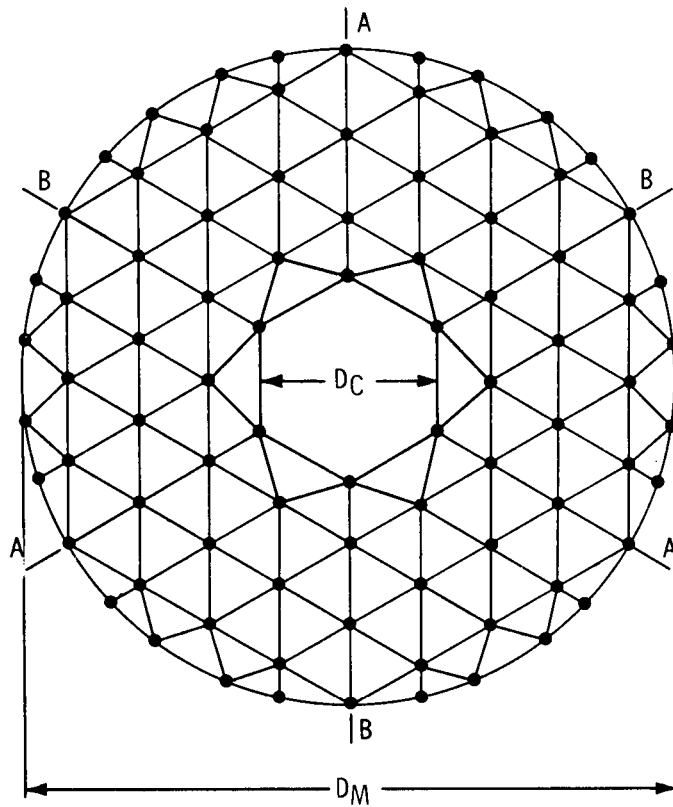
$$\frac{D_C}{D_M} = \frac{5}{16}$$

NOTE:
POINTS 'A' USED FOR
3-SUPPORT STUDIES
POINTS 'A' AND 'B' USED
FOR 6-SUPPORT STUDIES

Fig. 6-14  Finite element subdivision used for cassegrain plate
and thin shell mirror studies - both 80"Φ and 120"Φ
—transverse loading.
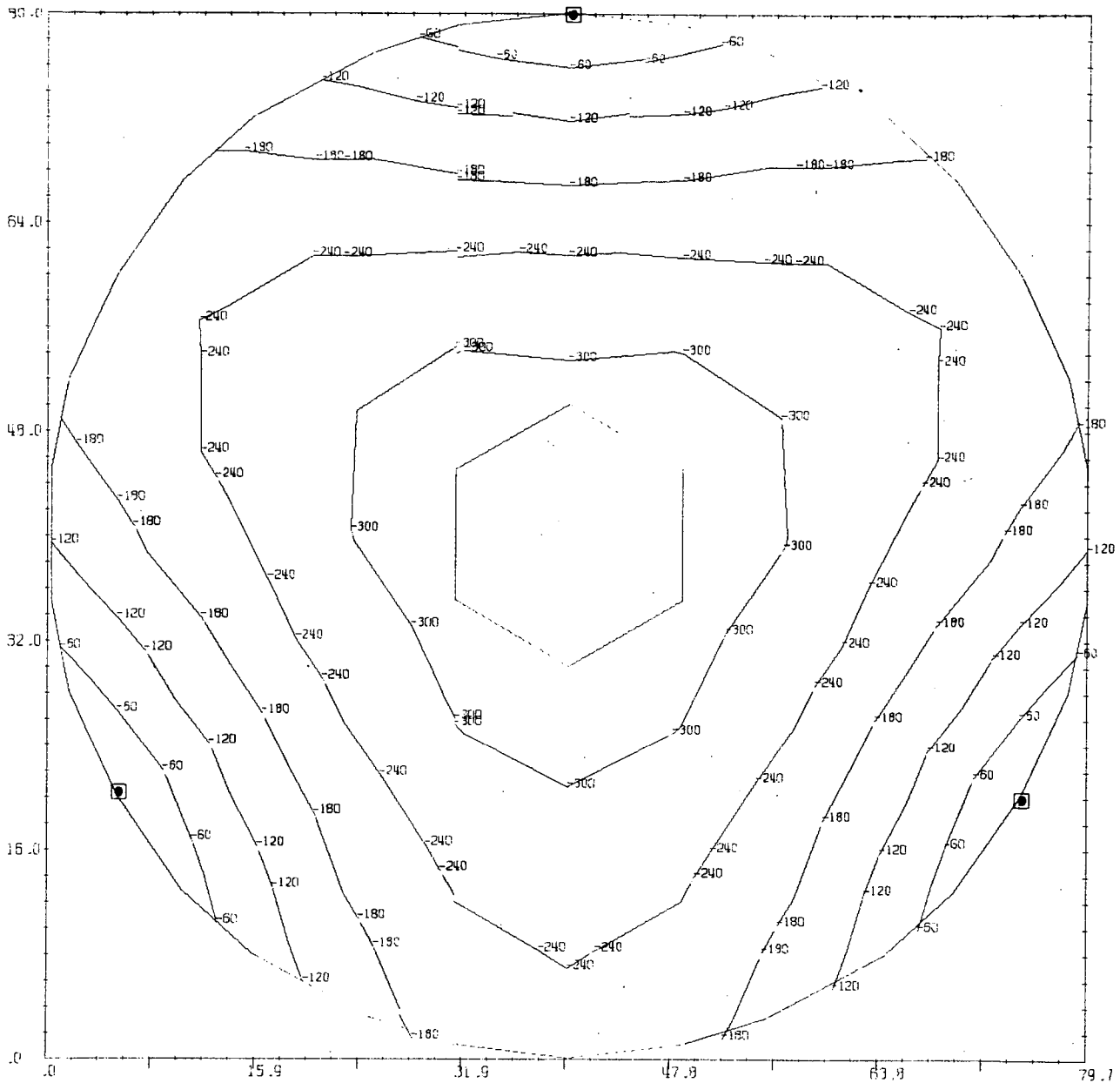
Fig. 6-15  Open Mirror 3 Supports at Edge

◙ - SUPPORT LOCATIONS

NOTE:        The contour intervals are presented here in a
             generalized form for $(\Delta_M)$.  Any specific values
             desired can be obtained from Eq. (6-4) by
             substitution of the appropriate parameters.

65
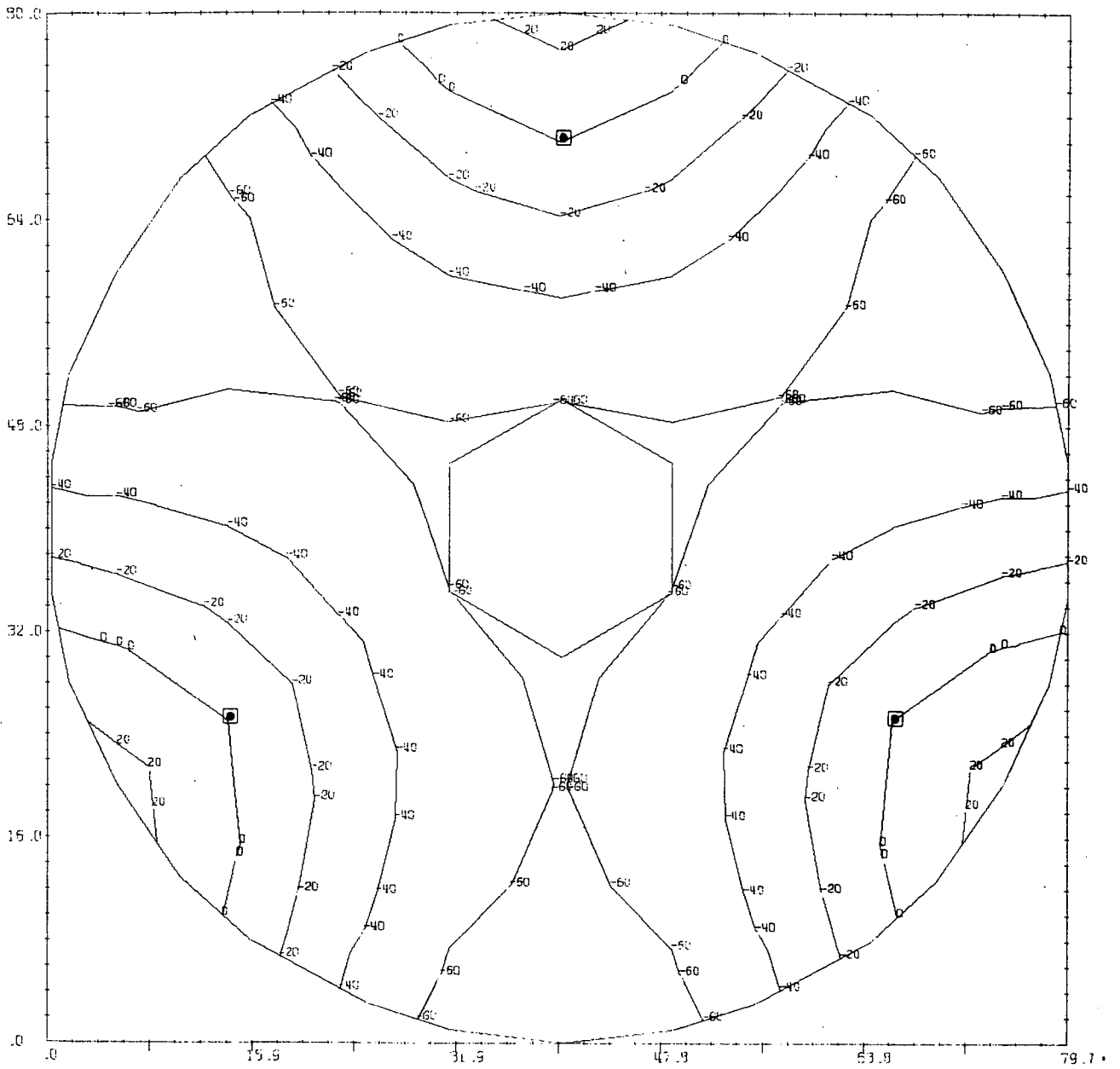
Fig. 6-16  Open Mirror 3 Supports 25% in from Edge

◉ – SUPPORT LOCATIONS

66
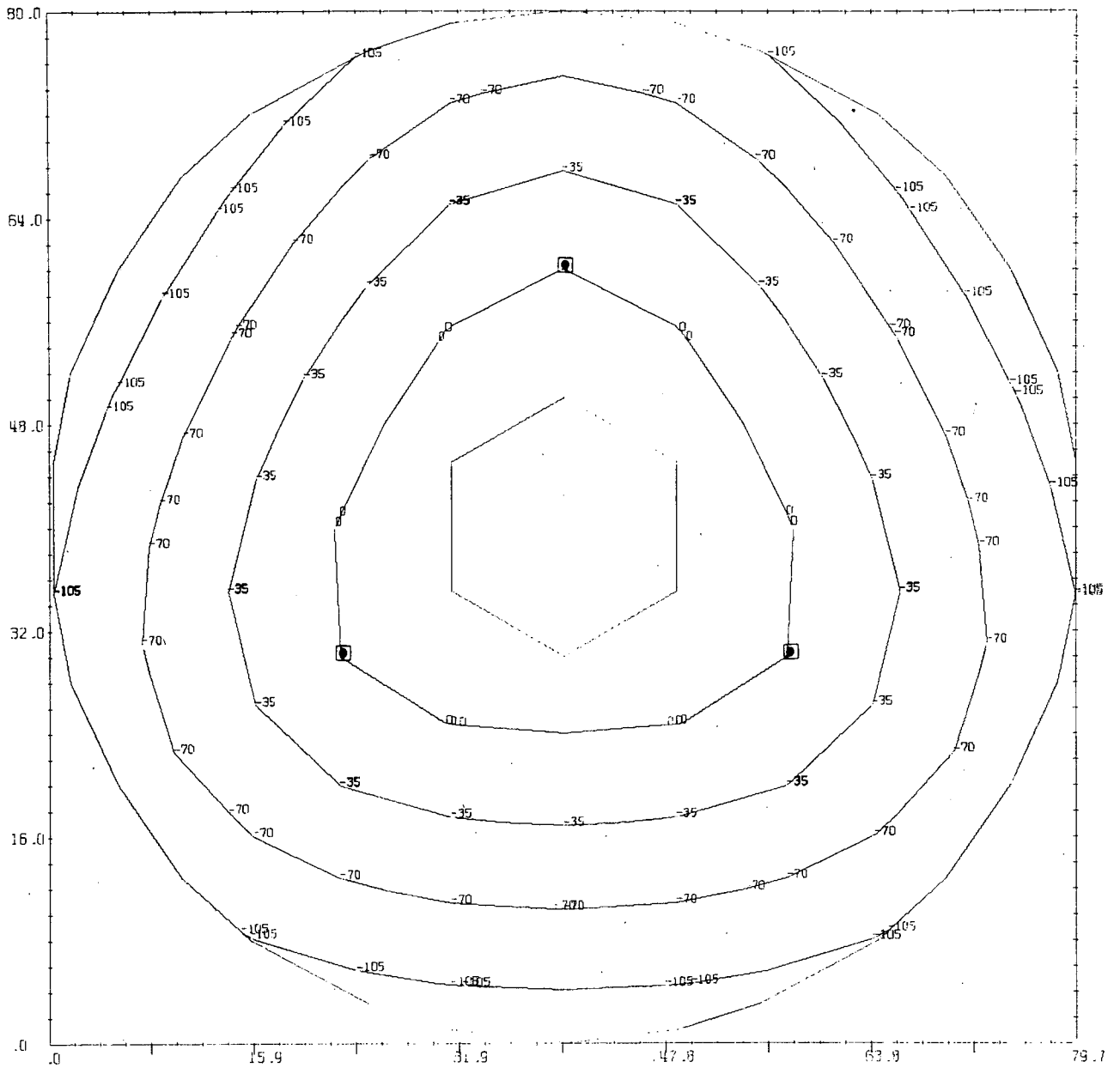
Fig. 6-17 Open Mirror 3 Supports 50% in from Edge

⊡ - SUPPORT LOCATIONS

67
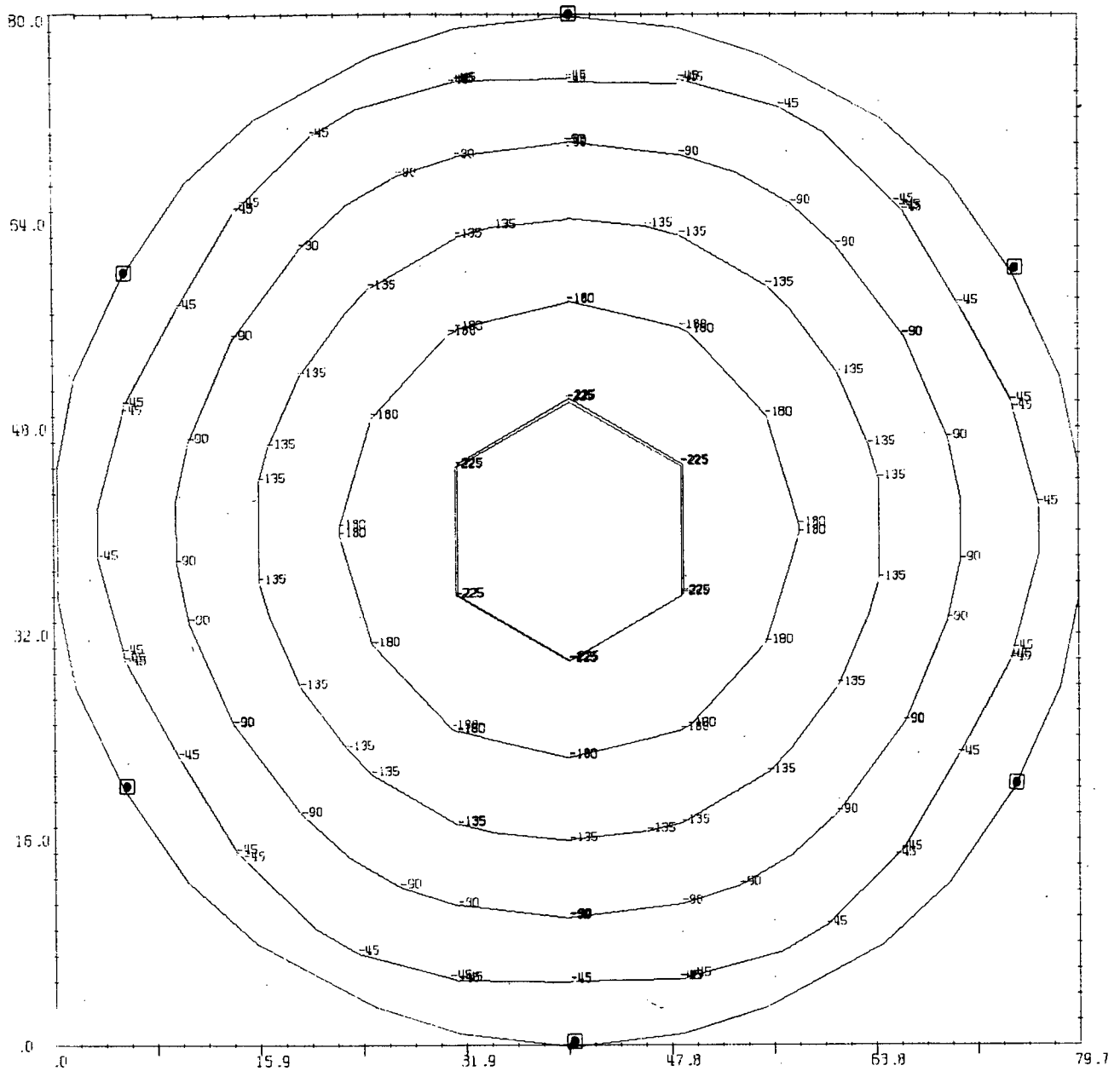
Fig. 6-18 Open Mirror 6 Supports at Edge

◉ – SUPPORT LOCATIONS

68
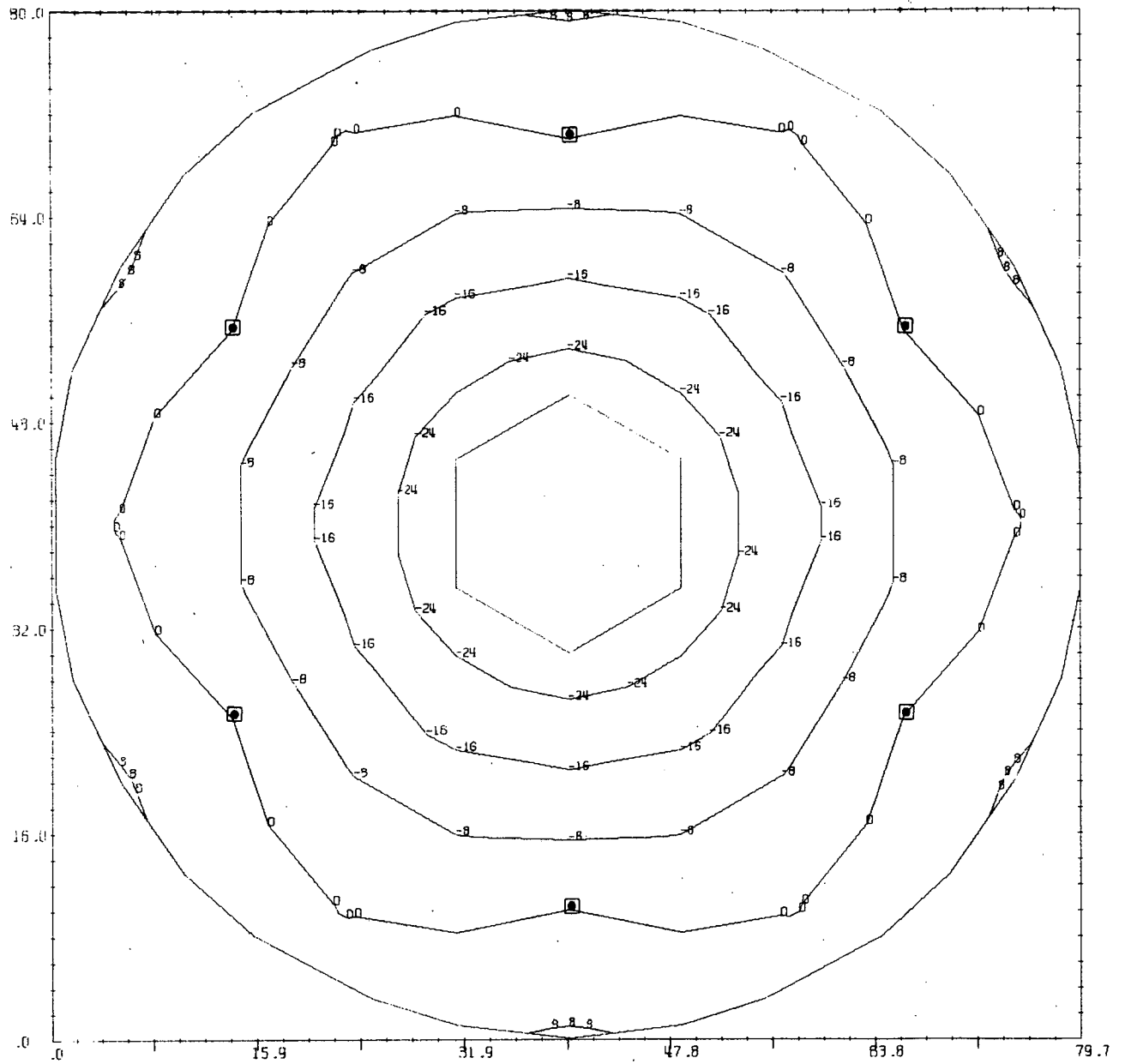
Fig. 6-19 Open Mirror 6 Supports 25% in from Edge

◉ – SUPPORT LOCATIONS

69
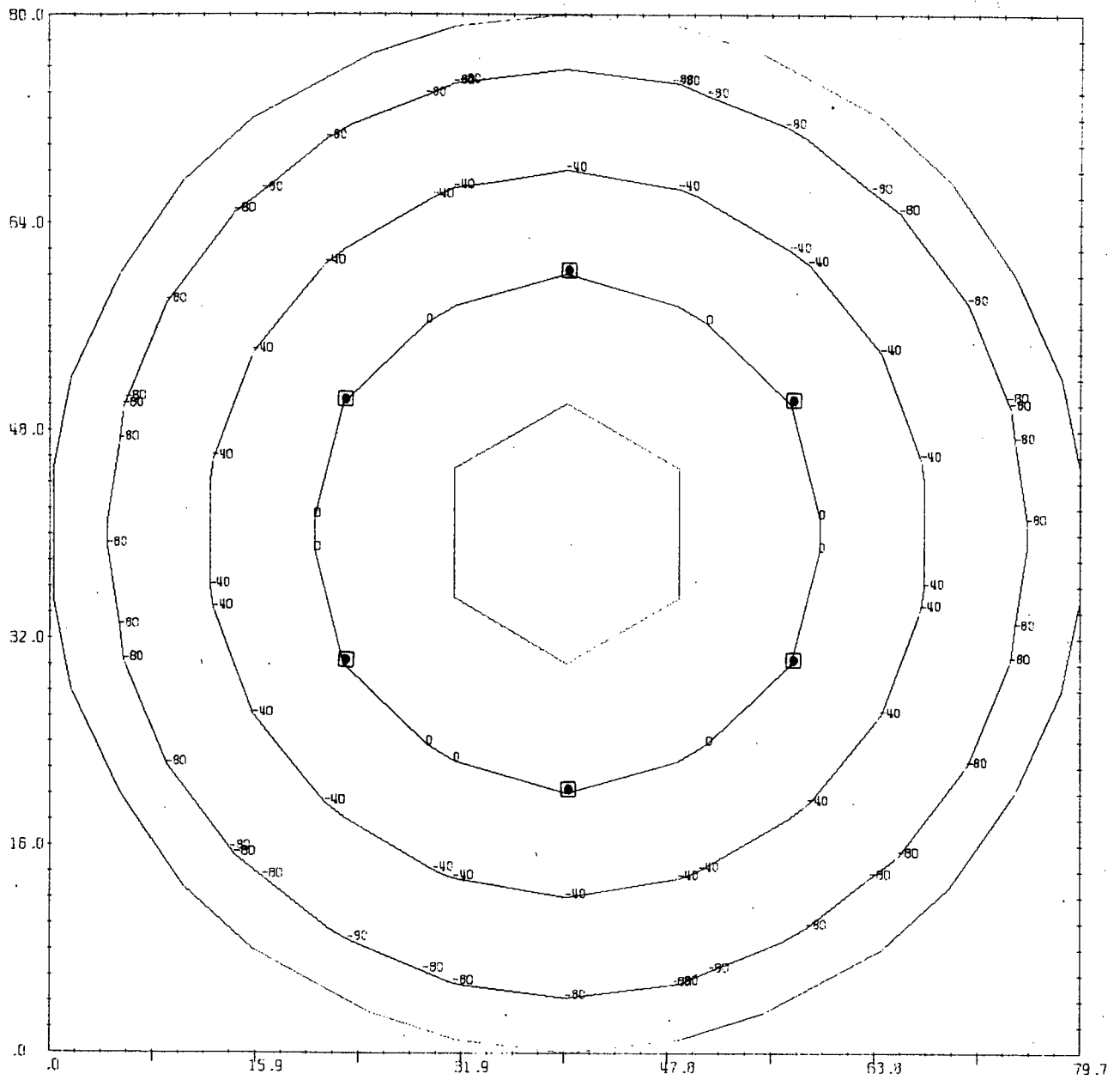
Fig. 6-20 Open Mirror 6 Supports 50% in from Edge

⊡ - SUPPORT LOCATIONS

70
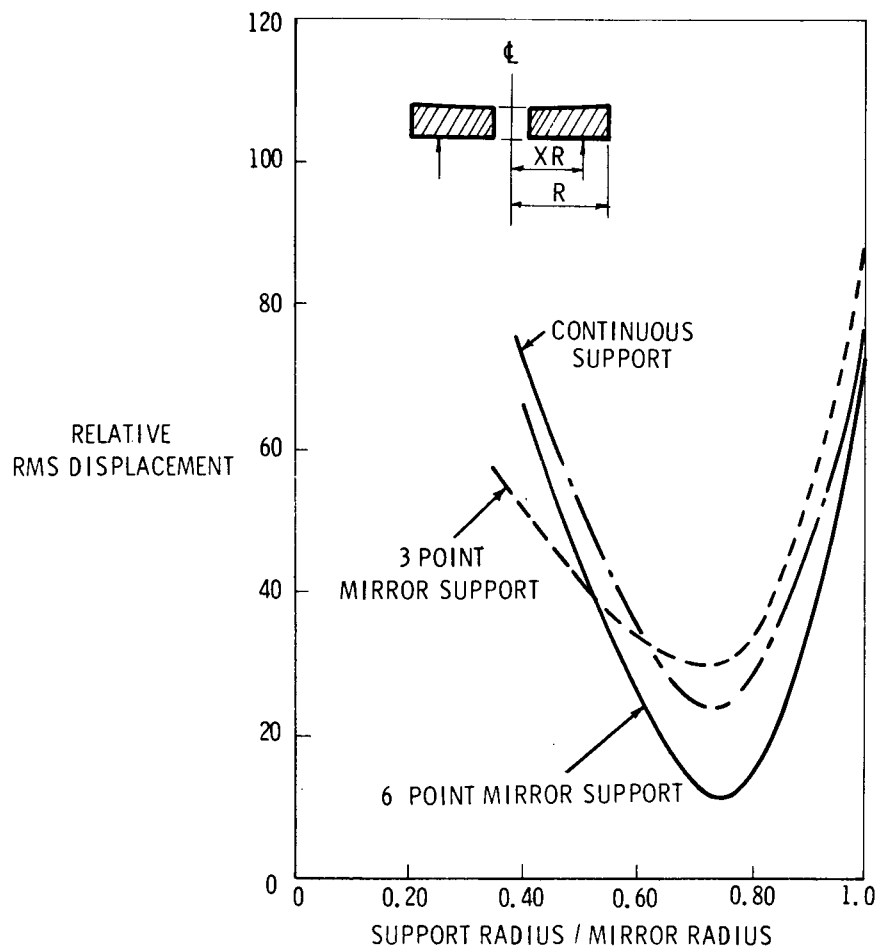
Fig. 6-21    Open mirror - face up.

71

## 6.4  Mirror Behaviour - Bending and Shear Deformations

The data obtained in Section 6.3 on optical mirror behaviour
was based on the thin plate linear bending theory.  It is assumed by
this theory that the transverse deflections are small relative to the
plate thickness and that the deflections result from strictly bending
behaviour.  In optical mirror structures, the first requirement is
always assured, but the second is not necessarily true in most cases.
When the plate is truly thin, that is, the spanlength is approximately two
orders of magnitude greater than the plate thickness, then the shear
deflection component is really small in comparison to the bending com-
ponent.

The typical solid mirror will have a span to depth ratio ranging
from 5:1 to 10:1 and shear deflections will form a large component of
the total.  If "order-of-magnitude" results are desired for mirror de-
flections, then the thin plate theory may be quite adequate, but for pre-
cision evaluations, shear deflections must be included.  These have not
always been obtained in practise, as closed-form solutions for thick
plates are relatively limited.  It is only recently that finite difference
and finite element methods have brought the general case nearer to
solution.

### 6.4.1  Thick Plate Behaviour - A Classical Solution

A classical closed-form solution that is very useful for thick
plate parametric studies is that of Love.[19]  Assuming a rigid continuous
boundary for the circular plate, the transverse deformations (W) under a
uniform pressure loading (P) can be expressed by the following equation.

$$W = - \frac{1}{8} \frac{P}{C} (R^2 - r^2) \left\{ \frac{1}{8} \left( \frac{5+\sigma}{1+\sigma} R^2 - r^2 \right) + \frac{1}{5} \left( \frac{8+\sigma+\sigma^2}{1-\sigma^2} \right) h^2 \right\} \qquad (6-6)$$

where  R  is the circumferential and support radius,  r  is the radius at
which W is calculated,  $\sigma$ is the poisson ratio, t is the plate depth, and
C is the plate stiffness expressed by

72

$$C = \frac{Et^3}{12(1 - \sigma^2)} \tag{6-7}$$

where E is the elastic modulus. The pressure P can represent the selfweight loading intensity ( $\gamma$ t) where $\gamma$ is the material density.

The first part of (6-6) within the braces expresses the bending deflections, the second part of the shear deformations. The relative importance of the shear term increases, obviously, with the increase of t relative to R. For example, the behaviour of a 120" diameter plate, loaded by its own weight and with a Poisson ratio of 0.18 is shown in Fig. 6-22 with percent shear deformation plotted against the mirror depth. At a span to depth ratio of 24:1, the shear deformation is less than one percent of the total deformation. At 10:1, it is 3%; at 6:1, 8%; and at 4:1, it is 16%.

Under ideal boundary conditions such as these, the amount of shear deflection is not excessive, and the approximate thin plate theory is probably quite adequate. Shear deflections, however, are very sensitive to load and support concentrations and if a three-point support were used, the percentage of shear deflection would on the average, double.

It has been assumed, moreover, that the mirror is perfectly isotropic. If the shear-supporting material, in the web, is removed to some degree by "lightweighting" or is replaced by an "egg-crate", the shear deflection component will increase very strongly. This, too, will happen when the core material is a low-density foamed glass or silica.

In effect, the curves on Fig. 6-22 represent the most favorable conditions for use of the thin plate approach; in all other cases the shear deflection is much larger.

In optical mirror literature, the classification of mirrors by stiffness with respect to gravity effects has occasionally been discussed. Oral tradition for a long time has held that the stiffness of the blank is
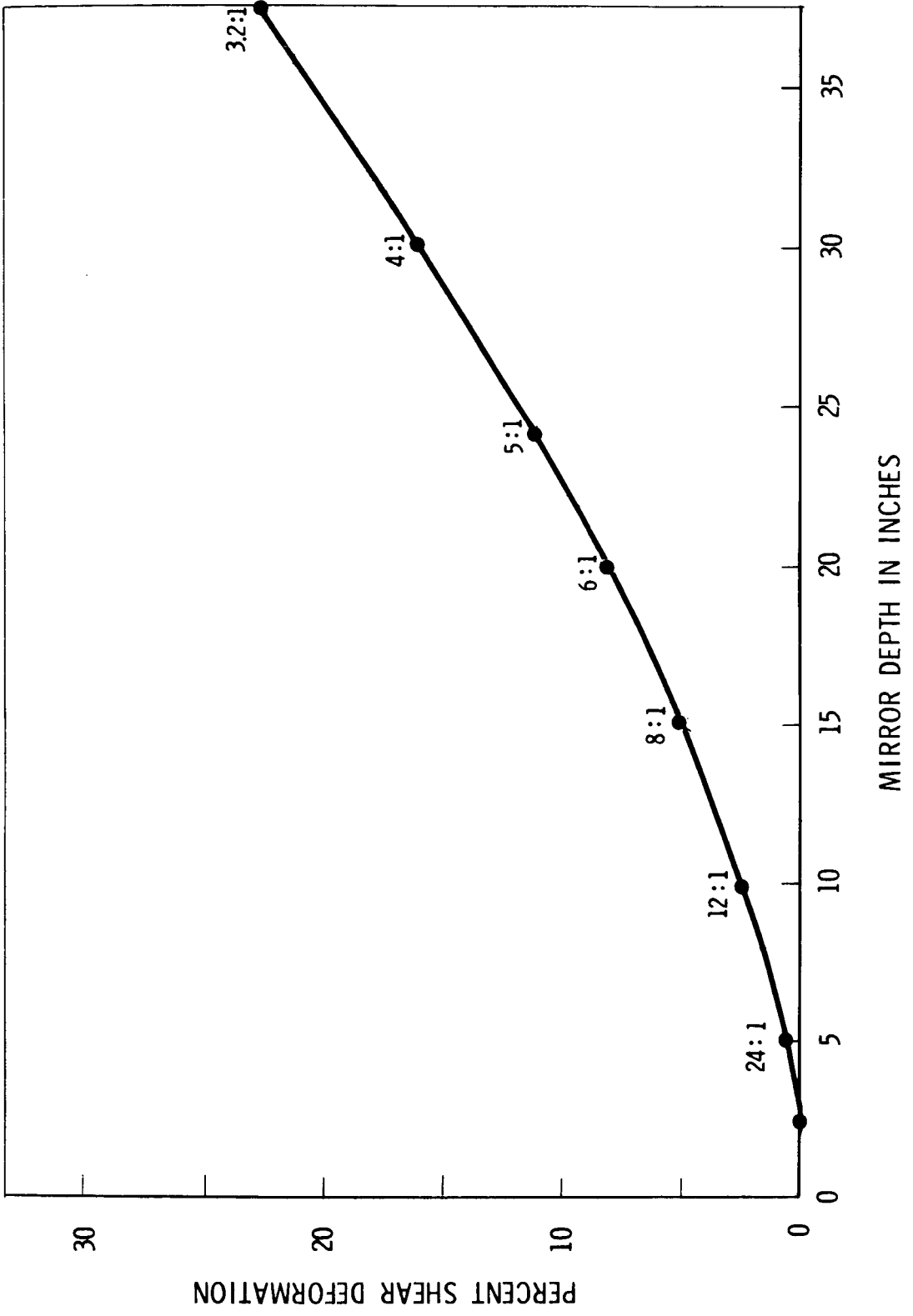
FIG. 6-22 120" MIRROR, CONTINUOUS SUPPORTS, SELF-WEIGHT LOAD

74

related to the diameter to depth (D/t) ratio and the best value for this was 6:1. Couder[20], observing a number of mirrors in practise and comparing his results to thin plate theory, felt that the proper measure of mirror stiffness was a $(R^4/t^2)$ relation of radius and thickness. Rule[21] has recently quoted a $(D^2/t)$ empirical relation as an occasionally suitable design tool. These all are rules of thumb that may be valid for a limited range of mirror blank radius to depth proportions, but they cannot be entirely justified on the basis of exact elasticity theory.

A comparison of the approximations with a rigorous closed-form elasticity solution for a deep mirror can be made through Love's equation (6-6). If this equation is simplified to represent the maximum central deflection in a mirror under gravity loads parallel to the optical axis, the following is obtained:

$$W = K_1 \cdot \frac{R^4}{t^2} + K_2 \cdot R^2 \tag{6-8}$$

where $K_1$ and $K_2$ are terms representing products of material density and elasticity constants. The first term represents the bending deformations and the second the shear contributions in this case.

The Couder relation can be expressed as:

$$W_C = K_3 \cdot \frac{R^4}{t^2} \tag{6-9}$$

and Rule's "empirical" relation by

$$W_E = K_4 \cdot \frac{D^2}{t} \tag{6-10}$$

It is clear that Couder's expression relates only to the bending deflections in the mirror. This is to be expected, as the major verification of his hypothesis was performed with a relatively thin mirror (74.6 cm. in diameter and 3.44 cm. thick), although he extended the

range of its validity to much thicker mirrors. The "empirical" expression does not appear to be related to the rigorous theory at all, being probably a "best-fit" relationship.

To establish the value of (6-9) and (6-10) as design tools, a comparison of these with the exact solution (6-8) can be made. If it is assumed that they are valid at the one point in their range where most mirrors have been fabricated; i.e., where $D/t$ ratio is 6, then the coefficients $K_3$ and $K_4$ can be determined so that all three cases coincide at that point. Assuming that the mirror diameter desired is 120", the deflections, and hence stiffnesses, for various mirror thicknesses can be computed. The three cases are shown, plotted semi-logarithmically, in Fig. 6-23.

As would be expected, the deflections from the Couder approximation are about 9% too high at a $D/t$ of 24 and about 27% too low at $D/t$ of 3. The "empirical" relation predicts only one quarter of the actual deflection at $D/t$ of 24 and is high by about a factor of 2 for the $D/t$ of 3. The empirical relation may well be better suited for mirrors with concentrated point supports than for the continuous support case. With either approximation the errors can be significantly high, and their use should be minimized since exact analysis techniques are now available.

Recent work by Selke[24,25,26], using the Reissner[27,28] extension to Kirchhoff's assumptions including now the transverse shear deformation energy, has resulted in a Bessel function solution for thick circular plates on concentric rings. Selke's shear corrections terms differ from Love's by about 3% for most mirror materials, with the total deformations then differing from Love's by 0.5 and 0.1% for $D/t$ ratios of 4:1 and 10:1 respectively.

Additional current work comes from Malvick and Pearson[29,30,31]. Using a tensor formulation in nonorthogonal curvilinear coordinates and difference elements for the dished mirror with a central hole, and employing a propagation type numerical solution for the resulting equilibrium problem, a number of specific cases have been analyzed. No common reference point with Selke's or Love's solutions is, however, available.

LOVE'S EQUATION — W
EMPIRICAL — $W_E$
COUDER — $W_C$

MAXIMUM MIRROR DEFLECTION IN INCHES

MIRROR THICKNESS IN INCHES

$D/t = 6/1$
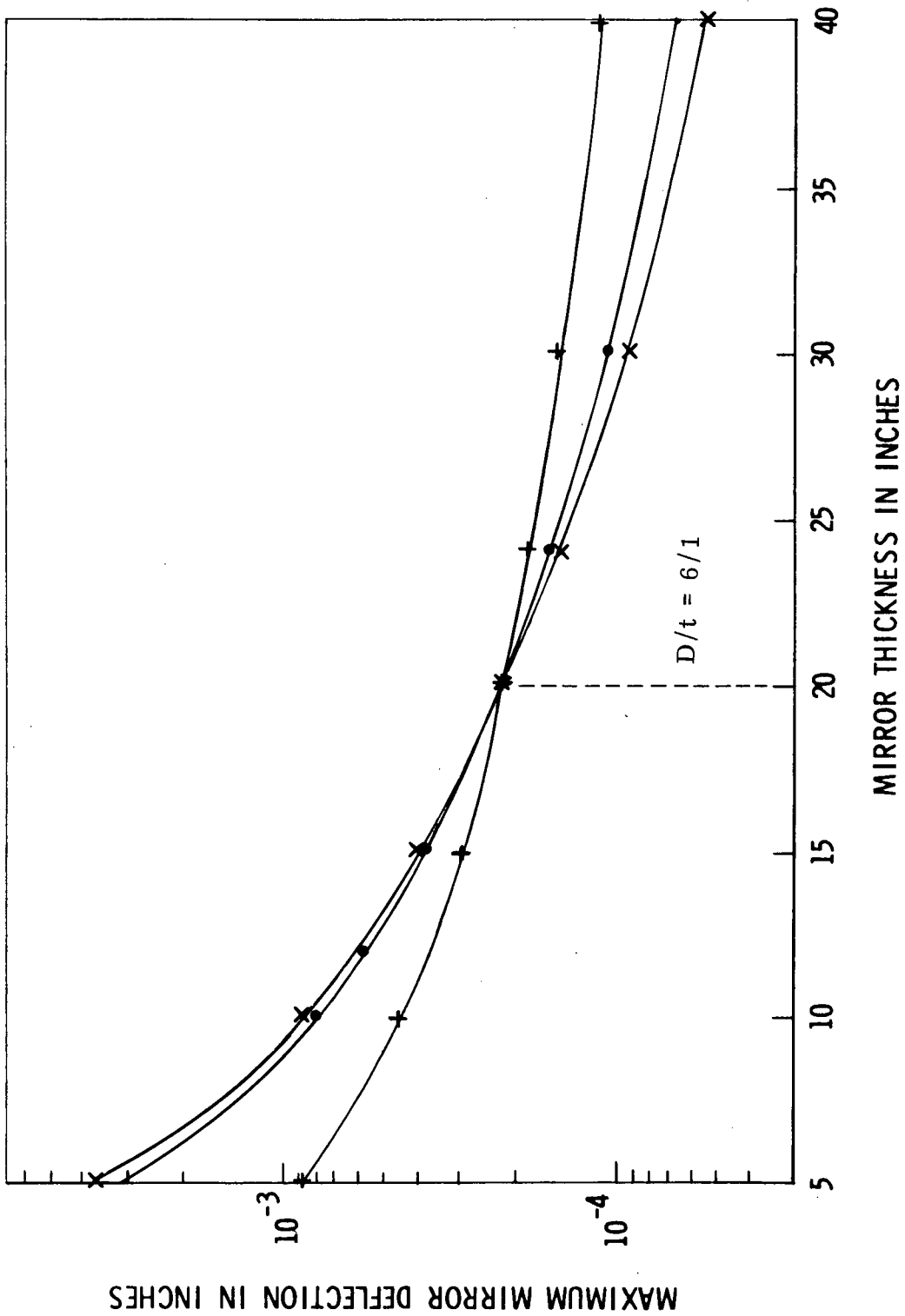
Fig. 6-23  120" mirror – continuous supports, self-weight load comparison of approximate expressions with the closed-form theory.

## 6.4.2 Thick Plate Mirror Behaviour - Finite Element Solution

While closed-form solutions such as A. E. H. Love's are absolutely accurate if the analyst does not deviate from the initial assumptions of the theory, most practical problems in mirror design, however, differ enough in support characteristics to limit the value of this solution. The use of finite element methods reduces dilemma considerably as there are few practical limitations to the approach, and with care, good results are obtainable.

It is possible, in the finite element analysis of thick mirrors, to formulate a plate element that includes finite shear deformations. It is questionable that the elements would resemble plates or even slabs in any way if the span to depth ratio of the mirror is 4:1. It is for this reason that the solid isoparametrics have been used in the following studies. Because there are no limiting assumptions, these elements will give good results if properly implemented. Obviously, the computational costs with 3-D elements are very much higher than with the simple plate or the plate with shear elements.

A study was performed on six curved face solid mirrors 120" in diameter. Two surface radii were considered, with three thicknesses for each (Fig. 6-24). Each mirror was evaluated with both continuous edge supports and 3 point edge supports, and the actual (3-dimensional) deflections were compared with deflections resulting from an equivalent pure bending (but also finite element) analysis. Symmetry sections were analyzed as per Fig. 6-25 and 6-26. The elements were divided in such a manner that later studies for support radius variation could be implemented with small modifications.

The results of this study are summarized in Table 6-4. With continuous supports, the differences between the 3-D and bending studies, which are due to shear deflections, are relatively low and predictable from the A. E. H. Love solution results as shown in Fig. 6-22. The slight differences between Fig. 6-22 and the percentages in Table 6-4 can be attributed to the fact that these mirrors are not flat
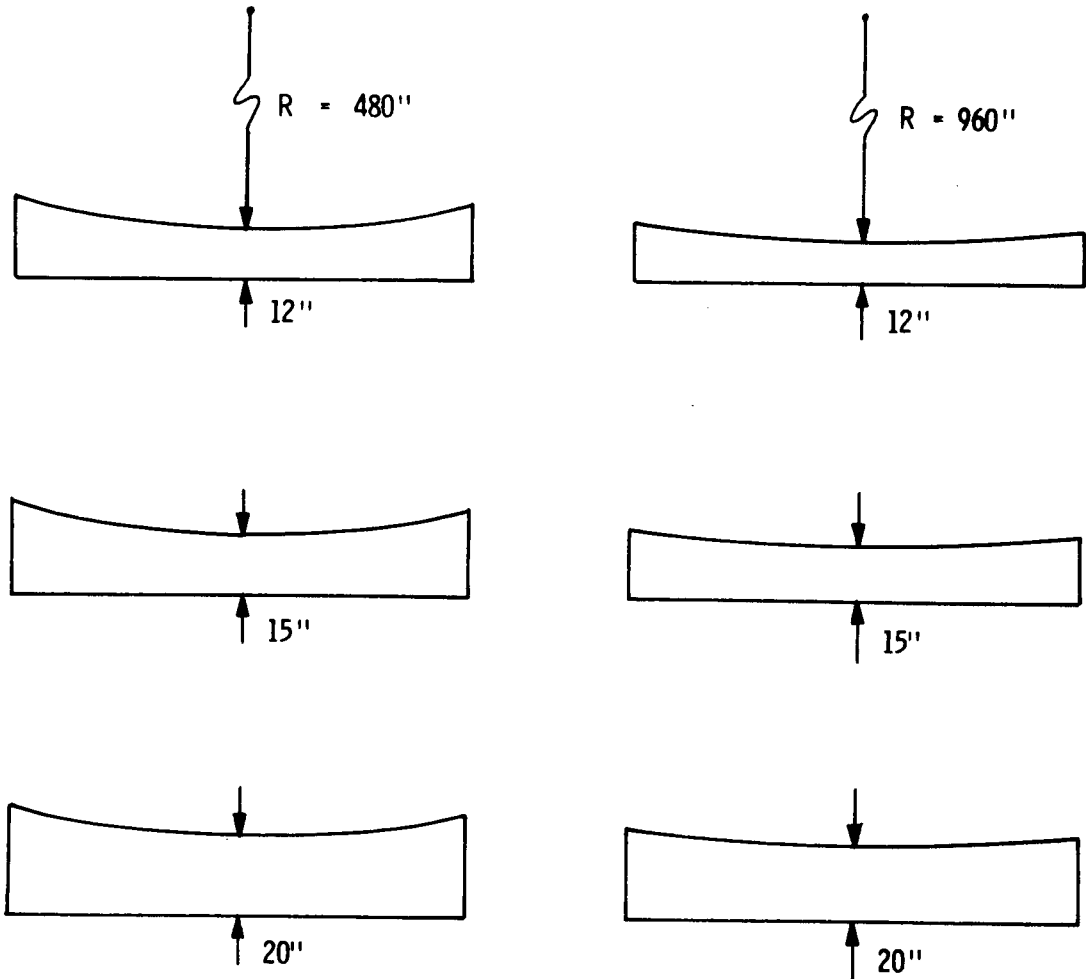
FIG. 6-24    THICKNESS AND RADIUS PARAMETERS FOR 120"
SOLID MIRROR STUDY
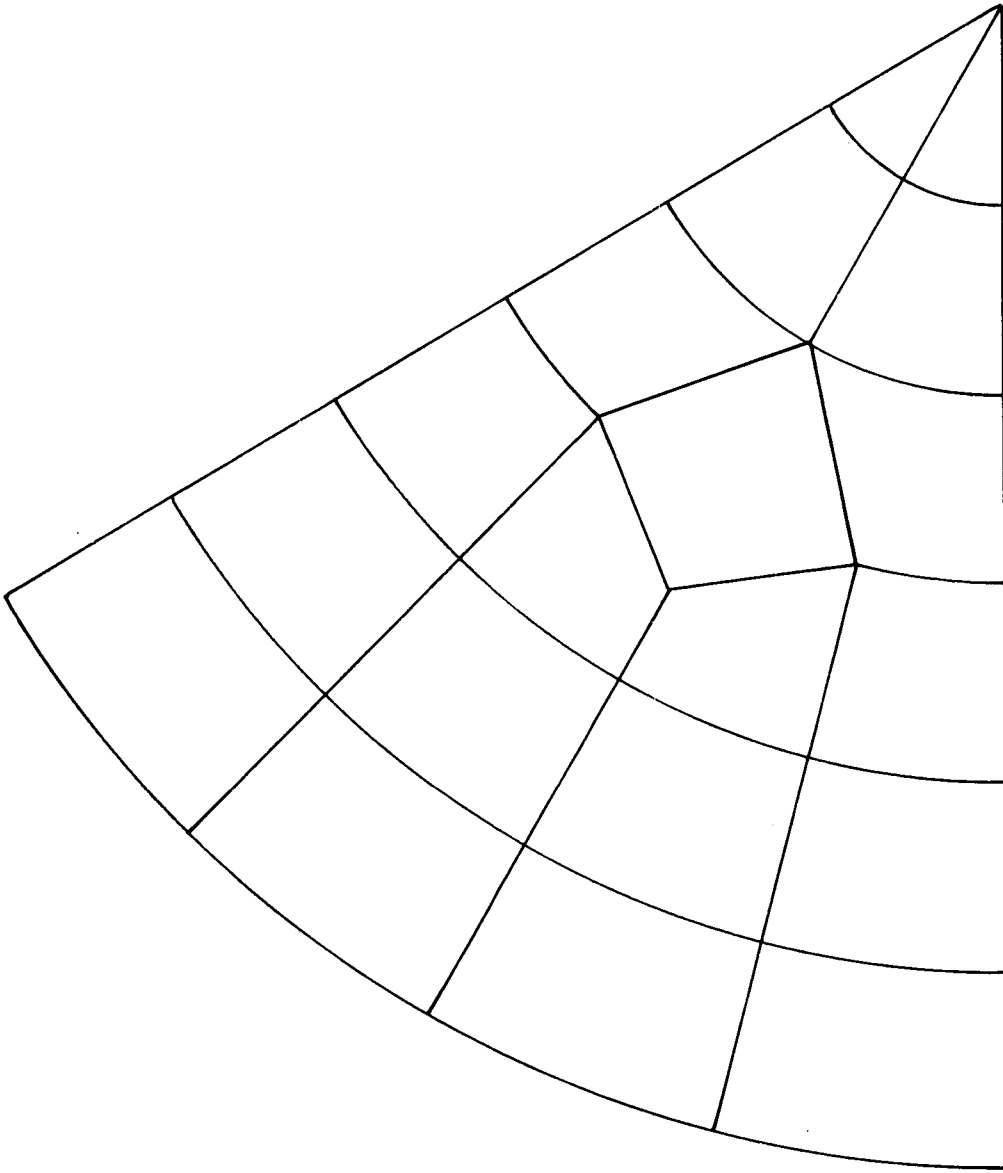
FIG. 6-25   FINITE ELEMENT ALLOCATION FOR 3-D ELEMENTS FOR
120" SOLID MIRROR
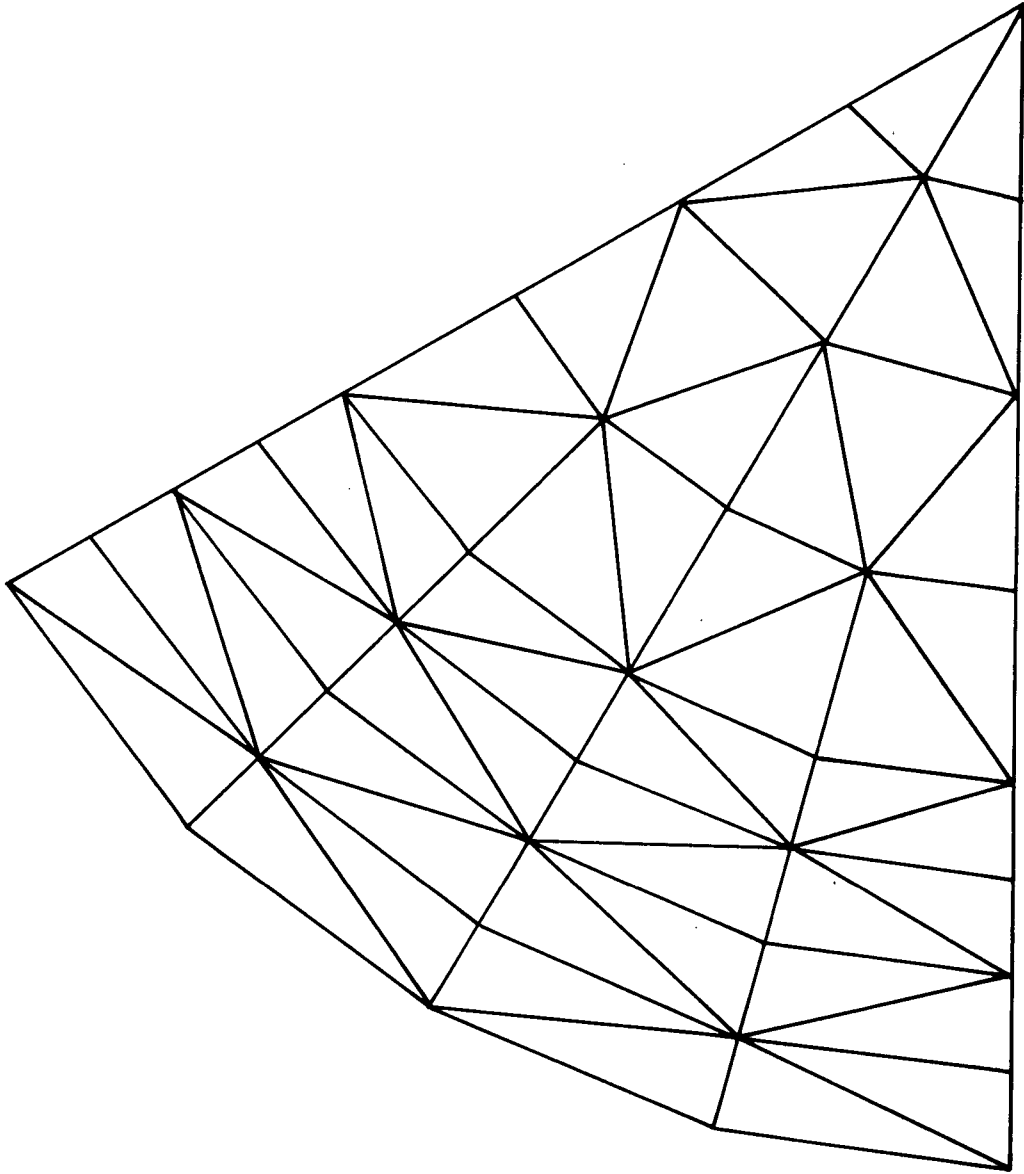
FIG. 6-26   FINITE ELEMENT ALLOCATION FOR BENDING ELEMENTS FOR
120" SOLID MIRROR

## TABLE 6-4

### 120" SOLID MIRROR, SILICA PROPERTIES
### MAXIMUM DEFLECTIONS $\times$ $10^{-6}$ IN.

R = 960"

| MIRROR THICKNESS | CONTINUOUS SUPPORTS | | | 3 POINT SUPPORTS | | |
|---|---|---|---|---|---|---|
| | 3-D | BENDING | ERROR | 3-D | BENDING | ERROR |
| 12 | 500 | 480 | 4% | 970 | 760 | 22% |
| 15 | 340 | 310 | 9% | 730 | 490 | 33% |
| 20 | 210 | 180 | 14% | 560 | 290 | 48% |
| R = 480" | | | | | | |
| 12 | 460 | 440 | 4% | 880 | 670 | 24% |
| 15 | 310 | 290 | 6% | 680 | 450 | 34% |
| 20 | 200 | 170 | 15% | 530 | 260 | 51% |

like the theoretical closed-form solution assumes.

With the three-point supports, the difference between the 3-D and bending approach is highly evident. For the thickest case, a 20" mirror with a span to depth ratio of 6, the bending theory predicts one half of the actual deflections. With the thinner mirrors this error level is expectedly smaller, but still significant.

An additional difference between the bending theory and the 3-D behaviour should be noted here. According to the bending theory, the total deformation field is defined by the displacements and rotations of a hypothetical middle surface, infinitesimally thin, but with finite stiffness. The transverse deformations of the actual top and bottom surfaces in the mirror can be obtained directly from the deformations of the middle surface, and with a properly thin mirror all three should differ by second-order magnitudes only.

In the three-dimensional model for the mirror, no such behaviour assumptions are made, and the top and bottom of the mirror surfaces can have quite different deformation patterns, especially if load or support concentrations occur. An example of this can be seen in Fig. 6-27 and Fig. 6-28. Fig. 6-27 represents the deflection contours for a bending model of the 120" diameter, 20" thick, mirror supported on three points at the edge. As the supports are rigid, the zero deflection contour is located at the support. Fig. 6-28 represents the deformations of the top (optical) surface of the same mirror but analyzed with the 3-D method. It is obvious that while the contours here cluster around the support area, the least deflection contour is not the zero level, but the $275\mu$" level. Apart from this initial offset, the contour patterns of the two cases are quite similar in appearance.

Fig. 6-29 develops this similarity even further. It is evident from the exaggerated deformation-scale drawing that the top and bottom surface deformations of the solid mirror differ considerably. The graph directly below plots these surface deformations again but using the vertical deflection at the center of the mirror (which incidentally is almost the same at that point for the top and bottom surfaces) as the
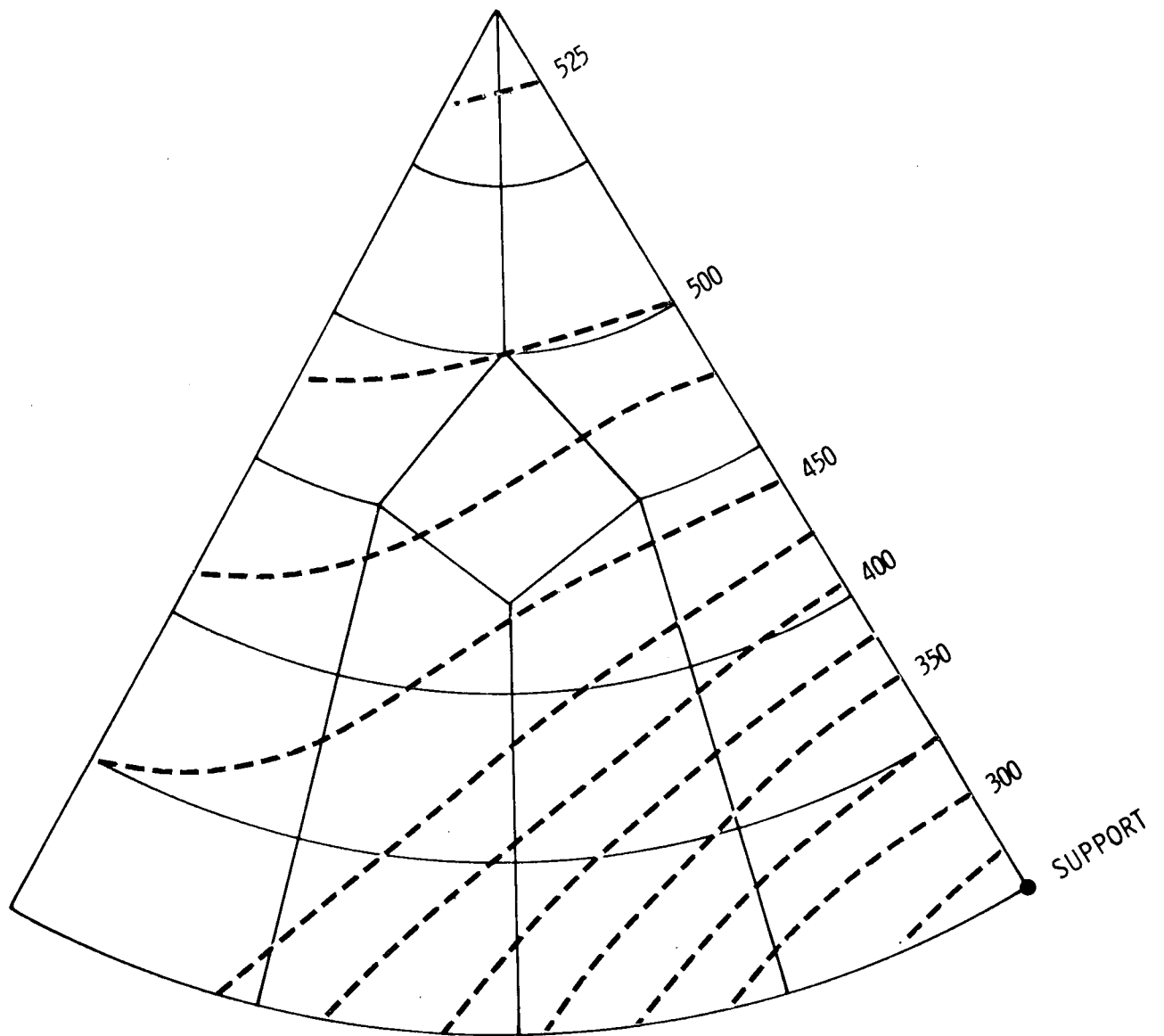
FIG. 6-27   TOP SURFACE TRANSVERSE DEFLECTIONS — 3-D MIRROR

(Intervals @ 25 x $10^{-6}$ in. )
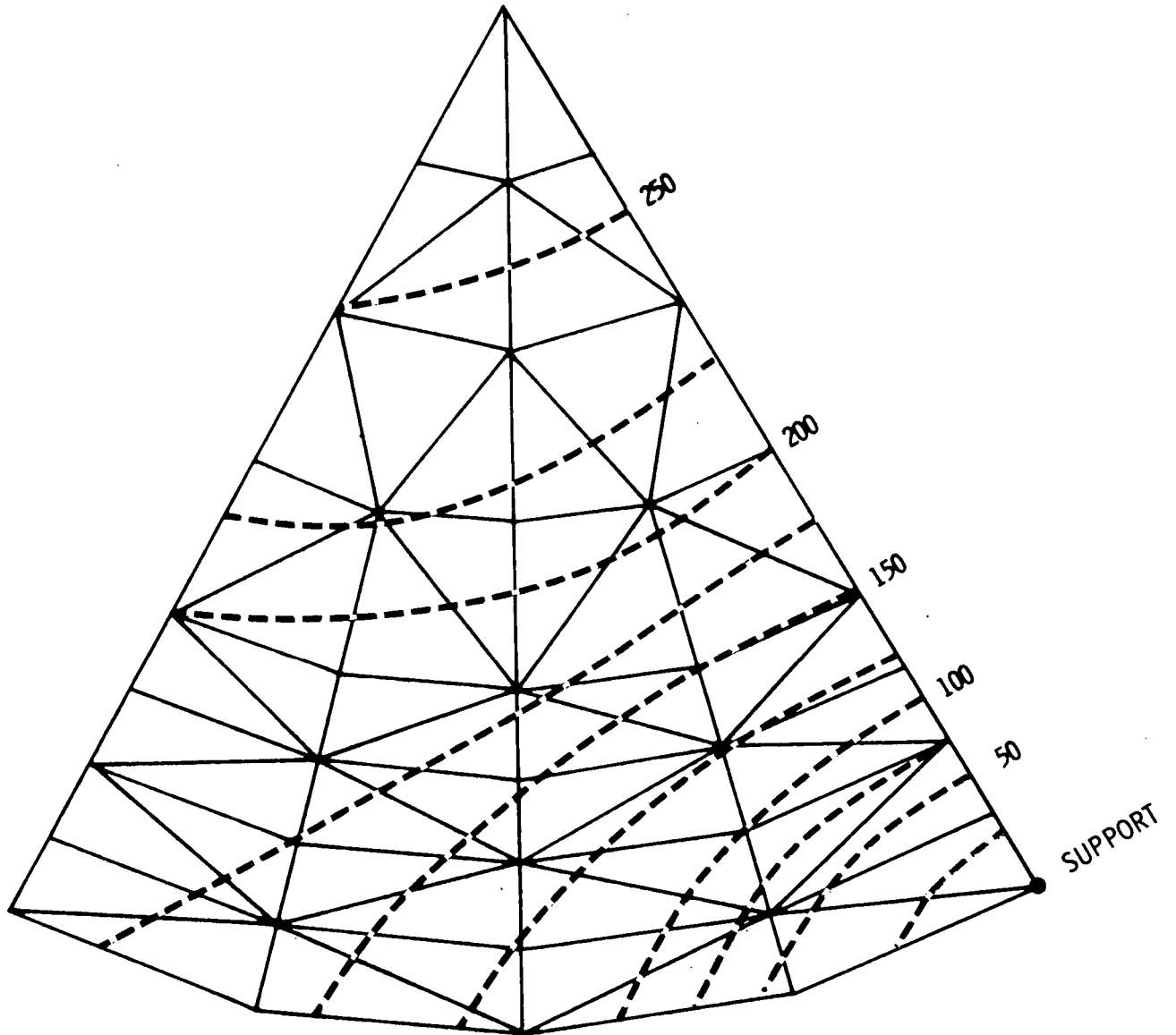
FIG. 6-28   TOP SURFACE DEFORMATIONS — BENDING MIRROR

(Intervals @ 25 x 10$^{-6}$ in)
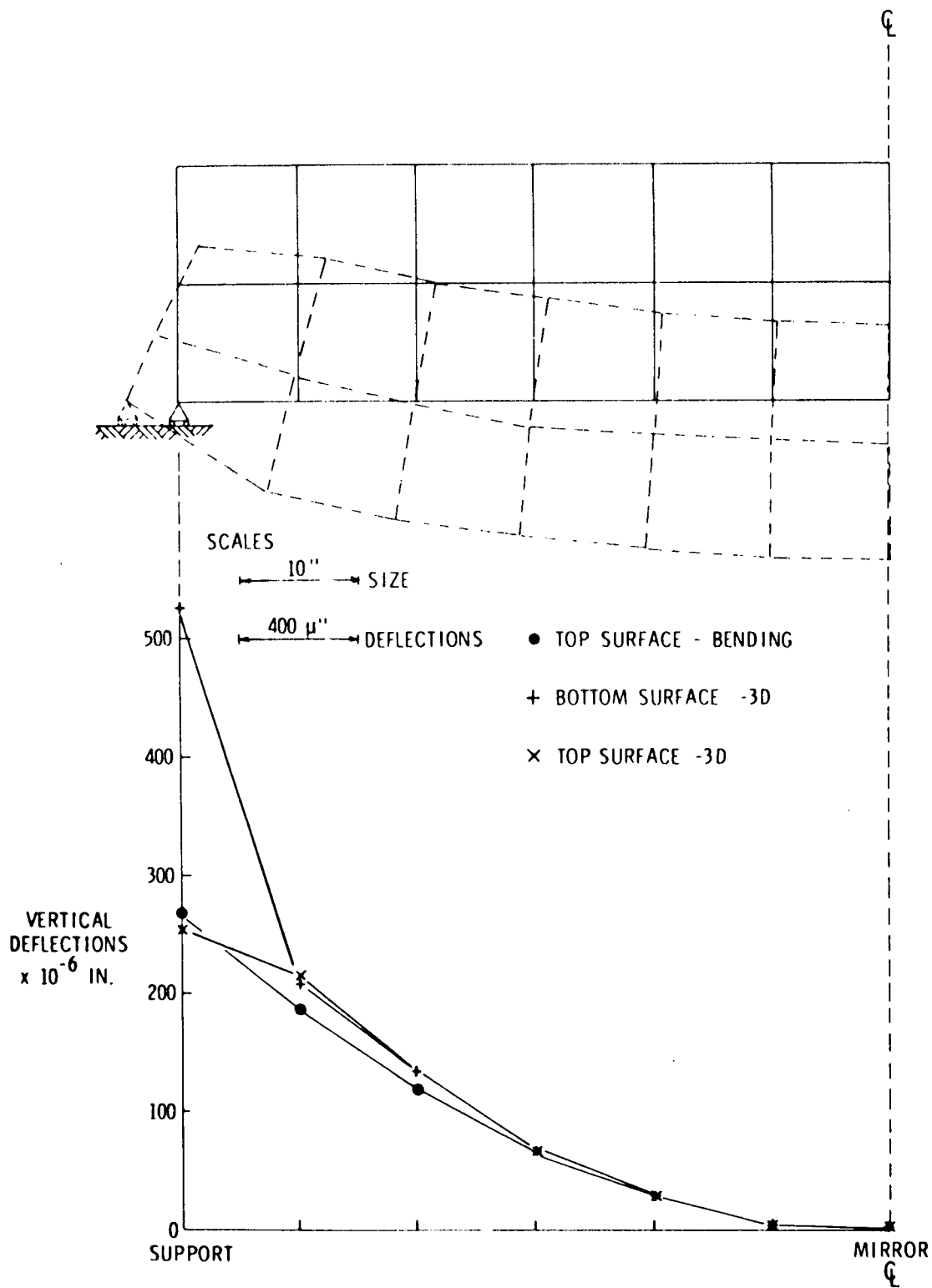
Fig. 6-29 Solid vs bending - 3 point mirror supports
deflections along radius line through supports.
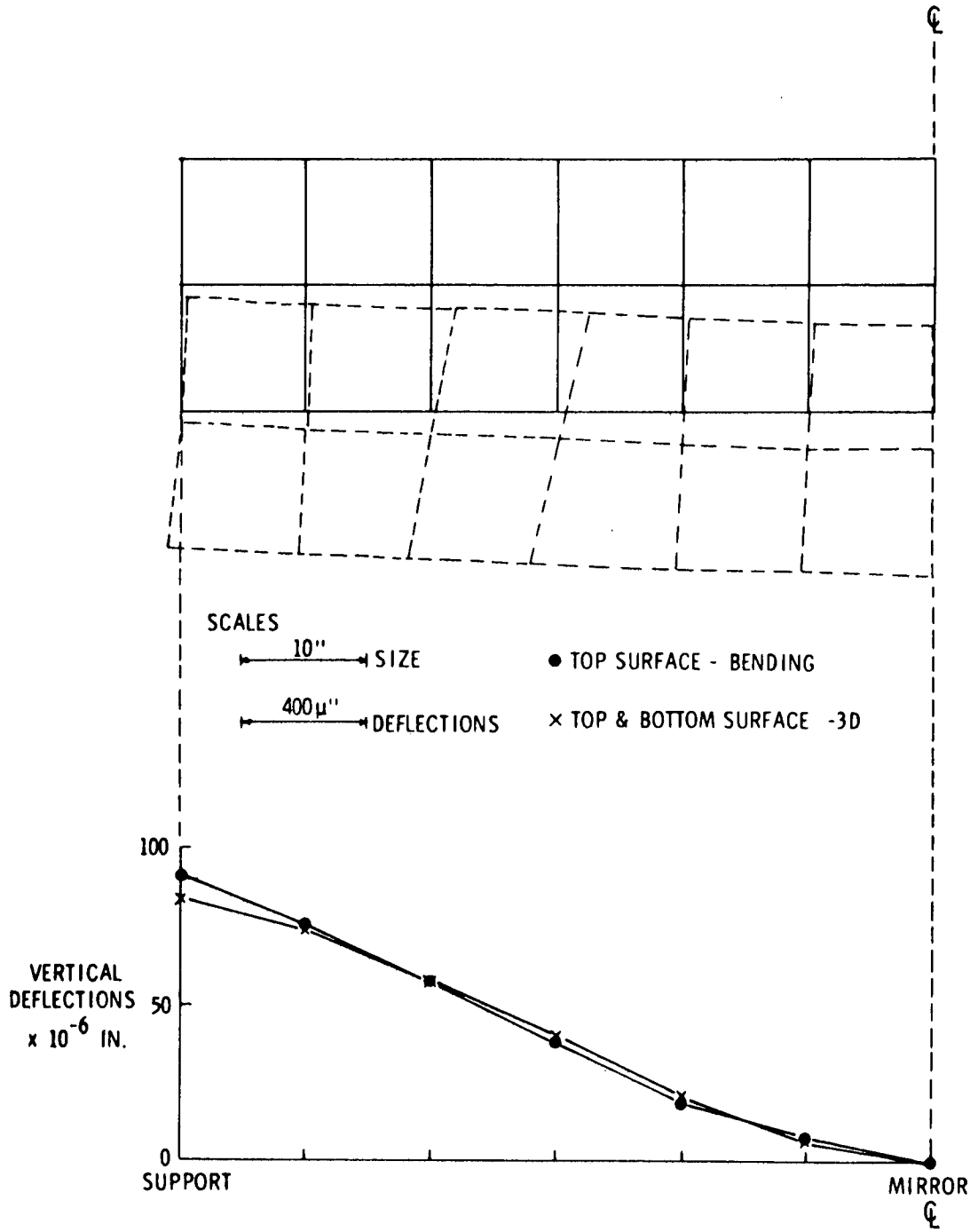
Fig. 6-30 Solid vs bending - 3 point mirror supports
deflections along radius line between supports.

SCALES

├────10"────┤ SIZE

├────200 μ"────┤ DEFLECTIONS   ● TOP SURFACE  -3D

+ TOP SURFACE - BENDING

✕ BOTTOM SURFACE  -3D

VERTICAL
DEFLECTIONS
× 10⁻⁶ IN.
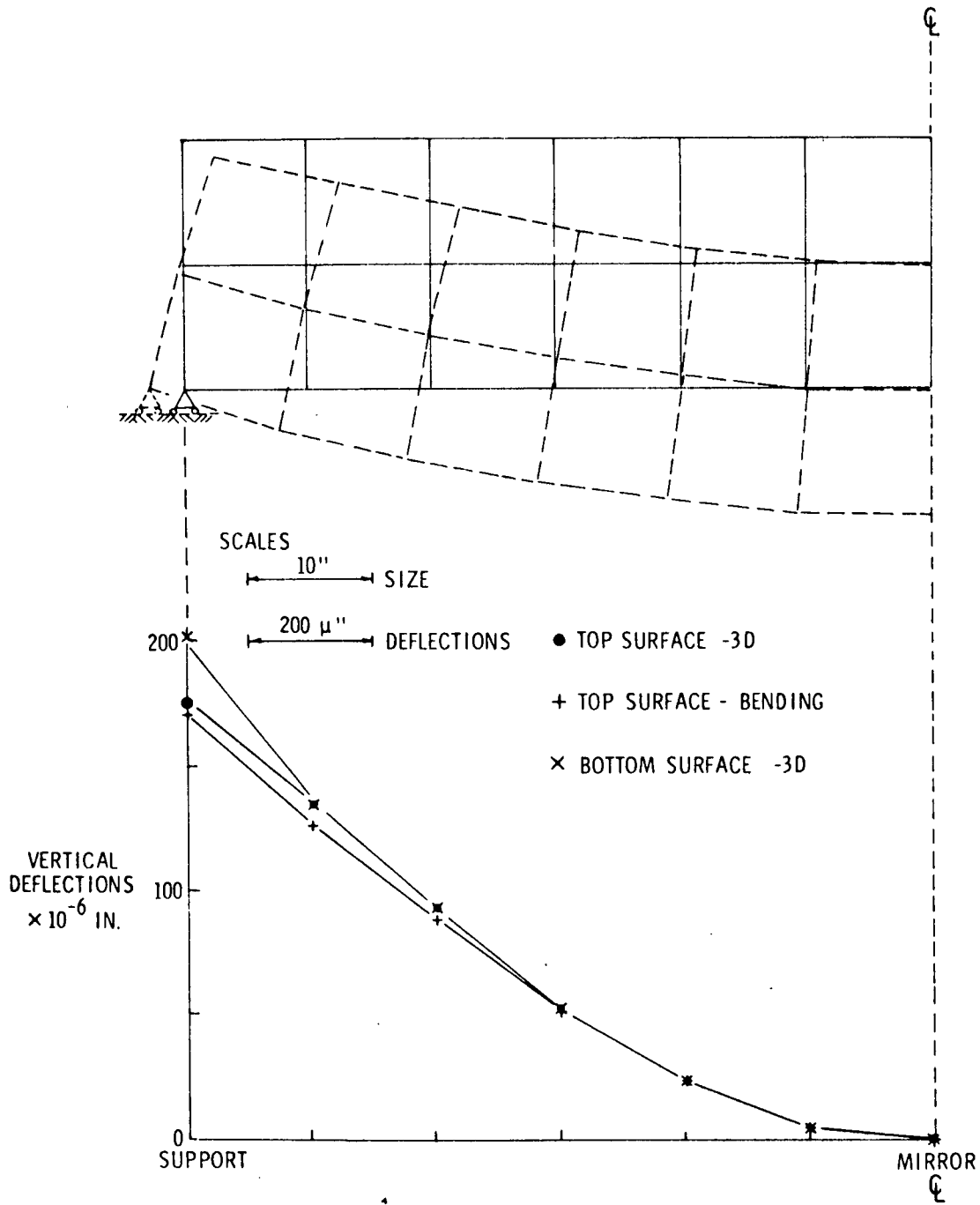
Fig. 6-31   Solid vs bending theory - mirror continuously
supported on circumference, deflections along
radius line.

origin of the figure. The bending theory results for the same mirror are plotted on the same basis and scale. The results are plotted for the 3-point supported mirror through a radius line connecting a support and the mirror center. Fig. 6-30 is analogous to Fig. 6-29, but deflections are plotted along a radius halfway between the supports.

It is evident that if the mirror deflection evaluation is based on relative displacements from an immovable point of reference, i.e., the supports, then the bending approach is truly inadequate as a design tool. If, however, the "rigid-body" component is removed from the optical surface deformations, as was done with the graphs in Fig. 6-29 and Fig. 6-30, then the top-surface 3-D and bending approaches appear to correspond quite closely.

If continuous edge supports are used, then the deformation patterns can be seen from Fig. 6-31. The top and bottom surfaces in the 3-D model have essentially identical deformation patterns across most of the mirror, departing somewhat near the supports. Again the 3-D top surface pattern resembles the bending results, and the differences are even less than with 3-point support case. The deformation profiles for other thick mirrors, which were summarized in Table 6-4 but are not presented here, point towards the same conclusions, but with lesser emphasis as the mirrors are thinner and the bending model is more valid in any case.

It is very evident from the data at hand, that when the mirror is supported at the back, then the bending theory can be used to compute the optical surface deformations. From the graphs in Figs. 6-29, 6-30, and 6-31, it is not certain, however, that this correspondence will be true under the more severe criteria based on the optical path difference and the Strehl ratio. A more detailed study of this data sometime in the future would be highly fruitful.

It is tempting to speculate that the thin plate bending approach, and hence Couder's approximation might be a completely appropriate general design tool for mirrors with a wide range of depth the diameter ratios. Couder observed it to be adequate for various sizes of

ring-supported solid mirrors, and verified it accurately for a very thin mirror. The results here confirm this to some degree, and further indicate that it may be suitable for the three-point edge supports as well, provided the mirror supports are at the back. Possibly other types of support will be found where agreement is good.

Some caveats are in order, however. It is clear from the present study that the location of the supports, whether at the optical surface, the bottom surface, or between, will have considerable effect on the deformation pattern. Whether the effect of many, evenly distributed supports under the mirror can be predicted from Couder's approximation is not known, nor is there any such information on the behaviour of mirrors with a large central opening. In general, there is sufficient disagreement between the bending and 3-D results as to make the use of an accurate 3-D analysis mandatory wherever precision results are needed. For order of magnitude design studies, the Couder approach is probably adequate.

### 6.4.3    Deep Mirror with Soft Core

Often to minimize the weight of a deep bending plate, the low-stressed core material around the neutral surface is replaced by a low-density, low-stiffness component which, by reducing the weight, increases the inherent efficiency of the whole. While such sandwich structures for optical mirrors are relatively uncommon, they occur often enough to pose some demands for adequate analysis capabilities. Sandwich mirrors are nearly always deep mirrors and must be analyzed by solid finite elements, but additionally the elastic, strength and density peculiarities of the face and core must be included in the study.

In order to test the deep sandwich mirror capabilities, the following example was analyzed. This is an idealization of an actual sandwich mirror proposed by NASA/MSFC Manufacturing Research and Technology Division. It is 21" in diameter, 3" deep with 0.38" front plate and 0.25" back plate. In this test example, the mirror has been assumed flat and of uniform thickness. The faces are solid fused silica and the core is silica foam with 85% voids. Four separate studies were performed - two types of supports and two configurations - with and without a rim plate. The loading was assumed to be 1g acting in the direction of the optical axis (Fig. 6-32).

A $60^{\circ}$ segment was divided into 5 solid elements, with isoparametric plate elements above and below each solid element. As the elements are conforming and of a very high order, this number was probably sufficient. Rim plates, also isoparametric, were added wherever needed. Symmetry conditions were imposed along the $60^{\circ}$ radial lines.

Deflection results are shown in Fig. 6-33, for points on the top surface in the direction of the optical axis. The mirror was assumed supported at the bottom surface on the rim, where the deflections then were zero. At the top surface, however, points immediately above the supports experienced some movements. This is again a contrast to the pure flexure case where the behavior is totally characterized by the middle surface, and a parallel of the behavior noted in Section 6.4.2.

The rimless case is contrasted with the pure flexure displacements using an equivalent bending stiffness for the latter. The

A           A

60°

3"

0.25 → ← → ← 0.38

FUSED SILICA

FOAMED SILICA

21" Φ

OPTIONAL 1/4" RIM
PLATES

TOP VIEW MIRROR

SECTION 'A-A'

3 POINT RIM
SUPPORT

"CONTINUOUS" RIM
SUPPORT
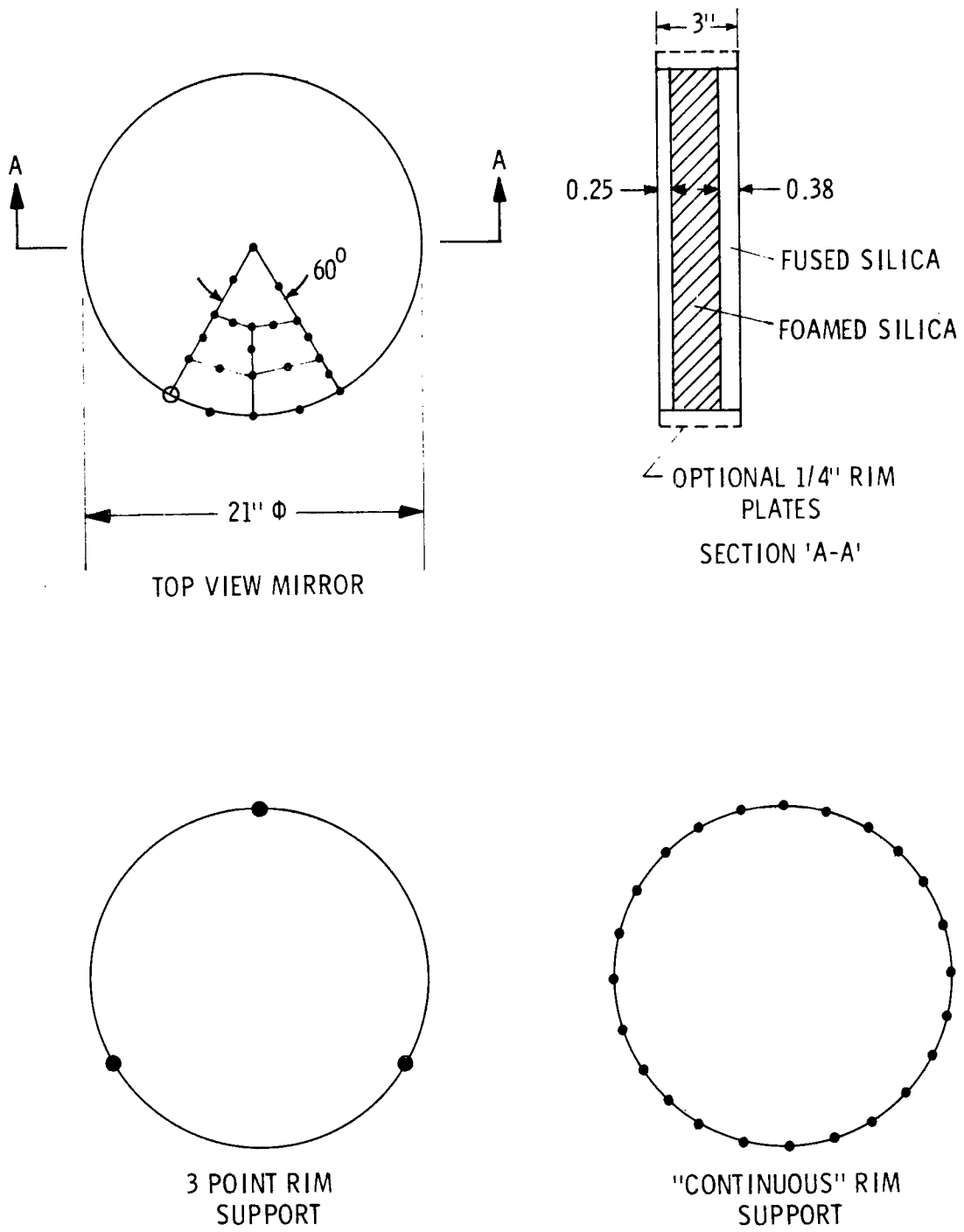
Fig. 6-32    Sandwich mirror.

92

results obtained clearly indicate the inadequacy of bending theory to deal with this problem. For continuous supports, the bending results differed by a factor of 2.5; with three discrete supports, by a factor of about 6.

The results also indicate the enormous sensitivities of this type of structure to concentrated supports (as well as loads). While the three support bending deflections differ from the continuous support deflections by a factor of 1.6, the sandwich structure has an analogous factor of 3.7. The difference is obviously the shear deformations. The effect of the rim on the sandwich is an indication of this behavior mode as well.

It should be noted here that factoring out the "rigid body" component of the optical surface deformations will not reduce the total deflections sufficiently to compare with the bending theory, as was possible in the solid mirrors considered in Section 6.4.2. It is evident that the shear deformations control the behavior here to such a degree that the bending approach to sandwiches of this type is not even a rough approximation to the actual mechanisms.

ELEMENT LAYOUT
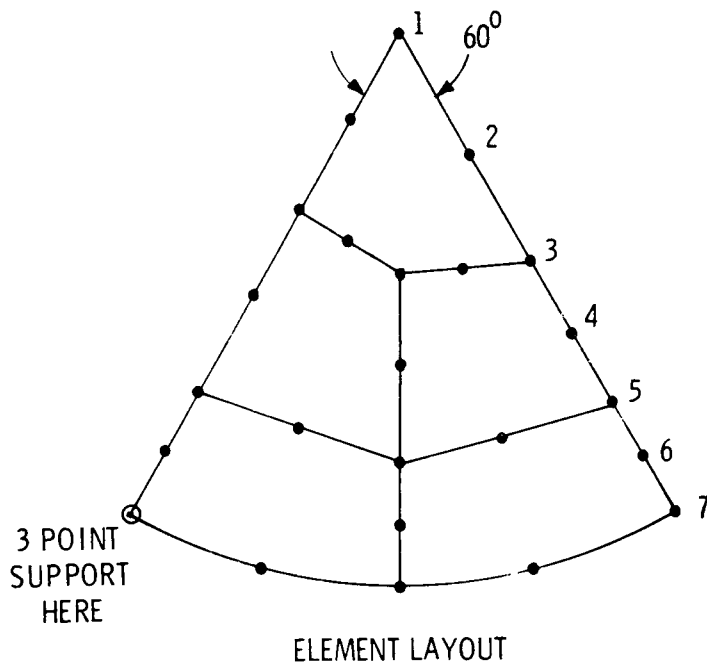
DISPLACEMENTS ON TOP SURFACE ALONG OPTICAL AXIS ($\times 10^{-6}$ IN)

| JOINT | CONTINUOUS SUPPORTS | | | 3 SUPPORTS | | |
|---|---|---|---|---|---|---|
| | NO RIM | 0.25 RIM | PURE BENDING | NO RIM | 0.25 RIM | PURE BENDING |
| 1 | 3.7 | 3.4 | 1.5 | 13.9 | 9.6 | 2.4 |
| 2 | 3.4 | 3.2 | | 13.5 | 9.2 | |
| 3 | 2.9 | 2.7 | | 12.6 | 8.3 | |
| 4 | 2.4 | 2.1 | | 11.5 | 7.3 | |
| 5 | 1.8 | 1.5 | | 10.1 | 5.9 | |
| 6 | 1.0 | 0.8 | | 7.6 | 3.8 | |
| 7 | 0.7 | 0.1 | 0.0 | 6.8 | 2.0 | 1.6 |

Fig. 6-33 Results - sandwich mirror analysis.

94

## 6.5    Lightweight Mirrors

The stiffness to weight characteristics of mirror structures are often improved by a "lightweighting" technique. This approach generally acts to minimize the material at the neutral surface of the mirror where it contributes relatively little to the bending stiffness. The total mirror weight then decreases more rapidly than the bending stiffness, and flexural displacements are reduced. The shear deflections, however, will increase and sometimes offset the improved bending behavior. As the mirror weight has been reduced, however, the net stiffness to weight ratio generally increases.

Lightweight mirrors may be assembled by fusing flange-plates to either a grid or a light-weighted core, or by machining from a solid blank. The fusing process is considerably more economical, but potential sources of trouble can arise with stress concentrations at the joints and lack of absolute uniformity in the degree of fusion at all points in the mirror. The machining process is much more costly, but good fillet radii can be achieved between joining surfaces and better dimensional control is possible. The mechanisms of internal stress relief by fabrication will probably be quite different in the two types. A direct comparison of this in two mirrors of equal stiffness but of differing fabrication techniques would be most valuable.

Until recently, the lightweight structure type has been quite difficult to solve analytically. Some approaches can be made using orthotropic plate theory, but these can become very complex with non-orthogonal grids, circular mirror structures and arbitrary support configurations. Equivalent stiffness approaches are not too illuminating either since these generally neglect the considerable shear deformations.

Finite element techniques make the analysis of lightweight mirrors relatively easy. As most of the components are plates, or can be idealized as plates, the bending and stretching elements can be used for both the ribs and the cover plates. Appendix A describes the formulation of such an element from uncoupled bending and plane stress behavior. This element was implemented early in this study, and has been tested extensively for speed and convergence. If only a part of the mirror blank has been lightweighted, then the solid isoparametric elements can be used wherever necessary in conjunction with the plate elements.

A number of candidate lightweight structures are analyzed here, first to demonstrate the capabilities of the approach utilized, to compare with results obtained by approximate means, and to study the sensitivity of the mirror behavior to parameter changes in the mirror lightweighting properties. The configurations are based on those given by Simmons[22] for 64" diameter lightweighted mirrors. While these mirrors were presumably lightweighted by machining, the analytical approach used is no less valid for the fused mirror structures. To simplify the analysis, the fillets and the backplate holes are ignored, although for a detailed study they could be included. As the supports are continuous along the edge and the loading comes from gravity along the optical axis, symmetry assumptions can be used and $30^\circ$ sectors are analyzed for the triangular and hexagonal configurations, and a $45^\circ$ sector for the square cavity case. (Fig. 6-34). As this is a deflection study, only a minimum number of elements is necessary to achieve adequate precision. A single element is used for the top and bottom plates for each triangle and rectangle, while each of the hexagons must be subdivided into at least six triangles. Single-rectangle elements are used for the ribs between the intersection nodes. If concentrated loadings and stress effects are desired, it is advisable to subdivide these elements further.

Table 6-5 shows a comparison of the relative maximum deflections of the various configurations in fused silica, ULE and CER-VIT. The triangular configuration deflects a shade less than the hexagonal, although its weight is considerably higher. The weights have been calculated assuming no fillets, backplate holes or the additional lightweighting holes found in triangular mirrors.

If the lightweighted mirror deflection is computed by assuming an equivalent bending stiffness, then that result will be in error by about 50%. This stems from neglecting the shear deformation, which in this structure type is quite substantial.

Even if the mirror were 12" thick and solid, the shear deflections would account for approximately 10% of the total. It is evident here too, that lightweighting does not necessarily reduce the total deflections in comparison to a solid mirror of the same outside dimensions. The weight of the mirror is however, substantially reduced, and improved dynamic behavior should be expected.
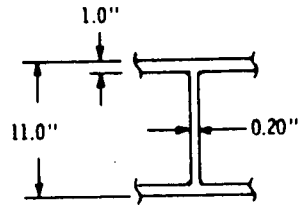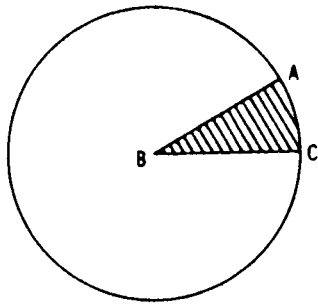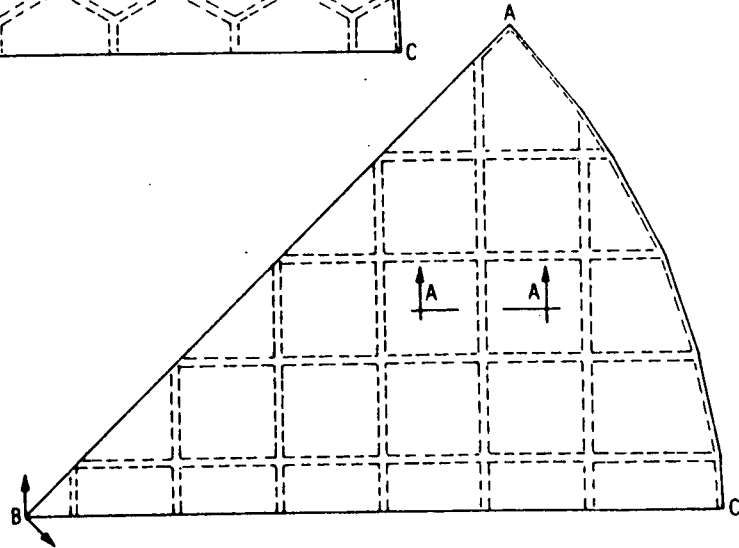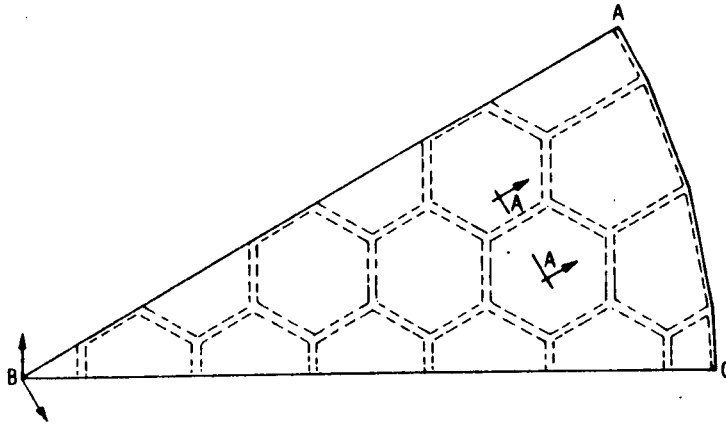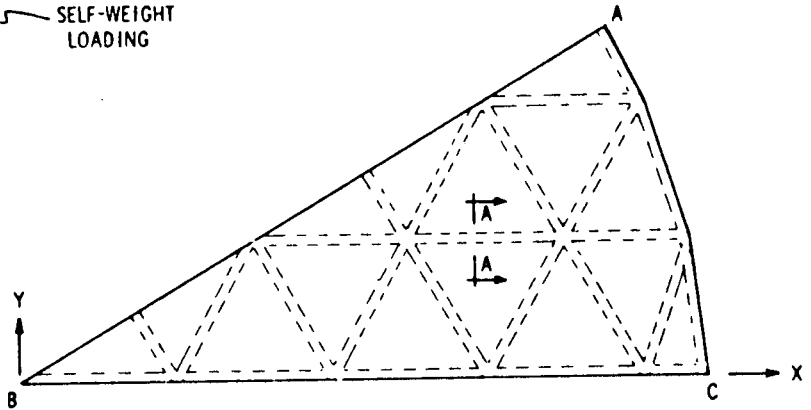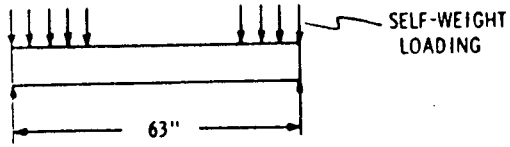
FIG. 6-34 LIGHTWEIGHT MIRROR CORE CONFIGURATIONS

97

## TABLE 6-5

### LIGHTWEIGHT VS SOLID MIRRORS
### 64" DIAMETER, 12" THICK

| CELL TYPE | SILICA | | ULE | | CERVIT | |
|---|---|---|---|---|---|---|
| | $\Delta$ x10<sup>-6</sup> in | Weight Lbs. | $\Delta$ x10<sup>-6</sup> in | Weight Lbs. | $\Delta$ x10<sup>-6</sup> in. | Weight Lbs. |
| TRIANGULAR | 54 | 885 | 58 | 885 | 49 | 1040 |
| SQUARE | 67 | 860 | 72 | 860 | 60 | 975 |
| HEXAGONAL | 55 | 830 | 59 | 830 | 50 | 945 |
| EQUIVALENT BENDING STIFFNESS | 28 | 885 | 30 | 885 | 25 | 1040 |
| SOLID 12" BENDING | 44 | – | 48 | – | 39 | – |
| BENDING + SHEAR | 49 | 3030 | 53 | 3030 | 44 | 3450 |

Fig. 6-35 shows the distribution of the mirror deformation contours under 1g loading for a lightweighted triangular mirror, a solid mirror of the same outside dimensions and a pure bending "equivalent bending stiffness" representation of the lightweighted triangular mirror. It is evident that the lightweight mirror surface deflections differ from its pure bending and solid counterparts by both magnitude and distribution of deformations.

While it is evident from these studies that there is some advantage to using a triangular or hexagonal core over a square one, considerable optimization is also possible within each configuration. As the computer running times on the triangular core mirror were much lower than the other cases, a number of parameter tests were performed using it. Keeping all other properties constant, web and/or flange thicknesses were doubled or halved, the total depth of the mirror was changed, keeping the webs and flange thicknesses constant, and finally the 1 1/2" back plate was removed from the mirror.

Certain significant trends can be observed in the data presented in Table 6-6. Deflections could be improved over the basic configuration by doubling the depth of the mirror, doubling the thickness of the web and halving the thickness of the flanges. Doubling the depth obtained the least deforming configuration, though obviously a large part of the advantage gained from increasing the depth for flexure resulted in a concurrent increase in the shear deformations.

The top or bottom plate (or flange) thicknesses seem to be at an upper limit of effectiveness in the original configuration. An increase in the plate thickness adds to both the bending stiffness and the total weight but results as well in an increase of the shear deformations so that the total benefit to the deflection behavior is slight.

The original web thicknesses could, however, be increased somewhat to reduce the shear deformations with relatively small penalty in weight.

It is recognized here that definite side constraints must be imposed on the sizes of the flange and plate members. Making the web or flange plates too thin can invite breakage or even buckling. If the

99

LIGHTWEIGHTED MIRROR
TRIANGULAR CELL
DEFLECTION CONTOURS

SOLID MIRROR
DEFLECTION
CONTOURS

"EQUIVALENT BENDING
STIFFNESS" FOR LIGHTWEIGHT
DEFLECTION CONTOURS

FIG. 6-35   DEFLECTION CONTOURS OF 64" MIRRORS, 12" THICK

(Deflections x $10^{-6}$ in.)

TABLE 6-6

LIGHTWEIGHT - VARIATIONS ON TRIANGULAR CELL - 64" DIAMETER MIRROR

| VARIATION | SILICA | | ULE | | CERVIT | |
|---|---|---|---|---|---|---|
| | Δ x $10^{-6}$ in. | Weight Lbs. | Δ x $10^{-6}$ in. | Weight Lbs. | Δ x $10^{-6}$ in. | Weight Lbs. |
| ORIGINAL | 54 | 885 | 58 | 885 | 49 | 1040 |
| 0.5 x WEB | 72 | 760 | 78 | 760 | 65 | 865 |
| 2.0 x WEB | 49 | 1135 | 53 | 1135 | 44 | 1295 |
| 0.5 x FLANGE | 49 | 570 | 53 | 570 | 44 | 650 |
| 2.0 x FLANGE | 53 | 1520 | 57 | 1520 | 48 | 1730 |
| 0.5 x (WEB, FLANGE) | 55 | 445 | 59 | 445 | 50 | 505 |
| 2.0 x (WEB, FLANGE) | 53 | 1770 | 57 | 1770 | 48 | 2020 |
| 0.5 x DEPTH | 139 | 730 | 150 | 730 | 125 | 830 |
| 2.0 x DEPTH | 31 | 1200 | 33 | 1200 | 28 | 1370 |
| 1 1/2" BACK PLATE REMOVED | 87 | 505 | 94 | 505 | 78 | 575 |

flange plate becomes too thin relative to the web stiffness and cell size, then the likelihood of the cell "imprinting" on the mirror figure becomes higher.

From the deflections and weights in Table 6-6 certain trends can be observed on the direction for optimizing the design of the lightweight mirror. If it is assumed that the structure with the least absolute deflection is optimal, then the solid unlightweighted configuration is a good candidate. Conversely, if a strictly minimum weight criterion is applied, then the least deforming mirrors may not be a good choice. If a minimum flexibility structure is proposed, i. e., least deflection to load (weight) ratio, then the solid mirror, and other heavier candidates will be acceptable. In effect, for a lightweight mirror, both weight and deflection must be reduced simultaneously. It is still not certain how this criterion should be analytically expressed.

If it is assumed, however, that both weight and deformation have equal significance, then a merit comparison could be implemented. In Table 6-7, the rank of the various mirror configurations with respect to weight and deformation are presented, and a composite ranking made on the average of both. The trends still very strongly point towards decreasing the flange, increasing the web and depth. Different mirror materials, incidentally, have little effect on this rank, unless perhaps beryllium or magnesium are considered.

TABLE 6-7

MERIT COMPARISONS

64" DIAMETER

| STRUCTURE | RANK | | |
| --- | --- | --- | --- |
| | WEIGHT | △ | TOTAL |
| TRIANGLE | 8 | 7 | 7 |
| SQUARE | 7 | 10 | 11.5 |
| HEXAGON | 6 | 8.5 | 6 |
| SOLID 12" MIRROR | 13 | 3 | 9.5 |
| TRIANGLE VARIATIONS | | | |
| 0.5 x WEB | 5 | 11 | 9.5 |
| 2.0 x WEB | 9 | 3 | 4 |
| 0.5 x FLANGE | 2 | 3 | 1 |
| 2.0 x FLANGE | 10 | 5.5 | 8 |
| 0.5 x (WEB, FLANGE) | 1 | 8.5 | 2 |
| 2.0 x (WEB, FLANGE) | 12 | 5.5 | 13 |
| 0.5 x DEPTH | 4 | 13 | 11.5 |
| 2.0 x DEPTH | 10 | 1 | 3 |
| 1 1/2" BACK PLATE REMOVED | 2 | 12 | 5 |

## 6.6 Segmented Mirror-Support Study

In the general case the active segmented mirror concept can include untold possible combinations of individual segments. If these are constrained to being geometrically compatible, repeatable and easy in manufacture, and to form a multiply symmetrical whole, then the possibilities drop significantly. One configuration that has been proposed is the hexagon surrounded by parts of other hexagons (Fig. 6-36). The structural design objective here is to find that combination of segments which deforms least under the environmental conditions. It should be recognized that while the system is an active one, it is nevertheless based on the assumption that the segments have, individually, small surface deviations.

It is assumed that the major design loadings result from testing in a 1g environment with a vertical optical axis. The design objective is to minimize the deformations over the sum of the segments. The system is assumed to consist of originally plane mirrors, and deformations will be obtained through finite element analysis with bending elements. A new, best-fit plane will then be determined, and the root mean square (rms) deviation from that plane computed. The combination that has the least rms error will be considered optimal.

Optimal support locations are determined for each segment so as to minimize the individual rms displacement. As the opening in the central hexagon remains constant, the support locations are differently proportioned at each size. This is true of the outer segments as well. Assuming that all segments have the same thickness, the rms of the entire system can then be computed at the various segment proportions.

A definite optimum range can be observed in the graph on Fig. 6-36. In the limit where A approaches B, the outer segments disappear and the mirror center experiences large deformations caused by long spanlengths. As A tends smaller, the opening in the inner

segment limits further decrease while the outer segments have acquired considerable spanlengths. This effect is, of course, not so intense as when A = B, since the supports total 18 versus 3.

Using existing programs this study can be extended to other geometrical combinations, to curved mirrors and other loading conditions.
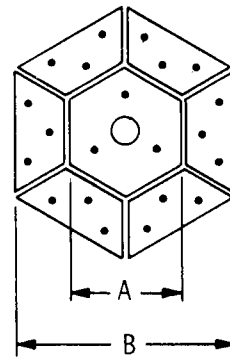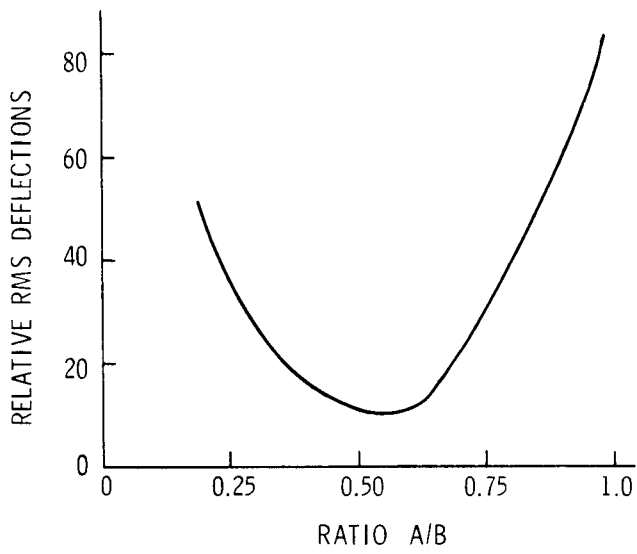
NOTE: UNIFORM THICKNESS AND
ELASTIC PARAMETERS
SELF-WEIGHT LOADING
PARALLEL TO OPTICAL
AXIS

Fig. 6-36   Segmented mirror proportions.

## 6.7 Active Flexible Mirror

The active flexible mirror is analyzed as a thin, shallow shell. The same element plan-view layouts as in Fig. 6-1 and 6-14 are used, but each element node has a Z component as well. At this preliminary stage, the mirror is considered to be assembled from a series of flat triangular plates with the nodes on a sphere with each element acting in both bending and stretching. The mirrors studied here are 120" in diameter, of uniform thickness and with a 480" radius of curvature. Mirror material properties used were for silica, although other material effects can be obtained by simple scaling.

The objectives here are to determine the range of validity of the shallow shell, as opposed to a pure bending approach for the mirror, to establish the effect of mounting the mirror horizontally, to test some of the automatic interpretation routines and to evaluate some necessary parameters for the actuator designs.

As no attempt is to be made here to determine the optimum location for the fixed supports for the flexible mirrors, the three-point edge support will be used throughout the analysis.

Table 6-8 summarizes a number of finite element studies for the gravity loading case parallel to the optical axis. Three different mirror thicknesses were analyzed both in the shallow shell and flat plate cases and the mirrors were assumed to be solid. It is evident upon comparing the maximum deflections for the six cases that significant differences occur when the shells and plates are both thin, but minimal differences can be observed when both are 10" thick. The data thus demonstrates the much greater efficiency of the shell action for load carrying purposes, as opposed to the pure bending action.

The distribution of the deflections differs considerably between the two cases in the 1" thickness. Fig. 6-37, which represents the shell deformations, has the maximum deformations at the edge, while the plate deforms maximally at the center (Fig. 6-38). This is to some degree evident in the 2" thick mirrors, Fig. 6-39 and 6-40, but

TABLE 6-8   CURVED VS FLAT MIRROR - SOLID

| | | MIRROR THICKNESS | | |
|---|---|---|---|---|
| | | 1" | 2" | 10" |
| MAXIMUM DEFLECTION (inches) | CURVED | 0.093 | 0.023 | 0.0013 |
| | FLAT | 0.134 | 0.034 | 0.0013 |
| ACTUATOR D/F (inches/lb.) | CURVED | $2.4 \times 10^{-4}$ | $3.5 \times 10^{-5}$ | $3.5 \times 10^{-7}$ |
| | FLAT | $2.4 \times 10^{-4}$ | $4.5 \times 10^{-5}$ | $3.5 \times 10^{-7}$ |
| CURVED CORRECTED TO SPHERE, FLAT TO PLANE | | | | |
| SPHERE RADIUS (inches) | CURVED | 478.75 | 479.18 | 479.87 |
| OPT. PATH DIFF. (maximum in inches) | CURVED | 0.092 | 0.023 | 0.0046 |
| | FLAT | 0.134 | 0.034 | 0.0013 |
| RMS DEFLECTION (inches) | CURVED | 0.023 | 0.0068 | 0.0039 |
| | FLAT | 0.035 | 0.0086 | 0.00034 |

the distribution and magnitudes are almost identical for both 10"
cases. These can be seen in Figs. 6-41 and 6-42.

When the mirrors have a center opening, as in a Cassegrain
system, similar observations can be made. Table 6-9 summarizes
this data for 1" and 10" mirrors. Again the differences are significant
for the thin mirrors, but are minimized as the thickness increases.
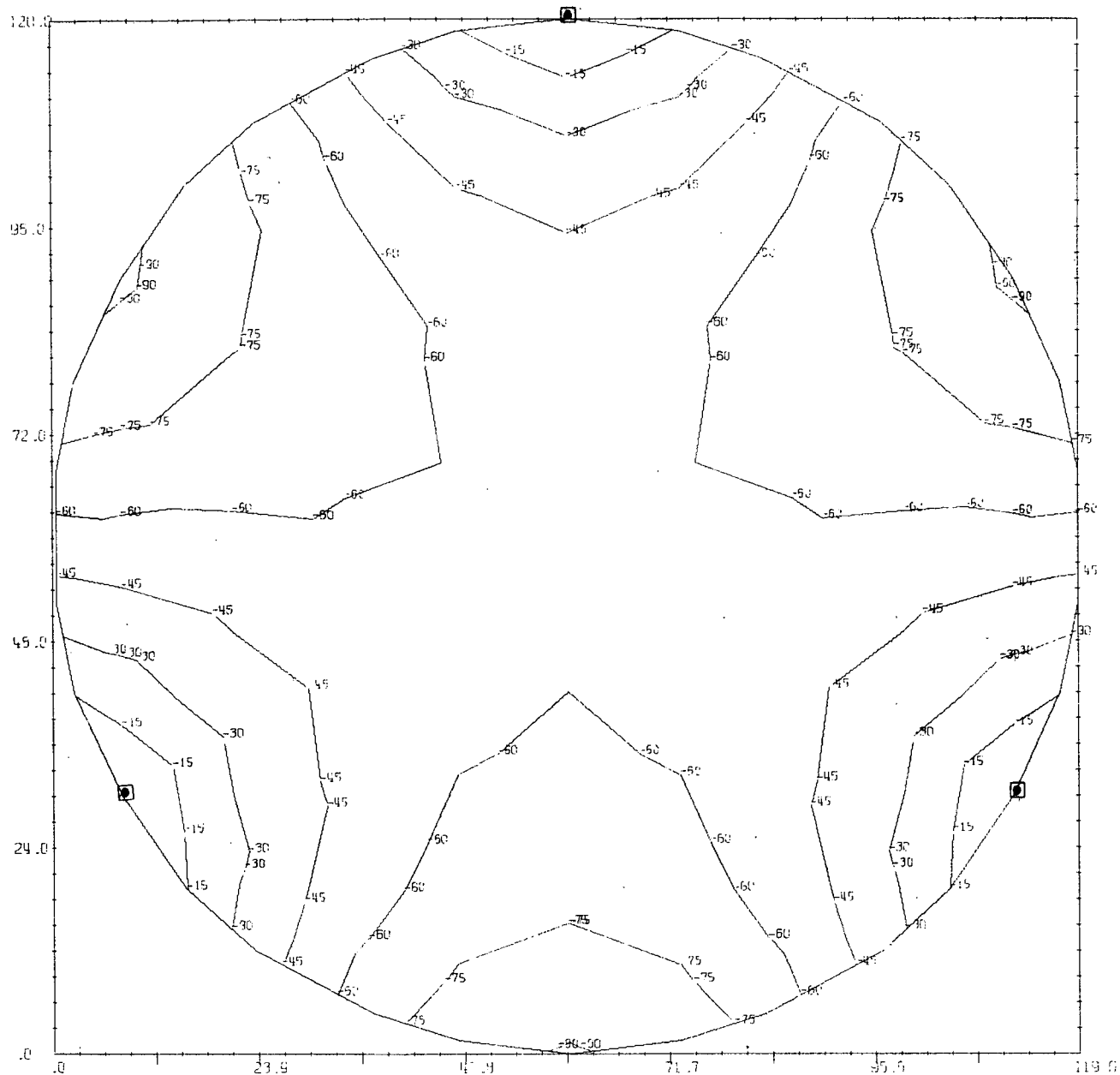
Fig. 6-37 Curved mirror 1" thick — optical axis vertical.

(scale x $10^{-3}$ inches)

◙ SUPPORTS

110
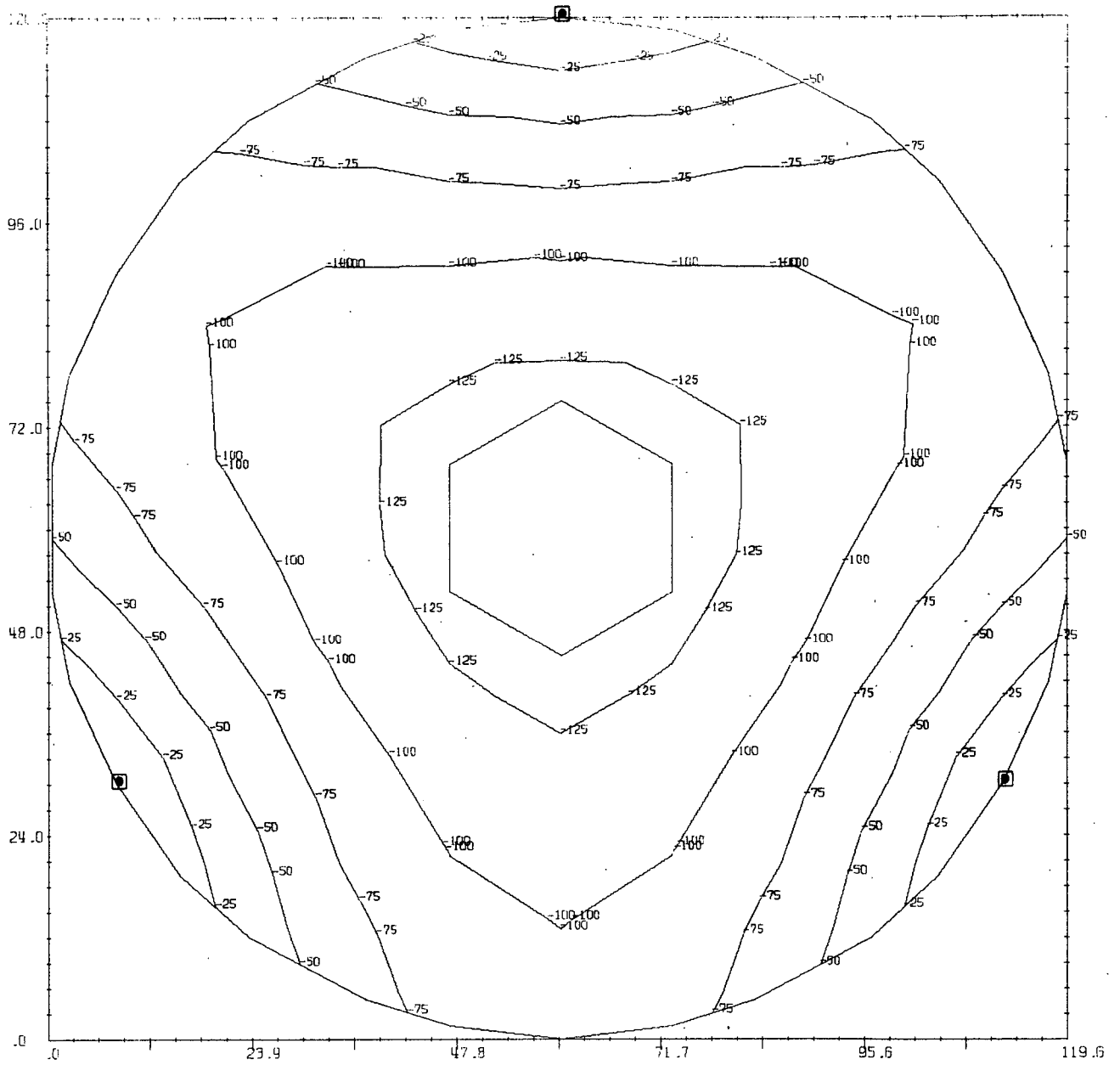
Fig. 6-38   Flat mirror 1" thick — optical axis vertical.

(scale x $10^{-3}$ inches)

◙ SUPPORTS

111
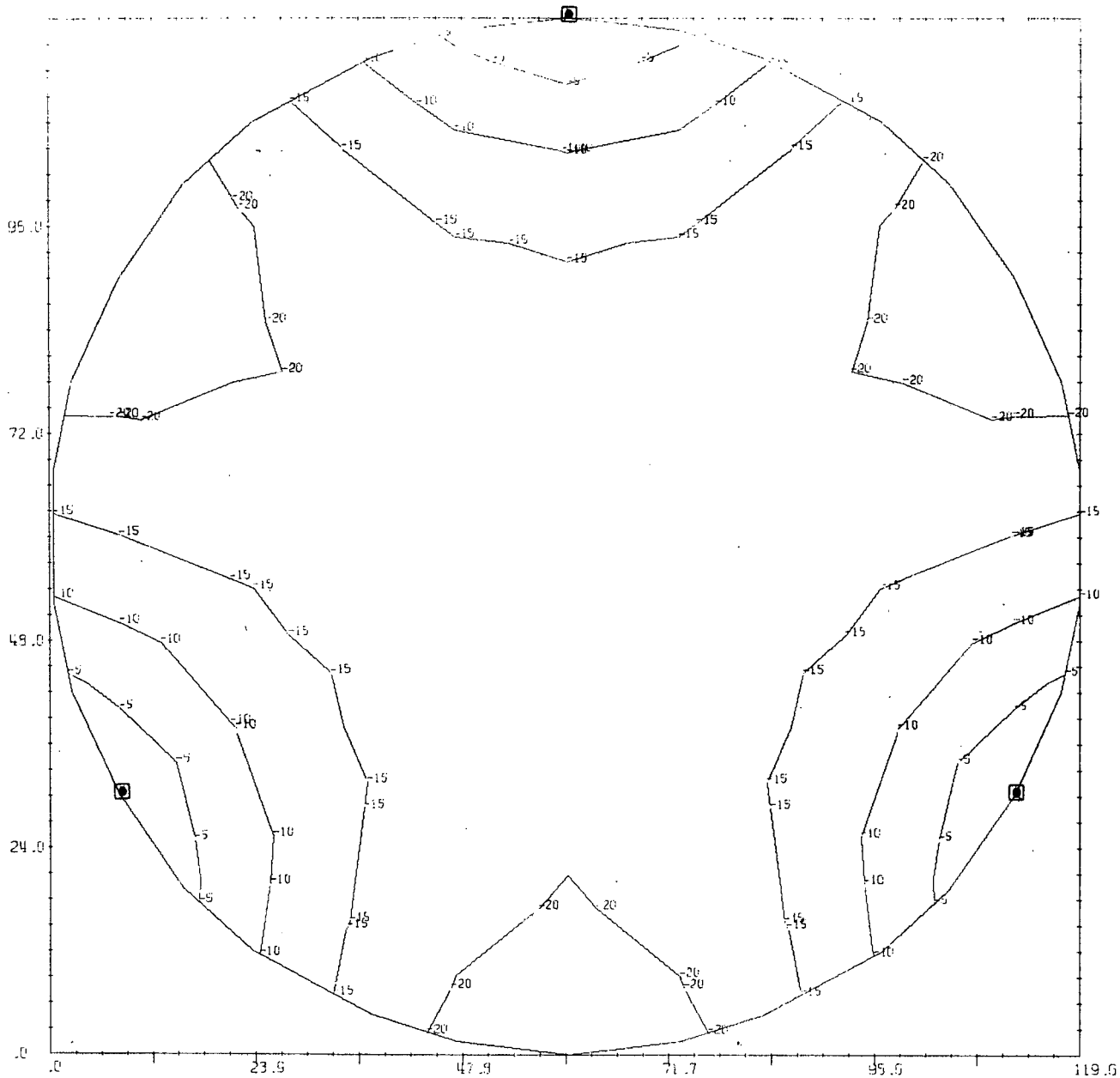
Fig. 6-39 Curved mirror 2" thick — optical axis vertical.

(scale x $10^{-3}$ inches)

◙ SUPPORTS

112
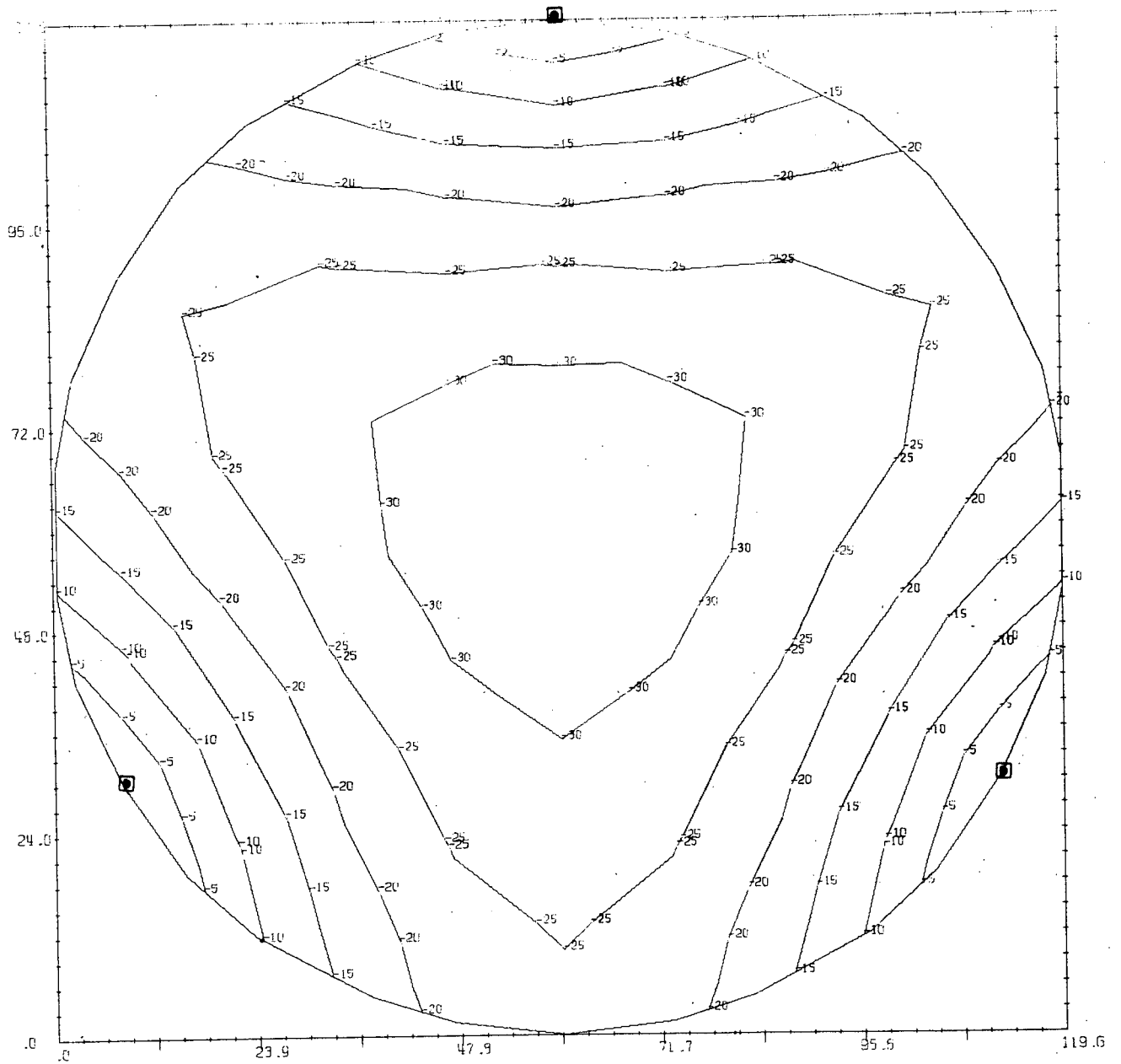
Fig. 6-40    Flat mirror 2" thick — optical axis vertical.

(scale x $10^{-3}$ inches)

◙ SUPPORTS

113

C3
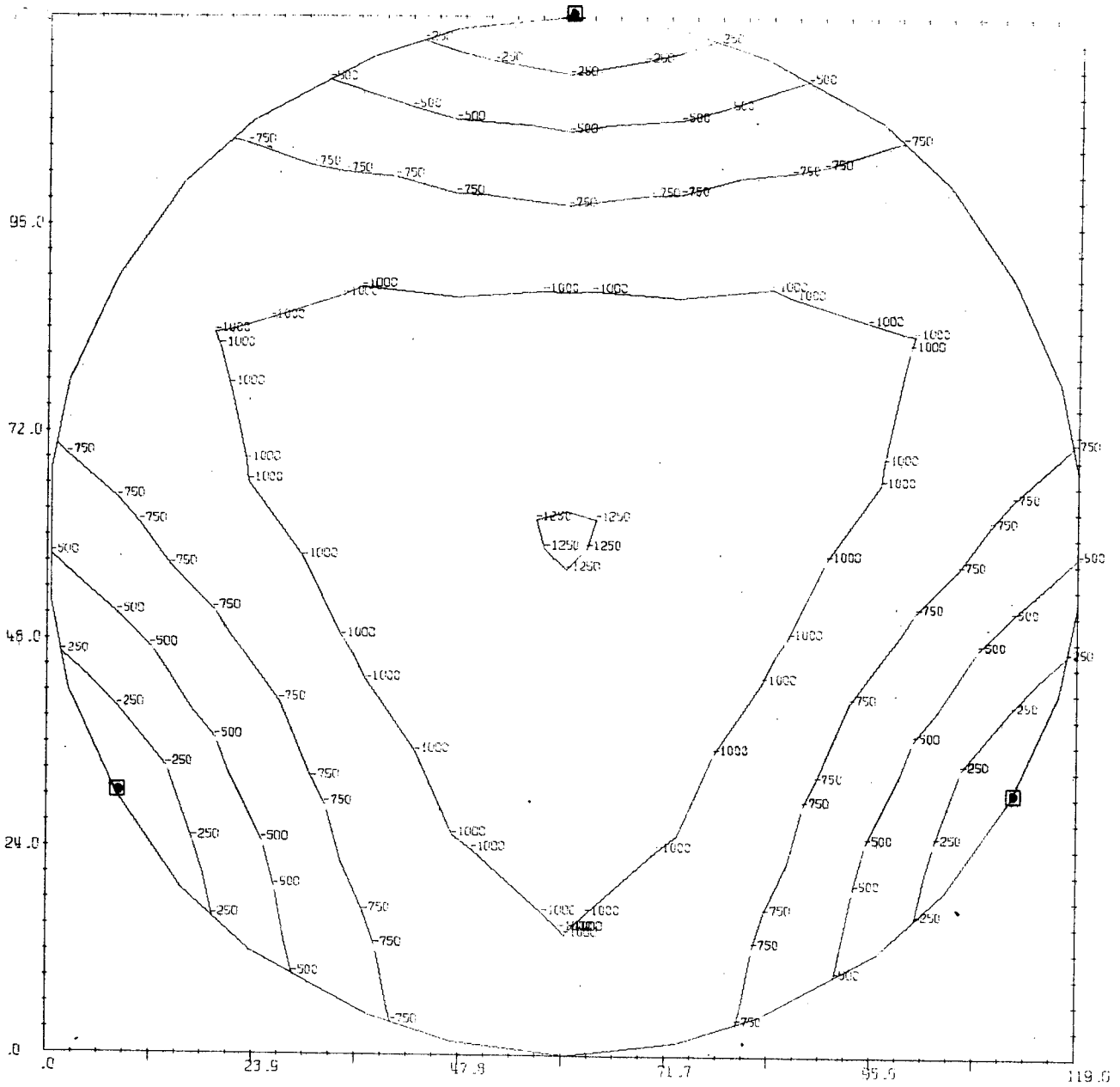
Fig. 6-41 Curved mirror 10" thick — optical axis vertical.

(scale x $10^{-6}$ inches)

◙ SUPPORTS

114
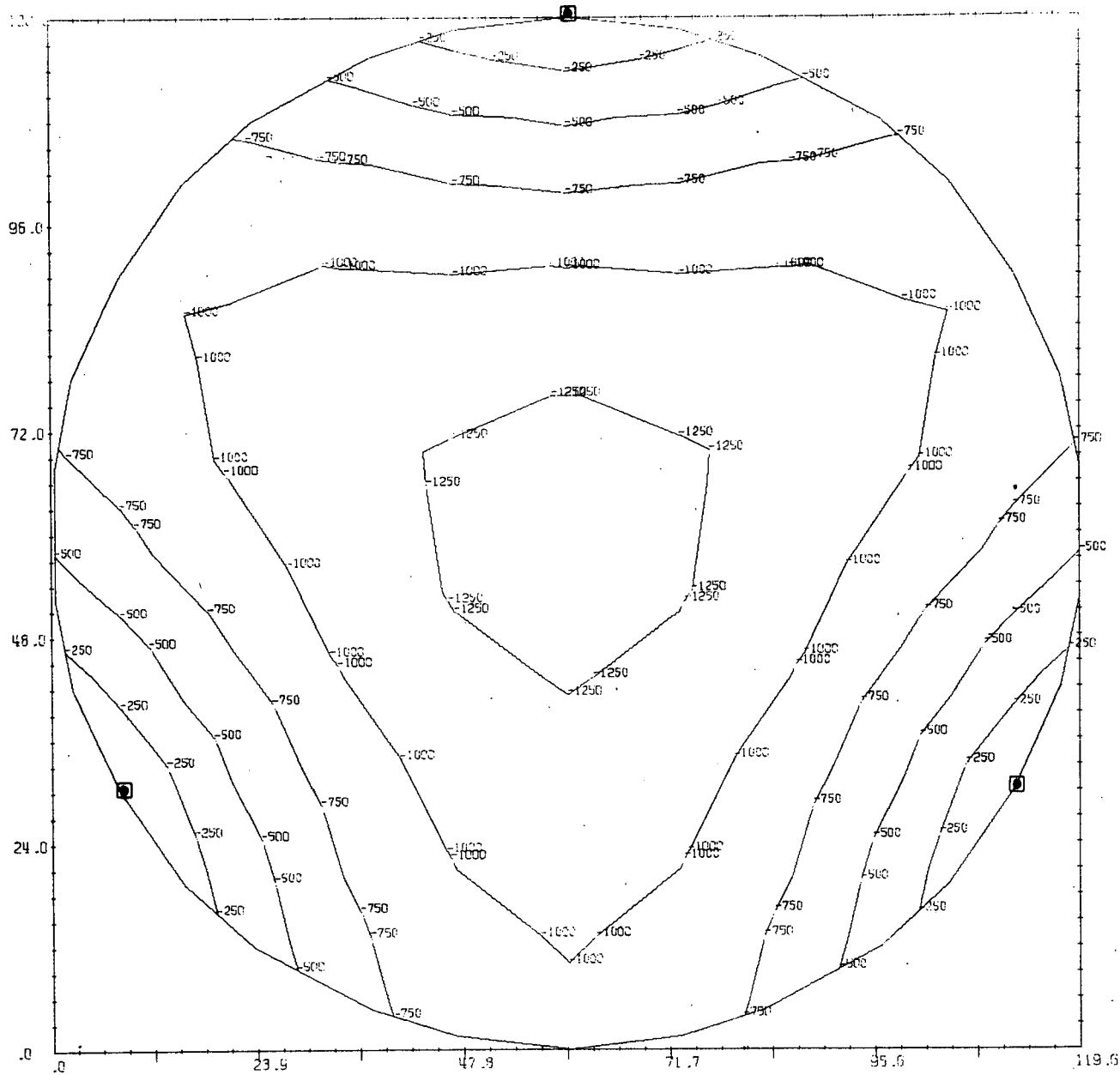
Fig. 6-42   Flat mirror 10" thick — optical axis vertical.

(scale x $10^{-6}$ inches)

◙ SUPPORTS

115

TABLE 6-9   CURVED VS FLAT MIRROR - OPEN

| | | MIRROR THICKNESS | |
|---|---|---|---|
| | | 1" | 10" |
| MAXIMUM DEFLECTION (inches) | CURVED | 0.088 | 0.0013 |
| | FLAT | 0.1367 | 0.0014 |
| ACTUATOR D/F (inches/lb.) | CURVED | $2.6 \times 10^{-4}$ | $3.9 \times 10^{-7}$ |
| | FLAT | $4.0 \times 10^{-4}$ | $4.0 \times 10^{-7}$ |
| CURVED CORRECTED TO SPHERE, FLAT TO PLANE | | | |
| SPHERE RADIUS (inches) | CURVED | 478.79 | 479.86 |
| OPT. PATH DIFF. (inches maximum) | CURVED | 0.088 | 0.005 |
| | FLAT | 0.1367 | 0.0014 |
| RMS DEFLECTION (inches) | CURVED | 0.021 | 0.0044 |
| | FLAT | 0.036 | 0.00036 |

If the mirrors are so mounted that the optical axis is normal to the gravity direction, then a reduction in the deformation field is observed. This test is obviously meaningless with a flat mirror, as a plane stress condition would produce uniform out-of-plane deformations unless very precise solid elements were used.

With the shell structure it is a very meaningful test and the surface deformations are reduced by almost an order of magnitude (Table 6.10), though relatively less in the thicker shells as the local bending of the shell is diminished. The figures 6-43, 6-44, and 6-45 demonstrate this effect. The mirrors, incidentally, are supported at three equidistant points on the rim, in a statically determinate manner.

The automatic interpretation routines were tested on the deformation results of these mirrors. A best-fit sphere was determined for the curved mirrors and a best-fit plane for the flat ones. Maximum optical path difference, and the RMS deviation from the best-fit surface for each case. It is evident that fitting a sphere to deformation results produced by three-point supports does not necessarily improve the results. Curve-fitting with continuous edge supports would certainly have decreased the residuals. Because of time and funding constraints, this unfortunately could not be done. Essentially these comments cover all of the Tables 6-8, 6-9, and 6-10, where all results are interpreted in this manner. Programs have been written, but not tested, to fit parabolas and hyperbolas as well. Figs. 6-46 and 6-47 show plots of the residual deformations resulting after a best-fitting sphere has been passed through the displacements originally plotted in Figs. 6-37 and 6-43.

TABLE 6-10    EFFECT OF OPTICAL AXIS ORIENTATION

| | | MIRROR THICKNESS | | |
| --- | --- | --- | --- | --- |
| | | 1" | 2" | 10" |
| MAXIMUM DEFLECTION (inches) | V | 0.093 | 0.023 | 0.0013 |
| | H | 0.013 | 0.003 | 0.00013 |
| ACTUATOR D/F (inches/lb.) | | $2.4 \times 10^{-4}$ | $3.5 \times 10^{-5}$ | $2.4 \times 10^{-7}$ |

| RESULTS CORRECTED TO BEST-FIT SPHERE | | | | |
| --- | --- | --- | --- | --- |
| SPHERE RADIUS (inches) | V | 478.75 | 479.18 | 479.87 |
| | H | 479.89 | 479.91 | 479.96 |
| OPTICAL PATH DIFFERENCE (inches, maximum) | V | 0.092 | 0.023 | 0.0046 |
| | H | 0.019 | 0.007 | 0.0045 |
| RMS DEFLECTION (inches) | V | 0.023 | 0.007 | 0.0039 |
| | H | 0.006 | 0.005 | 0.0042 |
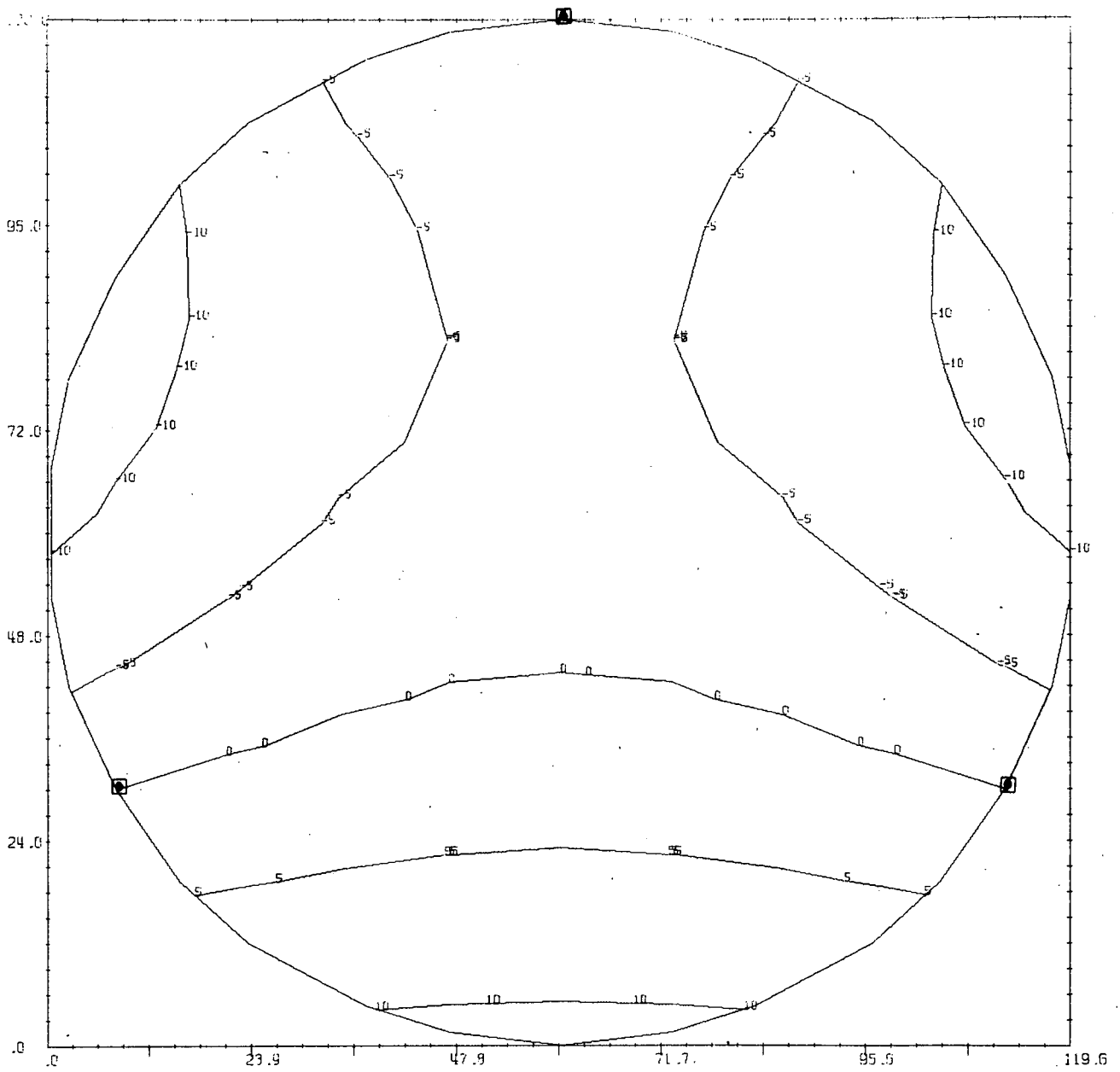
Fig. 6-43  Curved mirror 1" thick — optical axis horizontal.

(scale x $10^{-3}$ inches)

▣ SUPPORTS

119
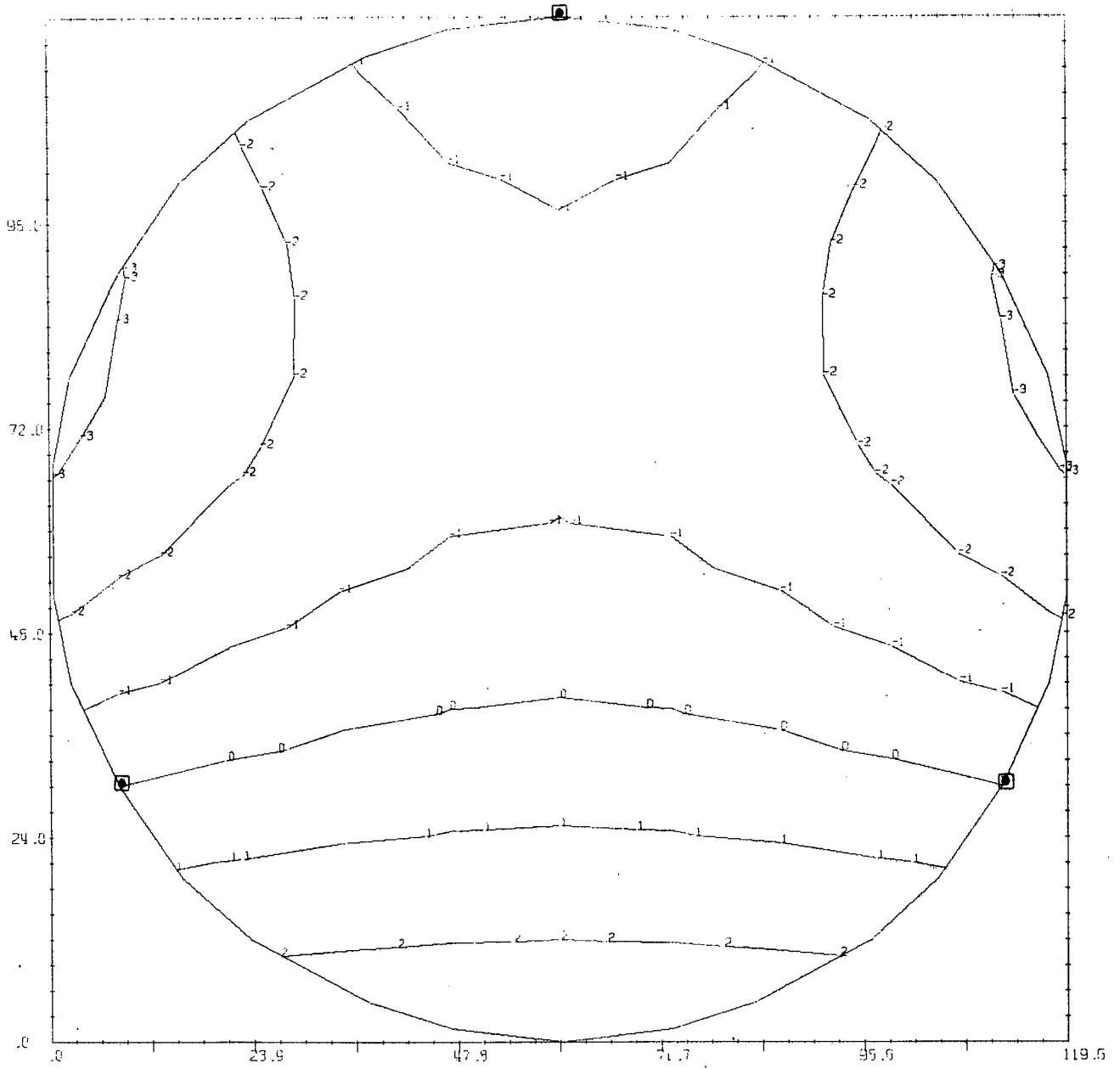
Fig. 6-44   Curved mirror 2" thick — optical axis horizontal.

(scale x $10^{-3}$ inches)
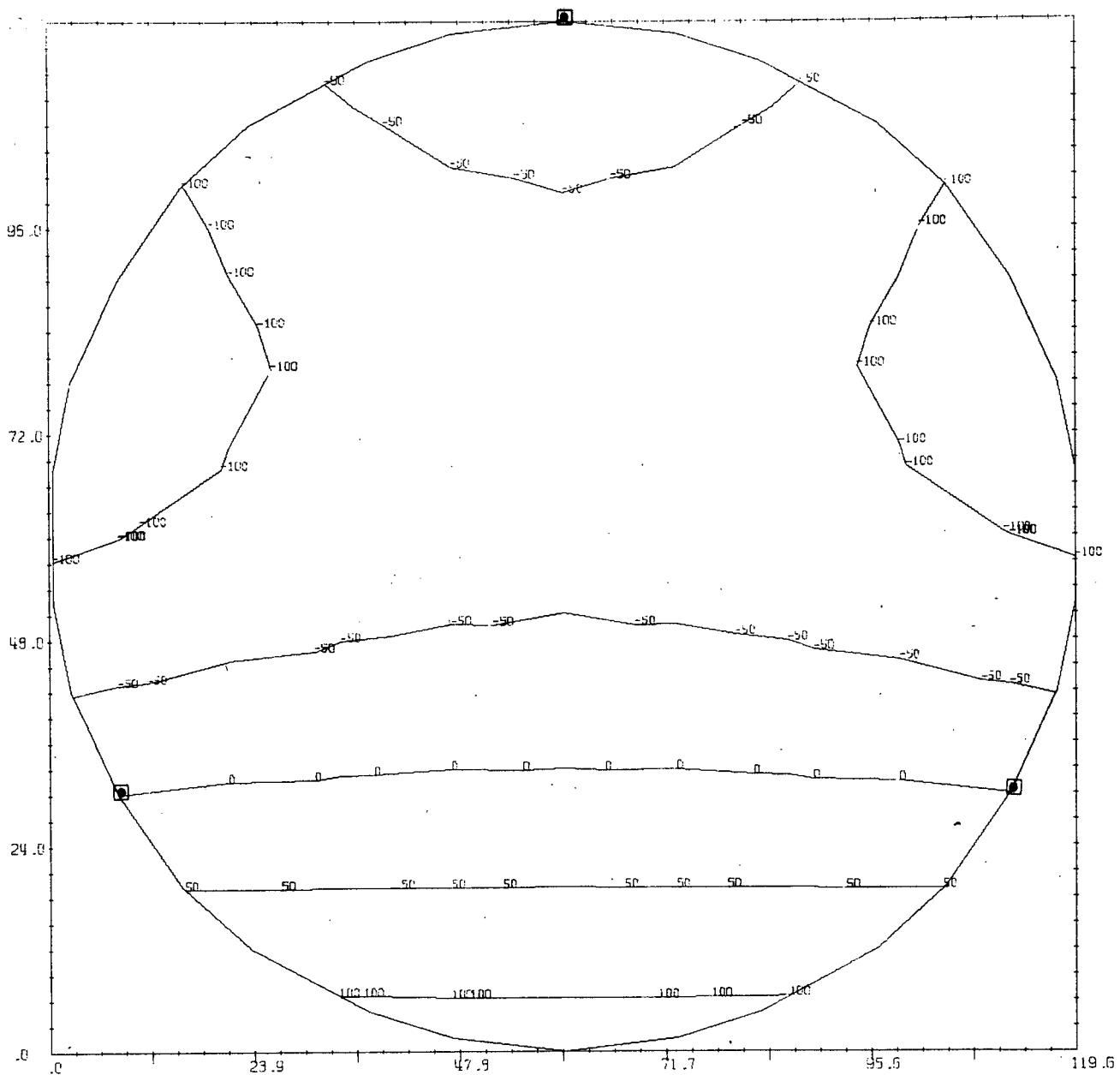
◙ SUPPORTS

Fig. 6-45 Curved mirror 10" thick — optical axis horizontal.

(scale x $10^{-6}$ inches)

◙ SUPPORTS

121
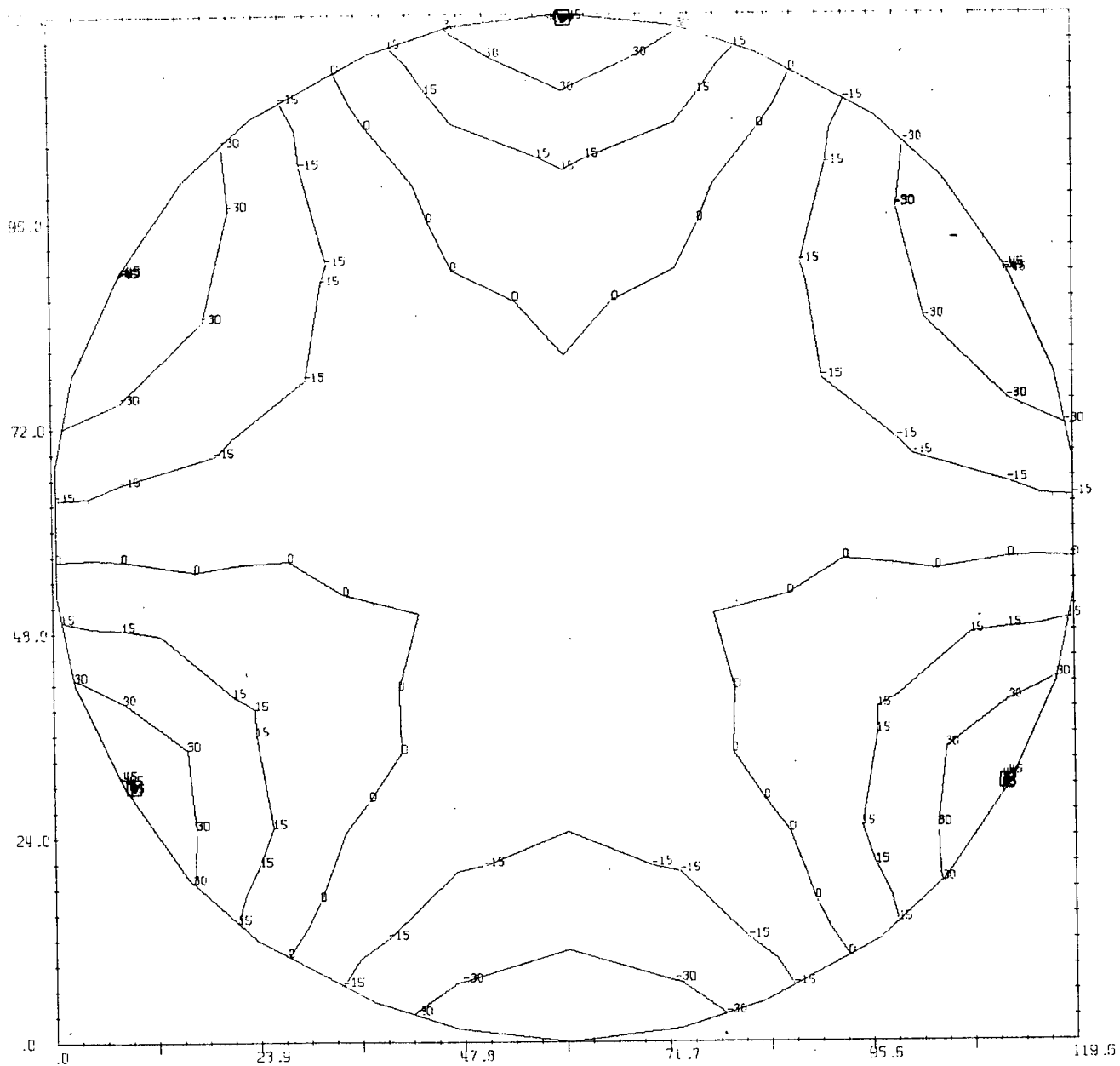
Fig. 6-46   Curved mirror residuals of best-fit sphere, to Fig. 6-37.

(scale x 10$^{-6}$ inches)
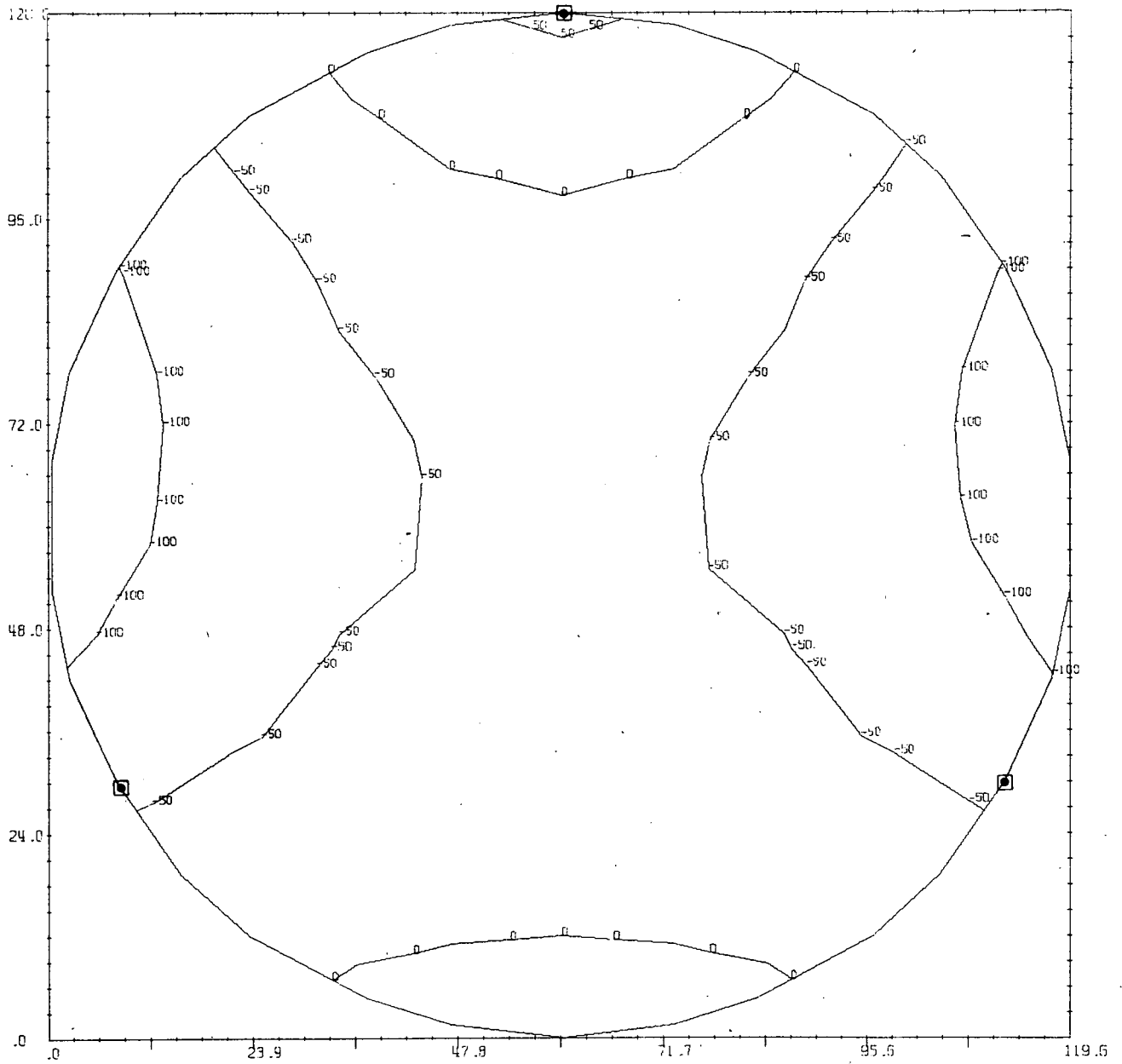
▣ SUPPORTS

Fig. 6-47   Curved mirror residuals of best-fit sphere, to Fig. 6-43.

(scale x $10^{-4}$ inches)

◙ SUPPORTS

The effects of actuators on the mirror can be determined in several ways. The simplest criterion is to evaluate the mirror on the basis of deformation under a unit load at a given point in all mirrors. This data is shown in Tables 6-8, 6-9, 6-10, and this data simply compares the relative stiffnesses of the mirrors to load concentrations. It is evident here that the curved mirror is much stiffer than the flat, if both are thin, but the difference disappears quite rapidly with increasing thickness.

A more meaningful comparison is based on using a number of symmetrically placed actuators and using these to cancel out a given mirror disturbance, such as the gravity effect. From such a study the required actuator strength and stroke length can be obtained. It is assumed here that the actuators will move to cancel out the disturbances at their own locations only. This is identical to the simplified linear control algorithm as defined by MacKinnon, et al. [23]

An influence surface study is performed on the structure in Fig. 6-14. A unit load is placed at each element node in turn and the resulting deflections at all nodes are obtained. Therefore to eliminate the deflection at a node

$\Sigma$ (deflection contributions) = disturbance actuators

or

$$[\Delta] \bullet (R) = (D) \tag{6-11}$$

where

$\Delta_{ij}$ = influence matrix of deflections at actuator location i due to unit force by actuator at location j (reduced flexibility matrix)

$R_j$ = vector of participation coefficients of actuators j (actuator forces)

$D_i$ = disturbance at actuator location i (deflection)

Matrix $\Delta$ is inverted, and values of R can be obtained for each set of D.

124

Distributing the actuators over approximately equal tributary areas, configurations of 3, 6 and 9 actuators are considered. The results of this study can be seen in Figs. 6-48, 6-49, 6-50 and Table 6-11.

Four types of disturbance are considered. First, the mirror is assumed mounted with its optical axis vertically and the deformation pattern as shown in Figs. 6-37 through 6-42 can be observed. Then the optical axis is turned horizontally (Figs. 6-43 through 6-45) and the disturbing deformations recorded. Finally, it is assumed that thermal errors of a maximum amplitude of $100\lambda$ and $1\lambda$ occur on the mirror and have a distribution similar to the gravity deformations. From this an estimate can be made of the in-orbit needs of the active mirror.

Table 6-11 summarizes these results for the 1" curved-shell mirror. It is evident that with an increase in the number of actuators, the load and stroke requirements of the actuators are reduced. It is also evident that to cancel the full gravity effects, very powerful actuators are needed if only a few will be used.

The mounting of the mirror on a horizontal axis reduces the actuator requirements for gravity loads by about an order of magnitude (Fig. 6-48). The value of the thermal disturbance used is a purely arbitrary number, as the actual disturbance is still unknown. If the actual thermal errors lie in this range, then the in-orbit actuator requirements appear not as severe.

It is strongly evident, however, that in order to test such a mirror with actuators in the earth's gravity field, the test actuators will have to be different from the in-orbit devices, or some other means be found to support the weight of the mirror.

In the limit, assuming that each actuator is to carry two lbs. of the mirror weight, the actuators will be spaced closely enough so that the actuator surface force is statically equivalent to the gravity force (by Saint Venant's Principle) and the weight of the mirror is approximately 800 lbs. per inch of thickness; then a total of 400 actuators (per inch of mirror thickness) will be required. It is not known whether a 1" thick, 120" diameter mirror can be fabricated satisfactorily. Alternately, the other limit will come from crowding the actuators.
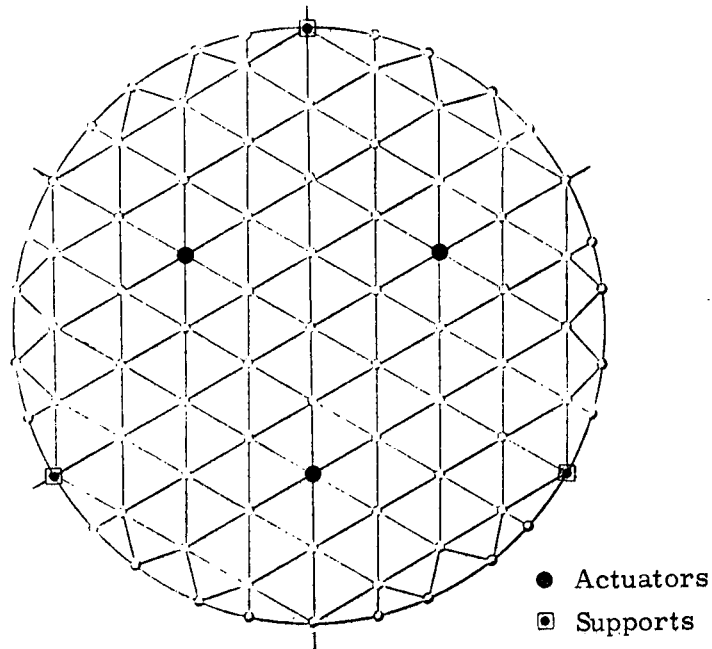
● Actuators
◉ Supports

Actuator forces in lbs., displacements in inches.

| LOADING | MIRROR TYPE | | | |
|---|---|---|---|---|
| | CURVED 1" | CURVED 10" | FLAT 1" | FLAT 10" |
| Gravity ‖ Axis | | | | |
| Act. Force (lbs.) | 247 | 2160 | 216 | 2160 |
| Act. Disp. (inch) | 0.059 | 0.00076 | 0.078 | 0.00078 |
| Gravity ⊥ Axis | | | | |
| Act. Force | 25.3 | 361 | - | - |
| Act. Disp. | 0.0061 | $126 \times 10^{-6}$ | - | - |
| Thermal 100 λ | - | | | |
| Act. Force | 7.75 | 3030 | 3.76 | 3760 |
| Act. Disp. | 0.0018 | 0.0013 | 0.00134 | 0.00134 |
| Thermal 1 λ | | | | |
| Act. Force | 0.078 | 30.3 | 0.038 | 37.6 |
| Act. Disp. | $18 \times 10^{-6}$ | $13 \times 10^{-6}$ | $13.4 \times 10^{-6}$ | $13.4 \times 10^{-6}$ |

FIGURE 6-48      3 SYMMETRICAL ACTUATORS

● Actuators
◉ Supports

Actuator forces in lbs., displacements in inches.

| LOADING | MIRROR TYPE | | | |
|---|---|---|---|---|
| | CURVED 1" | CURVED 10" | FLAT 1" | FLAT 10" |
| Gravity ⊥ Axis<br>Act. Force<br>Act. Disp. | 154<br>0.038 | 1710<br>0.00048 | 171<br>0.048 | 1710<br>0.00048 |
| Thermal of 100 λ<br>Act. Force<br>Act. Disp. | 4.10<br>0.0014 | 2730<br>0.00122 | 2.73<br>0.00122 | 2730<br>0.00122 |
| Thermal of 1 λ<br>Act. Force<br>Act. Disp. | 0.041<br>$14 \times 10^{-6}$ | 27.3<br>$12.2 \times 10^{-6}$ | 0.0273<br>$12.2 \times 10^{-6}$ | 27.3<br>$12.2 \times 10^{-6}$ |

FIGURE 6-49          6 SYMMETRICAL ACTUATORS
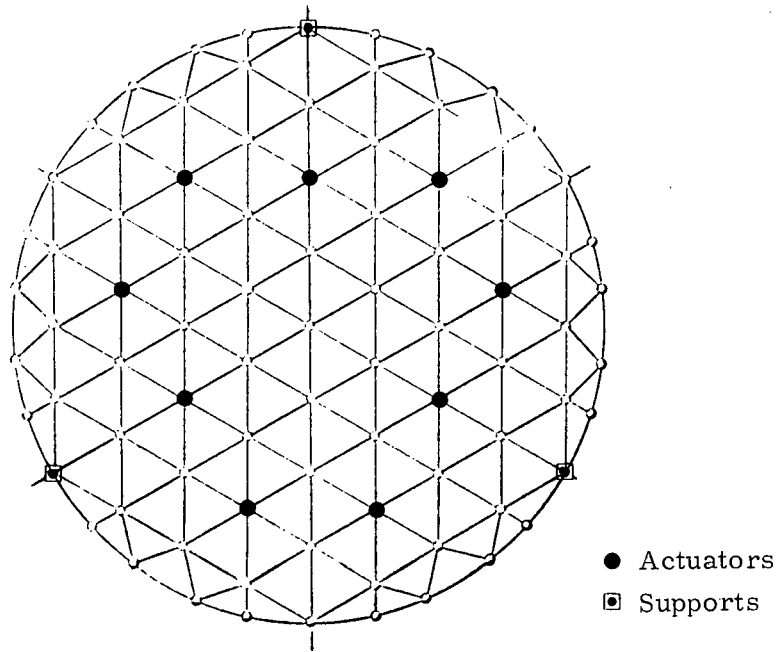
● Actuators

◉ Supports

Actuator forces in lbs., displacements in inches.

| LOADING | MIRROR TYPE | | | |
|---|---|---|---|---|
| | CURVED 1" | CURVED 10" | FLAT 1" | FLAT 10" |
| Gravity ‖ Axis | | | | |
| Act. Force | 92 | 1280 | 128 | 1280 |
| Act. Disp. | 0.0313 | 0.000296 | 0.0296 | 0.000296 |
| Thermal of 100 $\lambda$ | | | | |
| Act. Force | 2.87[#] | 2560[#] | 2.56[#] | 2560[#] |
| Act. Disp. | 0.00097 | 0.000105 | 0.000106 | 0.000106 |
| Thermal of 1 $\lambda$ | | | | |
| Act. Force | 0.0029 | 25.6 | 0.0025 | 25.6 |
| Act. Disp. | $9.7 \times 10^{-6}$ | $10.5 \times 10^{-6}$ | $10.6 \times 10^{-6}$ | $10.6 \times 10^{-6}$ |

FIGURE 6-50          9 SYMMETRICAL ACTUATORS

128

TABLE 6-11

CURVED 1" MIRROR -- ACTUATOR EFFECTS

Actuator forces in lbs., movement in ins.

| GRAVITY LOADING PARALLEL TO OPTICAL AXIS | | |
|---|---|---|
| ACTUATOR ARRANGEMENT | ACTUATOR FORCE | ACTUATOR MOVEMENT |
| 3 Symm. | 247 | 0.059 |
| 6 Symm. | 154 | 0.038 |
| 9 Symm. | 92 | 0.031 |
| THERMAL DISTORTION OF 100 $\lambda$ | | |
| 3 Symm. | 7.75 | 0.0018 |
| 6 Symm. | 4.10 | 0.0014 |
| 9 Symm. | 2.87 | 0.00097 |

These calculations have assumed, of course, that the actuators are infinitely stiff and are supported by an absolutely rigid reaction-plate. To refine the calculations further, the actuator influence matrix should be obtained using the designed stiffnesses of the actuator and supporting mechanisms.

While it is possible to obtain a perfect mirror figure measured at the actuator locations only, some amount of residual "ripple" will remain in the mirror. This can be evaluated using the Strehl ratio technique described in Chapter 5 to determine the effect on diffraction. Assuming that approximately 200 actuators will eventually be used, a finite element study must be performed to study this ripple effect, using at least 3 elements between actuators. With a triangular grid, this would require a minimum of 1400 nodes, each with 6 degrees of freedom with a fairly ill-conditioned structural system. This task will be attempted only at the very last stages of such a structural study, as the preparation time and running times will be quite astronomical. Until this is really needed, approximate approaches will be employed.

Further studies on the active mirror should include the extension of the influence matrix approach to many actuators and to more anti-symmetrical and asymmetrical disturbances. When actuator and support stiffness data becomes available these, too, will be included in the influence matrix.

# CHAPTER 7

# SUMMARY AND CONCLUSIONS

1. Finite element structural analysis methods have been developed and implemented for all types of optical mirror structures undergoing all types of loading.

2. Necessary computer graphics and interpretation aids have been developed. A plotting routine to verify geometric compatibility of the finite element input for complex structures has been developed. Other routines to determine best-fit surfaces for deformed mirror data, to automatically compute the optical path difference, Strehl ratio, and to plot deformation and best-fit residuals data have been developed, and to the most part, debugged.

3. The environmental conditions that the mirror will experience have been outlined. Information is still lacking on systems-dependent conditions, such as launch environment and thermal distributions. When these become available, they will be used in the existing programs for detailed design studies.

4. An evaluation of candidate mirror materials has been conducted, and the present study has included as possible candidates fused silica, ULE, CER-VIT and beryllium. Due to manufacturing reasons it seems likely that beryllium will not be available at the 120" size.

5. Using the finite element approach, a large amount of data has been collected on the behaviour of plate, slab, "lightweight, "

shell and other mirror types. Good correspondence has been obtained with the closed-form solutions, where these are available, and considerable confidence is expressed in the validity of the results.

6. There is at this time insufficient evidence to favor any one structural configuration over any other for the 3-meter mirror of the Large Space Telescope. The necessary structural analysis tools are now available, and further data must be sought on environments and material properties.

# CHAPTER 8

# SUGGESTIONS FOR FURTHER DESIGN STUDIES

While the initial period in this study has concentrated primarily on the compilation of material, environmental, and design criteria, and on the formulation, production and verification of analysis methods, the next stage should be aimed towards producing a preliminary design for the 3-meter mirror structure. Some of the areas that must be covered during this phase include:

1. Inclusion of real mirror supports into the analysis phase. While idealized support conditions are very valuable for parametric studies, the actual operating deflections of the mirrors can only be obtained by a joint mirror-support study.

2. While there is considerable consistency in the finite element results, within themselves and also with closed-form solutions, the comparison of theory and laboratory experiment is very necessary for absolute confidence. Since the level of accuracy can be controlled in the finite element approach by increasing the number of finite elements, some experimentally-derived guide-lines are most desirable for both monolithic and lightweighted mirrors.

3. As the mirror is manufactured under earth gravity conditions, orbital operation would tend to relieve some of the internal stresses. It should be determined whether the level of internal stress could be near the failure level and whether the resulting deformations tend to degrade the mirror figure.

133

4. Further parametric studies should be performed on the lightweight and deep slab mirrors in order to establish definitely the detailed optical surface deformation patterns with respect to the mirror support types and locations.

5. Some tradeoff studies should be performed on the cell type, mirror depth and plate thicknesses in lightweight mirrors. Existing configurations do not appear to be especially optimal.

6. Further support studies should be performed on the shallow shell flexible mirror. The location of the supports or actuators; the stiffnesses necessary in the mirror to avoid local "dimpling" by the actuators, the strength and stroke of the actuators should be defined in a manner including both the control system and structure optimization.

7. When the (elastic) support conditions for the various mirrors have been defined, dynamic studies including both mirrors and the supports must be performed. Individually performed, the tests might be quite meaningless.

# APPENDIX A

## A GENERAL STRETCHING AND BENDING PLATE ELEMENT

For the analysis of problems where both stretching and bending are relevant, a pair of new elements was added to the STRUDL II system.

The addition of these new elements, called "GSBPE" and "GSBTE," permits the analysis of any continuous system composed by a series of planes, normal to each other and subjected to external loads producing a stretching and bending behavior; a typical example is the folded plate problem that arises in the analysis of "lightweight" or ribbed mirror structures.

"GSBPE" is rectangular in shape and "GSBTE" is triangular and with the characteristics described in Reference (3), Chapters 3 and 7. The element stiffness matrix includes a stretching part and a bending part, which are uncoupled. The stiffness matrix is first assembled in the local reference frame which is related to the plane in which the element lies, and then rotated to a unique global reference frame. During the assembly of the total stiffness matrix, the inter-action among different planes is brought into evidence. Two different types of nodal points must be established (Fig. A-1). The first type, to be called intersection node, includes the nodes connecting elements lying in different planes. The second kind, to be called simple node, includes nodes connecting elements lying in the same plane. For simple nodes the number of degrees of freedom to be considered is equal to 5: 3 displacement components and 2 rotations. The normal rotation, negligible for problems of this type, is not included. For intersection nodes six degrees of freedom are considered, including

135

E      generalized bending and stretching elements
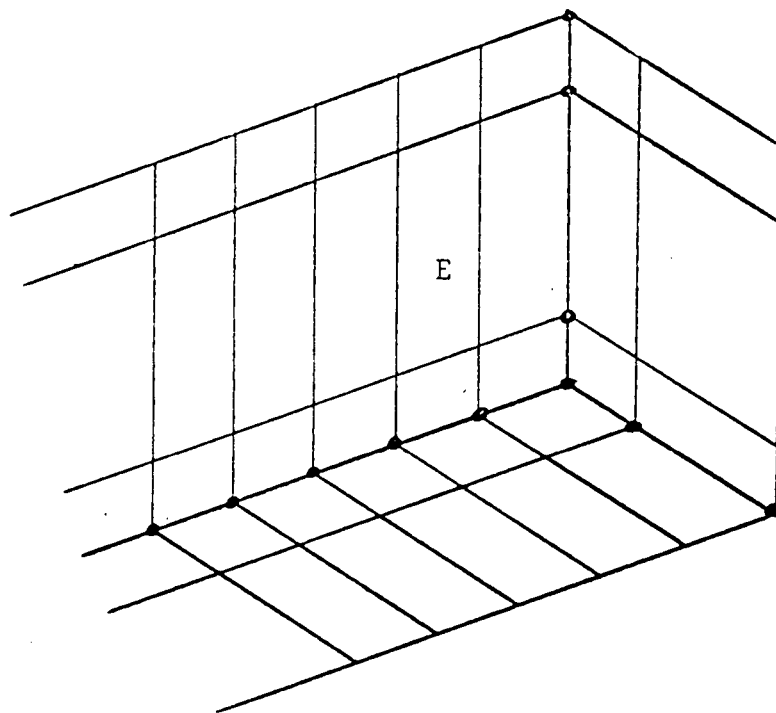
●     intersection nodes

┼     simple nodes

Fig. A-1. Intersection and simple nodes

three displacement components and three rotations, thus taking into account the proper interaction between the different planes.

The type of external loads which can be processed are nodal loads. Distributed loads are simulated by lumping the equivalent nodal loads. The material properties are represented by Young's modulus and poisson's ratio. The material is assumed to be homogeneous and isotropic, but the material properties may vary from element to element.

The results produced yield the nodal displacements and rotations, and element stresses, stress resultants, stress couples, and principal stresses. The element results are given at the center of gravity of each element.

The basic steps to be developed for the general stretching and bending elements are the computation of the element stiffness matrix, the computation of stresses from displacement and rotation components and the output program. As mentioned earlier, the element stiffness matrix, in the local coordinate system, contains stretching and bending parts, which result in five degrees of freedom per joint. The basic arrangement is represented schematically as follows:

$$
\begin{bmatrix}
X & X & O & O & O \\
X & X & O & O & O \\
O & O & X & X & X \\
O & O & X & X & X \\
O & O & X & X & X
\end{bmatrix}
\qquad (A.1)
$$

This matrix is expanded to allow six degrees of freedom per joint, including the rotation not taken into account in the stretching part, and becomes:

$$
\begin{bmatrix}
X & X & O & O & O & O \\
X & X & O & O & O & O \\
O & O & X & X & X & O \\
O & O & X & X & X & O \\
O & O & X & X & X & O \\
O & O & O & O & O & E
\end{bmatrix}
\qquad (A.2)
$$

137

where E is equal to 1, for simple nodes, and equal to 0 for inter-section nodes. This distribution is made to avoid obtaining structural instabilities in relation to the simple nodes. At the intersection nodes, since there will be a contribution to the stiffness matrix from elements lying in different planes, the zero row and column will become non-zero, once all the contributions are taken into account. That is not the case for simple nodes, where all connecting elements are in the same plane. Therefore, for the matrix to be regular, E must be equal to 1 for that type of node.

Once the element stiffness matrix is computed in the local frame, it is then rotated to the global frame. This rotation will be explained in two steps. First, consider an element with an arbitrary orientation with regard to its own plane:
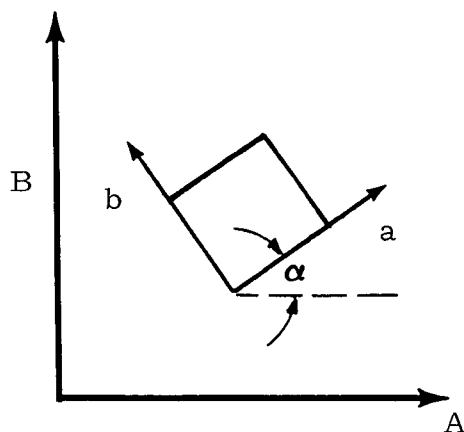


The element stiffness matrix is first generated in the a, b frame. Rotation to the A, B frame requires the use of the following rotation matrix:

$$R^{ab,AB} = \begin{bmatrix} \cos\alpha & -\sin\alpha & 0 \\ \sin\alpha & \cos\alpha & 0 \\ 0 & 0 & 1 \end{bmatrix}$$ 

(A.3)

138

The plane where the element lies may be XY, XZ, or YZ.
Therefore, there is an additional rotation required, involving a different
rotation matrix in each case. When the element lies in the XY plane, the
second rotation matrix is simply a unit matrix, so that no further manipu-
lations are needed. For the other two cases the rotation matrices are:

$$R^{XZ} = \begin{bmatrix} 1 & 0 & 0 \\ 0 & 0 & -1 \\ 0 & 1 & 0 \end{bmatrix} \tag{A.4}$$

$$R^{YZ} = \begin{bmatrix} 0 & 0 & 1 \\ 1 & 0 & 0 \\ 0 & 1 & 0 \end{bmatrix} \tag{A.5}$$

Although the procedure of the rotation of the stiffness matrices has been
divided into two steps for simplicity, it will actually be performed using
a unique rotation matrix for each element, which is:

$$R^{*, XY} = \begin{bmatrix} \cos \alpha & -\sin \alpha & 0 \\ \sin \alpha & \cos \alpha & 0 \\ 0 & 0 & 1 \end{bmatrix} \tag{A.6}$$

for elements lying in the XY plane, or

$$R^{*, XZ} = \begin{bmatrix} \cos \alpha & -\sin \alpha & 0 \\ 0 & 0 & -1 \\ \sin \alpha & \cos \alpha & 0 \end{bmatrix} \tag{A.7}$$

for elements lying in the XZ plane, or

$$R^{*,YZ} = \begin{bmatrix} 0 & 0 & 1 \\ \cos \alpha & -\sin \alpha & 0 \\ \sin \alpha & \cos \alpha & 0 \end{bmatrix}$$ 

(A. 8)

for elements lying in the YZ plane.

The displacement results will be obtained in the global frame after the solution procedure is completed. They will be first rotated to the local element frame using matrices (6), (7) or (8), according to the case, and from these stresses will be computed following the finite element analysis.

# BIBLIOGRAPHY

(1) Argyris, J.H., <u>Matrix Methods of Structural Analysis</u>, Pergamon Press (1964)

(2) Zienkiewicz, O.C., <u>The Finite Element Method in Structural and Continuum Mechanics</u>, McGraw-Hill (1967)

(3) Przemieniecki, J.S., <u>Theory of Matrix Structural Analysis</u>, McGraw-Hill (1968)

(4) Freeman, R.F., Porter, C.D., Mu, H.H. <u>Photoheliograph-Primary Mirror Development</u>, Report #750-F, J.P.L. (1968)

(5) Creedon, J.F., Robertson, H.J., "Evaluation of Multipoint Interaction in the Design of a Thin Diffraction-Limited Active Mirror", IEEE Aerospace Jrnl., March 1969

(6) Argyris, J.H., "Continua and Discontinua", Proc. Conf. Matrix Meth. in Struct. Mech., Wright-Patterson AFB (1965)

(7) Lang, T.E., <u>Summary of the Functions and Capabilities of SAMIS</u>, Tech. Report 32-1075 JPL (1967)

(8) Utku, S., Akyuz, F.A., ELAS, Volume I, <u>User's Manual</u> JPL (1968)

(9) McCormick, C. "Application of the NASA General Purpose Structural Analysis Program to Large Radio Telescopes", Structures Technology for Large Radio and Radar Telescope Structures, M.I.T. Press (1969)

(10) Logcher, R.D., Et al. <u>ICES-STRUDL II Engineering User's Manual</u>, M.I.T. CE Department (1968)

(11) Irons, B.M., Engatoudis, I., Zienkiewicz, O.C., "Curved Isoparametric 'Quadrilateral' Elements for Finite Element Analysis" Int. Jrnl. Solid Structures, Vol. 4, pp. 31-42, (1968)

(12) Kumanin, K.J., <u>Generation of Optical Surfaces</u>, Focal Press, (1968)

(13) Schroeder, J.B., "Materials Considerations for Large Spaceborne Astronomical Telescopes", Opt. Telescope Tech. Symp. NASA/MSFC, (1969)

# BIBLIOGRAPHY

(14)    Maringer, R.E., "Effects of Processing on the Dimensional
        Stability of Beryllium Mirrors". Opt. Telesc. Tech. Symp.
        NASA/MSFC (1969)

(15)    Hoffman, E.L., "Degradation of Mirror Surfaces in a Proton
        Environment", Opt. Telesc. Symp. NASA/MSFC (1969)

(16)    Smith, W.J., Modern Optical Engineering, McGraw-Hill
        (1966) p. 297

(17)    Ibid. p. 311

(18)    Marechal, A. and Francon, M., Diffraction, Structure
        des Images (Ed. de la Rev. d'Opt.) 1960

(19)    Love, A.E.H., "The Mathematical Theory of Elasticity"
        Dover (1944)

(20)    Couder, A., "Bulletin Astronomique", 7:201, 1931
        Translation by E.T. Pearson, K.P.N.O.

(21)    Crawford, D.L., Meinel, A.B., Stockton, M.W.
        "Support and Testing of Large Astronomical Mirrors"
        K.P.N.O and University of Arizona (July 1968)

(22)    Simmons, G.A., "The Design of Light-Weight Cer-Vit
        Mirror Blanks". Opt. Telesc. Tech. Symp. NASA/MSFC

(23)    MacKinnon, D., Madden, P., Farrell, P., "Optical Mirror
        Figure Control". MIT/CSDL #R-665, May (1970)

(24)    Selke, L.A., "Theoretical Elastic Deflections of a Thick
        Horizontal Circular Mirror on a Ring Support".
        Applied Optics, Vol. 9, No. 1 (Jan. 1970).

(25)    Selke, L.A. "Theoretical Elastic Deformations of a Thick
        Horizontal Circular Mirror on a Double-Ring Support".
        Applied Optics, Vol. 9, No. 6 (June 1970).

# BIBLIOGRAPHY

(26)    Selke, L. A. "Theoretical Elastic Deformations of Solid and Cored Horizontal Mirrors Having a Central Hole on a Ring Support", Applied Optics, Vol. 10, No. 4 (April 1971).

(27)    Reissner, E. "The Effect of Transverse Shear Deformation on the Bending of Elastic Plates", A. S. M. E. Journal of Applied Mechanics, V. 12, A-69 (1945).

(28)    Reissner, E. "On Bending of Elastic Plates", Quant. App. Math. V. 5, p. 55 (1947).

(29)    Malvick, A. J. and Pearson, E. T., "Theoretical Elastic Deformations of a 4 Meter Diameter Optical Mirror Using Dynamic Relaxation", Applied Optics, Vol. 7, No. 6 (June 1968).

(30)    Malvick, A. J. "Dynamic Relaxation: A General Method for Determination of Elastic Deformation of Mirrors", Applied Optics, Vol. 7, No. 10 (Oct. 1968).

(31)    Malvick, A. J. "Thermal Deformations of Solid Mirrors", Applied Optics, Vol. 9, No. 11 (Nov. 1970).